2-1-2021

Investigation of the Load-Induced Cracking and Rutting Performance of Specialty Hot Mix Asphalt Overlay Mixtures

Andrae Anthony Francois

INVESTIGATION OF THE LOAD-INDUCED CRACKING AND RUTTING PERFORMANCE OF SPECIALTY HOT MIX ASPHALT OVERLAY MIXTURES

by

Andraé Anthony François

A Dissertation

Submitted to the
Department of Civil and Environmental Engineering
College of Engineering
In partial fulfillment of the requirement
For the degree of
Doctor of Philosophy
at
Rowan University
April 22, 2020

Dissertation Advisor: Yusuf Mehta, Ph.D., P.E.

Dedications

I would like to dedicate this document to my parents, Gary Francois and Marilyn Thomas-Francois, as well as my sister, Marisa Adele-Marie Gray, for the unwavering love, support, and encouragement they provided throughout each phase of my academic career. I would also like to dedicate this dissertation to my extended family, especially David N. Thomas for the well wishes spiritual and technical support they provided throughout my graduate studies. Additionally, I would like to dedicate this dissertation to Rita N. Omekam: whose love and support spurred me on to complete this document. Lastly, I would like to dedicate this dissertation to my deceased grandparents, Lawrence Thomas, Adeline Thomas, and Rita Francois, who would have been very elated and proud to see me complete this major academic milestone.

Acknowledgements

I would like to thank Almighty God for providing me with the physical ability and mental fortitude to complete this dissertation. I would like to acknowledge and express my heartfelt gratitude to my advisor, Dr. Yusuf Mehta, for providing me with sound academic advice and astute technical guidance throughout my graduate studies. Additionally, I would like to specially thank the members of my dissertation committee, Dr. Douglas Cleary, Dr. Gilson Lomboy, Dr. Nasrine Benjilali, and Dr. Parth Bhavsar, for agreeing to serve on my committee and providing pivotal input that led to the overall success of this research effort. I would like to acknowledge the New Jersey Department of Transportation Bureau of Research for funding this research study, which was a continuation of an initial study entitled, "HVS Evaluation of Flexible Overlays on Composite Pavements." Lastly, I would like to thank the members of the Rowan University Center for Research and Education in Advanced Transportation Engineering Systems (CREATEs) who contributed to the fruition and success of this study. I would particularly like to acknowledge Dr. Ayman Ali, Dr. Dan Offenbacker, Ahmed Saidi, Zhuang Zhuo, Neirouz Bouhrira, and Cailin Purdy for the stalwart assistance they provided throughout this research study.

Abstract

Andraé François
INVESTIGATION OF THE LOAD-INDUCED CRACKING AND RUTTING PERFORMANCE OF SPECIALTY HOT MIX ASPHAL OVERLAY MIXTURES
2019-2020
Yusuf Mehta, Ph.D.
Doctor of Philosophy

This study was initiated with the aim of investigating the cracking performance, rutting performance, and cost effectiveness of specialty and composite HMA mixtures utilized in New Jersey to rehabilitate deteriorated rigid pavements. As such, four, plant-produced, specialty HMA overlay mixtures currently used in New Jersey were evaluated in this study. These overlay mixtures included: a dense-graded, 9.5-SP mixture, a gap-graded, 12.5-SMA mixture, a dense graded, 4.75-HPTO mixture, and a uniformly graded, 4.75-BRIC mixture. The 9.5-SP, 12.5-SMA, and 4.75-HPTO mixtures were produced using PG 76-22 binder while the 4.75-BRIC was contained a PG 70-28 binder. The laboratory cracking and rutting performance of the mixtures were assessed using the overlay test, the dynamic modulus test, uniaxial cyclic fatigue test, bending beam fatigue test, and asphalt pavement analyzer test. The field reflection cracking performance of the HMA overlay mixtures were assessed by performing accelerated pavement testing on six full-scale, field sections. The field sections contained a similar substructure. However, the overlays utilized on the field sections consisted of a 9.5-SP, 12.5-SMA, 4.75-HPTO, 9.5-SP & 4.75-BRIC, 12.5-SMA & 4.75-BRIC overlay, and 4.75-HPTO & 4.75BRIC. Based on the results of the study it was determined that the use of a 4.75-BRIC interlayer generally improved the reflection cracking performance and overall cost effectiveness of the conventional and specialty overlay mixtures.

Table of Contents

Table of Contents (Continued)

Table of Contents (Continued)

Table of Contents (Continued)

List of Figures

List of Figures (Continued)

Figure Page

List of Figures (Continued)

Figure Page

List of Tables

List of Tables (Continued)

Table Page

Chapter 1

Introduction

Hot mix asphalt (HMA) overlays have become the rigid (i.e., concrete) pavement, rehabilitation technique of choice for many state transportation agencies in the United States (US). This is because they have major advantages over other rigid pavement rehabilitation alternatives [1]. Some of the main advantages of HMA overlays include: their relatively quick and inexpensive application, long service life, low life cycle cost, and their ability to withstand heavy traffic and high shear stresses. HMA overlays primarily address functional deficiencies in deteriorated rigid pavements. Therefore, they are typically used to improve pavement ride quality, maintain pavement grade and slope geometry, reduce surface permeability, and minimize noise at the tire-pavement interface [1]. As a consequence, HMA overlays generally have a lower thickness than traditional HMA surface layers since they do not provide structural support for rigid pavement systems [2].

The layer thickness used for HMA overlays varies from state to state because there is little consensus among state transportation agencies in regard to the actual thickness that constitutes an HMA overlay. However, many state transportation agencies define HMA overlays as a surface course (i.e., pavement surface layer) that has a maximum thickness of 1.5 in. (38.1 mm) [2]. Since the field compacted density of HMA layers (particularly overlays) directly affects their performance: most state transportation agencies utilize HMA mixtures with a nominal maximum aggregate size (NMAS) of 12.5 mm or less (i.e., 9.5 mm or 4.75 mm) in HMA overlays [2]. This is because a study by

Brown et al. [3] determined that the ratio of HMA layer thickness to NMAS should range between 3:1 and 5:1 in order to ensure adequate field compacted density is achieved during HMA construction.

There are four types of HMA mixtures used in asphalt overlays in the US. These HMA mixtures which, differ based on gradation type, include: dense-graded aggregate (DGA) mixtures, stone matrix asphalt (SMA) mixtures, open graded friction course (OGFC) mixtures, and ultra-thin bonded wearing course (UTBWC) mixtures [4]. Dense-graded mixtures contain an even distribution of coarse fine, intermediate and aggregates. Stone matrix asphalt mixtures have a gap gradation (i.e., a small proportion of intermediate size aggregates). Open graded friction course mixtures consist of a small percentage of fine aggregates. Ultra-thin bonded wearing courses have a uniform gradation (i.e., a large proportion of aggregates that have a similar size) [5].

The four types of HMA mixtures used in asphalt overlays are subdivided into two broad categories; conventional and unconventional overlay mixtures, based on their specific applications. DGA and SMA mixtures are described as conventional overlay mixtures because they are typically used in asphalt overlays. OGFC and UTBWC mixtures are defined as unconventional overlay mixtures because they are specially designed to provide drainage, mitigate shallow rutting and stymie fatigue cracking, respectively [6].

Background

In recent years, researchers have investigated the impact of mixture gradation and binder type on the laboratory performance of conventional asphalt overlay mixtures to

determine their suitability for pavement rehabilitation applications [6, 7, and 8]. Suleiman [9] conducted one such study, which evaluated the rutting resistance of four different dense-graded, Superpave mixtures. All mixtures had a 4.75 mm, NMAS and were produced using a PG 64-28 or PG 58-28 binder. The researcher performed the asphalt pavement analyzer (APA) rut test on gyratory-compacted, specimens of the mixtures. All mixtures underwent 8,000 APA cycles; using a rut depth criterion of 9.5 mm. Based on the results of the study, the researcher determined that all mixtures were rut resistant (i.e., did not exceed rutting threshold). The researcher also found that the rut resistance of the mixtures improved as the percentage of crushed fine aggregates increased.

Rahman [10] evaluated the laboratory performance of twelve different dense-graded, 4.75 mm NMAS, Superpave mixtures. The researcher varied the aggregate source, natural sand content (i.e., fine aggregate content) (35%, 25%, and 15%), and binder type (PG 64-22 and PG 70-22) of the mixtures. Gyratory-compacted specimens of all mixtures were subjected to the Hamburg Wheel Tracking (HWT) rut test and the moisture susceptibility test while vibratory-compacted specimens of the mixtures underwent beam fatigue testing. The HWT test was allowed to run for 20,000 cycles at 50^{o}C; and the beam fatigue test was conducted at 25^{o}C under a constant strain of 300 micro-strains. Rahman [10] made two main conclusions based on the results of the tests. The first conclusion was that flexural strength of mixtures which, contained PG 64-22 binder, increased as the percentage of natural fine aggregates decreased. The second conclusion was that the PG 70-22 binder generally improved the fatigue performance of the 4.75 mm NMAS mixtures.

Cooley et al. [11] investigated the potential for using stone matrix asphalt mixtures with finer gradations (i.e., 9.5 mm or 4.75 mm NMAS) as thin overlays. The researchers evaluated the rutting performance of eight different SMA mixtures using the APA rut test. Cooley et al. [11] varied the NMAS (4.75 mm, 9.5 mm, 12.5 mm, and 19 mm) and break point sieve sizes of the mixtures (i.e., finest sieve sizes to retain at least 10% of aggregates). APA rut tests were performed on gyratory-compacted, specimens of each SMA mixture at 50^{o}C and 64^{o}C respectively. All specimens were subjected to 8,000 loading cycles using a rut depth threshold 5.0 mm. Cooley et al. [11] found that rut depth increased as test temperature increased. However, the magnitude of the rut depths remained relatively low (i.e., below the rutting threshold) despite the temperature increase. The researchers therefore, concluded that both the fine and coarse graded SMA mixtures were rut resistant.

Son et al. [12] assessed the suitability of 4.75 mm NMAS, SMA mixtures for wearing courses (pavement surface layers) by comparing the performance of a 4.75 mm, SMA mixture to that of a 9.5 mm, dense-graded and 12.5 mm, SMA mixture, respectively. Son et al. [12] conducted the dynamic modulus test and moisture susceptibility test on gyratory-compacted specimens of all mixtures. Based the results of the study the researchers determined that the 12.5 mm SMA mixture had the highest stiffness at low test frequencies while the 4.75 mm SMA mixture had the lowest stiffness at high test frequencies. Son et al. [12], therefore concluded that the 12.5 mm SMA mixture was the most resistant to rutting while the 4.75 mm SMA mixture was the most resistant to low temperature cracking. The researchers also reported that the 4.75 mm SMA mixture had the highest indirect tensile strengths in both wet and dry conditions.

However, the 4.75 mm SMA mixture was more moisture susceptible than the 12.5 mm SMA mixture.

Problem Statement

In summary, the studies outlined as well as other studies [13] – [15] have assessed the appropriateness of conventional mixtures for pavement rehabilitation applications based on their laboratory performance. Based on these studies transportation agencies such as New Jersey Department of Transportation (NJDOT) readily use various crack resistant, specialty conventional mixtures in their overlays to rehabilitate deteriorated rigid pavements. However, limited research was found in regard to studies that evaluated and compared the relative performance of different types of specialty mixtures. Furthermore, HMA overlays are particularly prone to reflection cracking due to the presence of cracks in the underlying layer [16]. However, few studies have explored the ability of specialty mixtures to resist reflection cracking. Therefore, there is a need to comprehensively assess the cracking, and rutting performance of various types of specialty HMA mixtures used in overlays in states like New Jersey (NJ).

In addition, reflection cracking is a major concern for HMA overlays because it reduces their overall effectiveness and service life [17]. Several studies, [18] – [20] have suggested that the use of a stress relieving interlayer in conjunction with specialty mixtures (i.e., composite overlays) delay the onset of reflection cracking in overlays. However, few studies have compared the relative performance of composite and specialty mixtures in order to determine whether composite mixtures are more viable rehabilitation options than specialty mixtures. Therefore, there is also a need to examine the relative

cracking and rutting performance of composite overlay mixtures as well as overall cost effectiveness of specialty and composite overlay mixtures.

Significance of Study

This study aims to address the various research limitations previously identified in regard to specialty and composite HMA overlay mixtures currently used by state transportation agencies. The study is designed to comprehensively examine the cracking and rutting performance of specialty and composite HMA overlay mixtures in order to determine the most suitable HMA overlay mixture(s) for rigid pavement rehabilitation. Determining the best performing mixture (or combination of mixtures) for asphalt overlays is essential for states like NJ where 50 percent of the pavements are composite pavements [21]. This is because state transportation agencies will be able to make better informed, cost effective, decisions when selecting rehabilitation alternatives for deteriorated rigid pavements.

Hypothesis

This study will seek to address the following research hypotheses:

1) The fatigue cracking, reflection cracking, and rutting performance of HMA overlays is influenced by the type of HMA mixture (i.e., specialty mixture) used to construct the overlay.
2) The service life and cost effectiveness of HMA overlays can be improved by using composite overlay mixtures (i.e., a surface course, specialty mixture placed over a stress relieving layer of binder rich intermediate course mixture).

Goal & Objectives

The main goal of this study is to compare the cracking performance, rutting performance, and overall cost effectiveness of specialty HMA mixtures and composite HMA mixtures utilized in New Jersey to rehabilitate deteriorated rigid pavements. To accomplish the overall research goal, this study had the following objectives:

- Evaluate the stiffness characteristics, laboratory fatigue cracking, reflection cracking, and rutting performance of four specialty, New Jersey mixtures that are utilized in HMA overlays (i.e., 9.5ME Superpave, 12.5 stone matrix asphalt, New Jersey high performance thin overlay (NJ HPTO), and binder rich intermediate course (BRIC)).
- Compare the relative laboratory fatigue cracking, reflection cracking, and rutting performance of three specialty New Jersey overlay mixtures (9.5ME Superpave, 12.5 stone matrix asphalt, and NJ HPTO) and three composite overlay mixtures (9.5ME Superpave & BRIC, 12.5 stone matrix asphalt & BRIC, and NJ HPTO & BRIC).
- Assess the field cracking and rutting performance of three specialty New Jersey overlays (9.5ME Superpave, 12.5 stone matrix asphalt, and NJ HPTO) and three composite New Jersey overlays (9.5ME Superpave & BRIC, 12.5 stone matrix asphalt & BRIC, and NJ HPTO & BRIC) .
- Develop a generalized methodology to process and analyze strain data obtained from full-scale, field sections in order to quantify the field cracking performance of the specialty and composite HMA overlays.

- Examine the cost effectiveness of the three specialty, New Jersey mixtures (9.5ME Superpave, 12.5 stone matrix asphalt, and NJ HPTO), and three composite mixtures (9.5ME Superpave & BRIC, 12.5 stone matrix asphalt & BRIC, and NJ HPTO & BRIC) based on the laboratory and field performance of the respective mixtures

Research Approach

The research approach adopted to achieve the objectives of this study is presented in Figure 1. The overall research approach encompassed both laboratory testing and full-scale, field testing. The purpose of the laboratory testing was to assess the laboratory performance of the specialty, New Jersey mixtures considered in this study as well as compare the relative laboratory performance of the specialty and composite New Jersey mixtures. The purpose of the field testing was to accurately quantify the relative cracking and rutting susceptibility of the specialty and composite HMA overlay mixtures based on realistic (or actual) pavement responses.

The first phase of laboratory testing outlined in Task 1 (Figure 1) was performed on laboratory-produced, specimen of the 9.5ME Superpave, 12.5 stone matrix asphalt, NJ HPTO and BRIC mixtures. The stiffness characteristics, laboratory fatigue cracking, reflection cracking and rutting performance of the mixtures were evaluated using the dynamic complex modulus (DCM) test, uniaxial cyclic fatigue test, overlay test (OT), and asphalt pavement analyzer rut test, respectively. The fracture properties of the HMA surface course mixtures (i.e., the 9.5ME Superpave, 12.5 stone matrix asphalt, NJ HPTO) was also assessed using the semi-circular bend test. Task 1 directly addressed the need to

assess the relative performance of various types of specialty HMA mixtures used in overlays since it facilitated a comparison of the fatigue cracking, reflection cracking, and rutting performance of all the mixtures evaluated in this study.

The field testing component of the study (outlined in Task 2 (Figure 1)) involved accelerated pavement testing (APT): where six full-scale, composite pavement sections were instrumented and subjected to accelerated, loading using a heavy vehicle simulator (HVS). The field sections contained a similar substructure however the HMA overlay utilized in each section was different. A 9.5ME Superpave overlay, 12.5 stone matrix asphalt overlay, and NJ HPTO overlay was used on three pavement sections while the overlays in the remaining sections consisted of the aforementioned HMA mixtures in conjunction with a BRIC interlayer. A generalized strain gauge data analysis procedure was developed and utilized to quantify and compare the relative cracking performance of the HMA overlays in the full-scale sections. It was necessary to develop such a procedure as part of the field testing because there is currently no standardized methodology to process and analyze strain gauge data obtained from full scale test sections. The rutting performance of the HMA overlays was assessed using a laser profileometer.

The second phase of laboratory testing described in Task 3 (Figure 1) was conducted on field-compacted, specimens (i.e., field cores) obtained from each of the full-scale, composite pavement test sections. The laboratory fatigue cracking, reflection cracking and rutting performance of the field-compacted specimens were assessed using the bending beam fatigue (BBF) test, overlay test, and APA, rut test, respectively. Task 3 essentially facilitated the relative performance comparison between the specialty HMA overlay mixtures and composite overlay mixtures.

Tasks 4 (Figure 1) entailed comparing and ranking the laboratory and field performance of the conventional, specialty, and composite HMA overlay mixtures based on the laboratory and field testing results. Additionally, Task 5 (Figure 1) involved determining the overall cost effectiveness of the specialty and composite overlay mixtures based on their field and laboratory cracking performance.

Research Outline

This research study is separated into eight chapters. The first chapter presents an overview of the study. It details the research problem, research hypothesis, and goals of the study. The first chapter also provides an overview of the approach adopted to achieve the research objectives. The second chapter provides a comprehensive literature review on the various types of HMA overlay mixtures. It also summarizes some of the studies conducted on these HMA overlay mixtures. Additionally, Chapter 2 also provides a detailed explanation of the cracking mechanism that occurs in HMA overlays along with the common laboratory tests that are used to assess HMA overlays during each phase of crack evolution. The rutting mechanism that occurs in HMA overlays as well as common laboratory rut tests is also explained in this chapter.

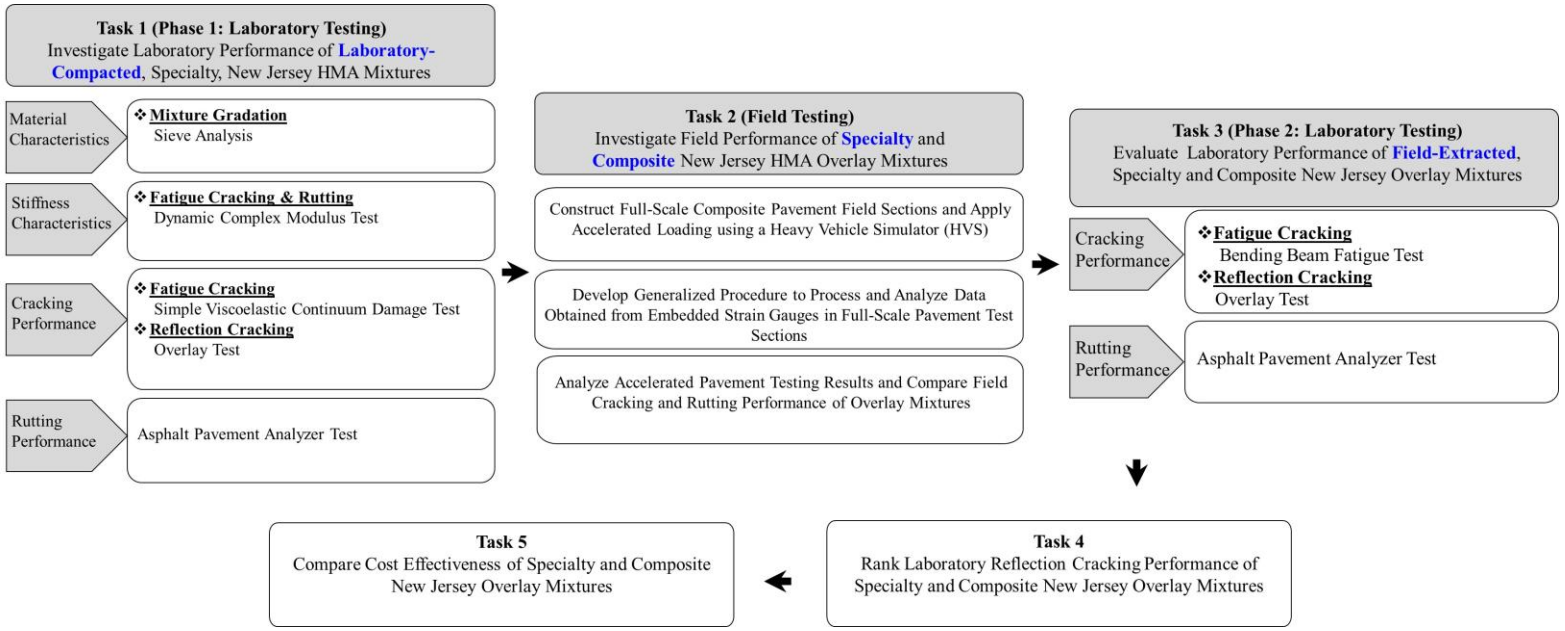

Figure 1. Research approach adopted in this study

The third chapter summarizes the material properties of the HMA mixtures assessed in this study. Information in regard to the gradation, volumetric properties (i.e., air void content), binder type and binder content of the mixtures is provided. The laboratory experimental plan and testing matrix is also discussed in this chapter. The fourth chapter presents the results of the laboratory testing and provides an interpretation and explanation of these results.

Chapter five provides a description of the full-scale, composite pavement field sections as well as the construction process used to construct these sections. The chapter also summarizes the types of sensors installed in the test sections and discusses the sensor installation process employed to instrument the field test sections. Additionally, the chapter outlines the overall field experimental plan and accelerated pavement testing scheme utilized in this study. Chapter six presents the results of the field testing (i.e., data obtained from the sensors installed in the composite pavement field sections). An interpretation of the sensor data obtained during APT is outlined. The generalized strain data analysis procedure developed to quantify the cracking performance of the HMA overlays is also explicated and demonstrated in this chapter using the strain data obtained from the composite sections during APT.

In chapter seven the laboratory and field testing results obtained for the HMA overlay mixtures are compared and ranked using statistical analyses. The chapter also describes the life cycle cost analysis that is employed to assess the service life and overall cost effectiveness of each HMA overlay mixture. In Chapter eight, the research study is concluded with a summary of the study's major findings, overall conclusions, study limitations, and recommendations for future research studies.

Chapter 2

Literature Review

This literature review is divided into three components. The first component of the literature review provides a detailed summary of the cracking mechanisms that are typically at play in HMA overlays. The second component outlines some of the laboratory tests that are used to assess the cracking performance of HMA overlays. The third component describes the type of HMA overlays that are utilized in New Jersey. The fourth and final section summarizes some of the key findings from laboratory and field studies that were performed on HMA overlays.

Overview of Cracking in HMA Mixtures

Fatigue cracking in HMA overlays. Fatigue cracking is one of the most common distresses that occur in HMA pavement layers. Fatigue cracking is defined as the accumulation of reflection cracking on HMA pavement layers due to the combined effects of repeated traffic and environmental loading [22]. Traffic loading induces bending and shearing stresses in HMA overlays. That is, HMA layers experience two peak shearing stresses and one bending peak stress during each loading pass of vehicular traffic (Figure 2) [22]. Daily temperature variation also gives rise to tensile stresses in HMA layers. This is due to the repeated contraction and expansion of the HMA layer [22]. When HMA overlays undergo repeated cycles of traffic and environmental loading (i.e., bending, shearing and tension) the fatigue process is triggered. This fatigue process cause cracks to form and propagate throughout the wearing course (i.e., HMA overlay).

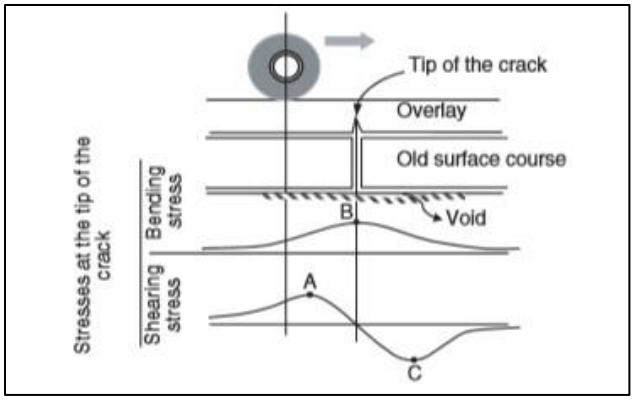

Figure 2. Illustration of stress that occur in HMA overlays due to traffic and environmental loading [24].

Stages of fatigue cracking in HMA mixtures. Cracks typically develop in HMA mixtures when they are subjected to repeated, tension loading. The crack formation process generally begins with the development of micro-cracks at regions of localized discontinuity in HMA mixtures. These localized discontinuities or stress raisers occur due to the presence of air voids in HMA mixtures. During the initial stage of cyclic (or repeated) tension loading, localized discontinuities briefly experience elastic deformation (region 1 (Figure 3)) [23]. This initial elastic deformation occurs because the entopic elasticity in the polymer chains of the asphalt binder tend to produce a dominant restorative force. However, as the tensile strains in the asphalt binder increases: the asphalt binder yields and the localized discontinuities undergo plastic (permanent) deformation (region 2 Figure 3)).

Permanent deformation occurs in asphalt binder; during this stage, because the polymer chains undergo disaggregation and realignment along the strained axis [24]. Localized discontinuities transform into a micro-crack once the plastic deformation limit of asphalt mixtures is reached. When the polymer chains in the asphalt binder realign

along the strained axis the tensile strength of asphalt mixtures increase with any further increase in tensile strain (i.e., strain hardening) (region 3 Figure 3)) [23]. This phenomenon occurs until the ultimate tensile strength of the asphalt mixture is reached. Once the ultimate tensile strength of the asphalt mixture is reached further increases in tensile strain overwhelm the covalent bonds in the polymer chains and they begin to break. This phenomenon causes the tensile strength of the asphalt binder to decrease as tensile strain increases until the asphalt binder undergoes catastrophic failure (i.e., macro-cracking) (region 4 Figure 3)).

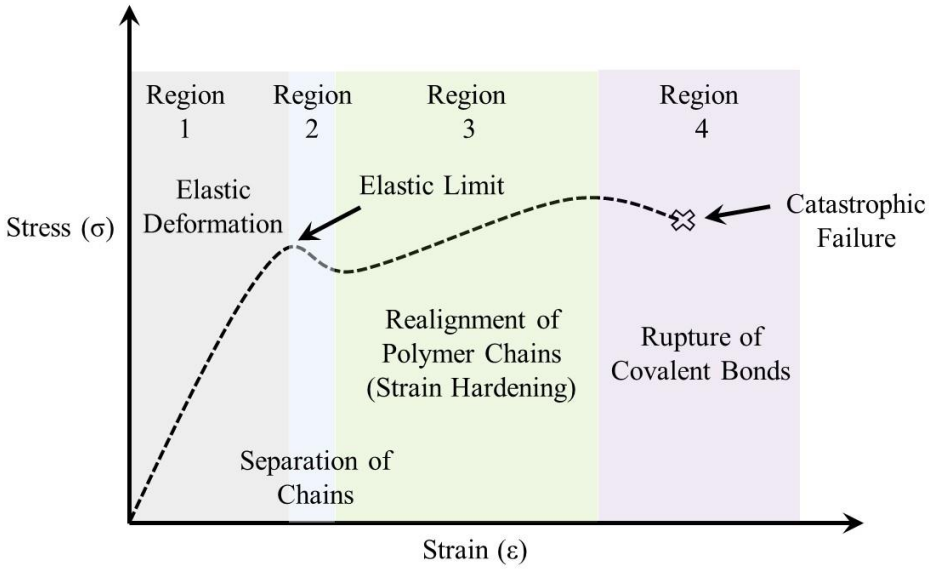

Figure 3. Stages of fatigue cracking in HMA mixtures.

Relationship between HMA overlay properties and fatigue cracking resistance. The fatigue cracking resistance of HMA overlays is strongly influenced by the mortar and binder type used in the HMA mixture. This is due to the fact that the mortar provides

HMA overlays with the necessary cohesion, tensile strength, and shear strength to resist effects of environmental and traffic loading [25]. The aggregate skeleton in HMA overlays also affects the fatigue cracking resistance of the overlay. This is because the shape and gradation of the aggregate skeleton provide the internal friction and bearing capacity required to resist traffic and environmental loading [25]. The nature (i.e., chemical properties) of the aggregates in the skeleton also plays a role in fatigue crack resistance of HMA overlays. This is owing to the fact that aggregate nature strongly influences binder adhesion and HMA mixtures' capacity to resist fragmentation [25]. Mixtures with low binder adhesion tend to have many weak points which make the mixtures more susceptible to fatigue crack initiation and propagation. For HMA mixtures with a low resistance to fragmentation, the coarse aggregates are more likely to crack making the mixture more prone to fatigue cracking.

Reflection cracking in HMA overlays. Reflection cracks can be described as transverse cracks that form in HMA overlays directly over joints and cracks in the underlying rigid pavement layer [26]**.** Reflection cracking is a primary concern for HMA overlays because it is one of the main distresses that occur in HMA overlays [27]. The onset of reflection cracking typically occurs during the early life of composite pavements. When reflection cracks fully propagate to the surface of HMA overlays, the overall structural capacity of the composite pavement system is adversely affected. This is because fully-propagated, reflection cracks permit the infiltration of water and debris which weakens the pavement structure (i.e., foundation) and reduces the overall service life of the composite pavement system [27]. Reflection cracks can also cause fine aggregate material to pump from the granular layer to the pavement surface. This creates

voids beneath the rigid pavement layer and decreases the overall structural stability of the composite pavement system [28].

Reflection cracking mechanism in HMA overlays. The effects of reflection cracking on the structural capacity and service life of composite pavement systems are exacerbated by two main external factors: traffic and environmental loading [29] - [30]. Traffic and environmental loading cause differential vertical and horizontal movements to take place in the vicinity of cracks and joints in the PCC layer of composite pavements (Figure 4). This differential movement is caused as a result of poor PCC slab support and poor load transfer efficiency across joints and cracks. The horizontal and vertical movements due to traffic and environmental loads produce points of stress concentration directly above crack and joints at the HMA overlay-PCC layer interface. The heightened stress at the HMA overlay-PCC layer interface causes an increase in tensile strains at the bottom of the HMA overlay [31]. When the magnitude of the tensile strains exceeds the tensile strain limit of the HMA overlay, reflection cracks initiate in the HMA overlays and they begin to propagate towards the surface [32]. The rate of reflection crack initiation and crack propagation depend on the characteristics of the HMA overlay mixture, condition of the composite pavement structure, load transfer efficiency across cracks and joints, and type of reflection cracking mitigation technique utilized (i.e., interlayer) [31].

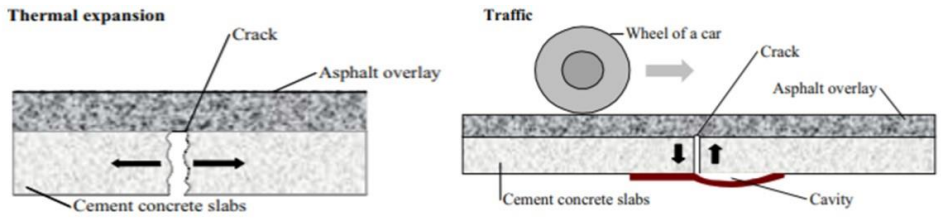

Figure 4. Reflection cracking mechanism in composite pavements [33].

Reflection cracking modes of failure. There are three modes of failure (i.e., mechanisms) associated with reflection cracking in HMA overlays. These modes of failure included: mode I, mode II, and mode III failure (Figure 5). Mode I failure is related to the horizontal movements (i.e., slab curling) of the PCC layer due to daily temperature variations [33]. These horizontal movements cause flexural and tensile stresses to develop in the HMA overlay. Mode II failure in HMA overlays is related to the differential vertical movement of the PCC layer at cracks and joints due to traffic loads [33]. These vertical movements cause shear and tensile stresses to develop in the overlay. Mode III failure in HMA overlays is linked to the parallel PCC slab movement in the rigid pavement layer due to structurally instability (i.e., lack of frictional resistance from supporting layers). It should be noted that Mode III failure is not common [33].

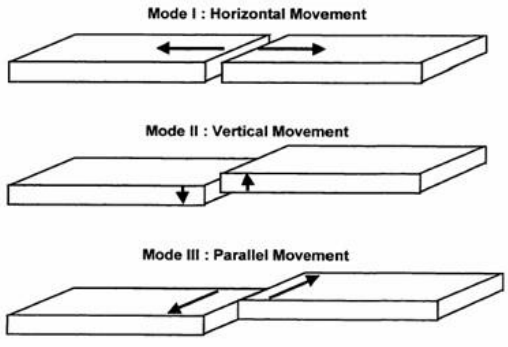

Figure 5. Movements in PCC layer that lead to reflection cracking in overlays [33].

Laboratory Tests Used to Assess HMA Overlay Performance

Dynamic complex modulus test. The dynamic complex modulus test (Figure 6) characterizes the material properties and linear viscoelastic behavior of HMA mixtures. The dynamic complex modulus test is used to determine the relationship between the stress and strain of asphalt mixtures under continuous sinusoidal loading. The dynamic complex modulus is defined as the ratio of the sinusoidal stress amplitude to the sinusoidal strain the amplitude; at the same time and angular frequency [34]. The dynamic complex modulus characterizes the elastic stiffness (i.e., storage or dynamic modulus (|E*|)) and viscous damping (i.e., loss modulus (E')) in asphalt mixtures. It can be graphically described in terms of vectors (Figure 6) [35]. The angle (φ) in (Figure 6) is referred to as the phase angle. The phase angle describes the lag in time between the applied stress and asphalt mixture strain response. This lag in applied stress and strain response arises because of the time-dependent, viscoelastic behavior of asphalt. The relationship between dynamic complex modulus, phase angle, storage modulus (dynamic modulus), and loss modulus is indicated in (Equation 1) and (Equation 2).

$$|E^*|(\omega) = E \times \cos(\varphi) \qquad (1)$$

$$E'(\omega) = E \times \sin(\varphi) \qquad (2)$$

Where

E Dynamic complex modulus, MPa

|E*| Storage Modulus, MPa

E' Loss Modulus, MPa

Φ Phase angle, degrees

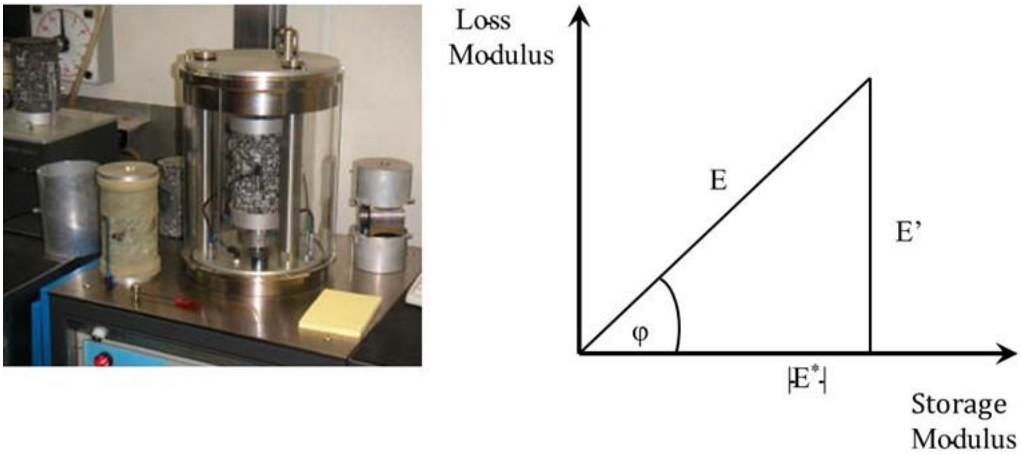

Figure 6. Dynamic complex modulus test setup and vector illustration of dynamic complex modulus [35].

The results of the dynamic complex modulus tests can be used to construct a dynamic modulus master curve. A dynamic modulus master curve indicates the stiffness of asphalt mixtures over a range of temperatures and loading frequencies. It is constructed at a specific reference temperature. The construction of the dynamic modulus master curve relies on the time-temperature superposition principle which involves shifting curves of measured dynamic modulus data at various temperatures until the curves merge into a single smooth function [34]. This shifting process is conducted with respect to time or frequency. The dynamic modulus curves at various temperatures are shifted using shift factors. The shift factors in this study were determined using Equation 1. In general, the dynamic modulus master curve can be modeled using various mathematical functions. However, in this study the dynamic modulus master curve was modeled using a sigmoidal function of the form expressed in (Equation 3).

$$\log\left|E^*\right| = \delta + \frac{\alpha}{1+\frac{1}{e^{\beta+\gamma(\log f_R)}}} \qquad (3)$$

Where

$\left\|E^*\right\|$	Dynamic modulus, MPa
f_R	Reduced frequency, Hz
δ, α, β, and γ	Master curve parameters

Uniaxial cyclic fatigue test. The uniaxial cyclic fatigue test (Figure 7) is a cyclic fatigue test that is used to assess the fatigue cracking resistance of asphalt mixtures. The test requires the application of a simple viscoelastic continuum damage (S-VECD) model to evaluate the evolution (i.e., growth) of fatigue damage in asphalt mixtures subjected to fatigue loading. The fundamental theory that governs the S-VECD model uses Schapery's work potential theory and damage based models developed by other researchers [36] and [37] to quantify damage in asphalt mixtures at the micro-structural level (Equation 4) [36]. The S-VECD model describes the cumulative damage asphalt specimens experience due to external fatigue loading over a range of loading modes and temperatures [38].

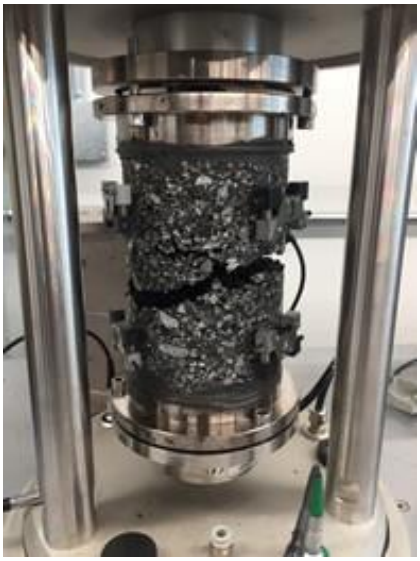

Figure 7. Uniaxial cyclic fatigue test setup.

Response of asphalt mixture specimen to cyclic tension fatigue loading. When cyclic tension loading is applied to asphalt specimen like the one illustrated in (Figure 7), the relationship between the stress and strain in the specimen is defined by (Equation 4) and Equation (5). The stress-strain relationship that characterizes the response of asphalt specimen during each cyclic tension loading cycle is represented by a hysteresis loop (Figure 8). The change in the area enclosed by the hysteresis loop during each loading cycle represents the total energy dissipated due to internal damping and the formation of microcracks [38]. Schappery's use of the correspondence principle to replace actual strains with pseudostrains allowed the effect of viscous damping on total dissipated strain energy to be eliminated. The relationship between actual strains and pseudostrains is defined by (Equation 4) and (Equation 5).

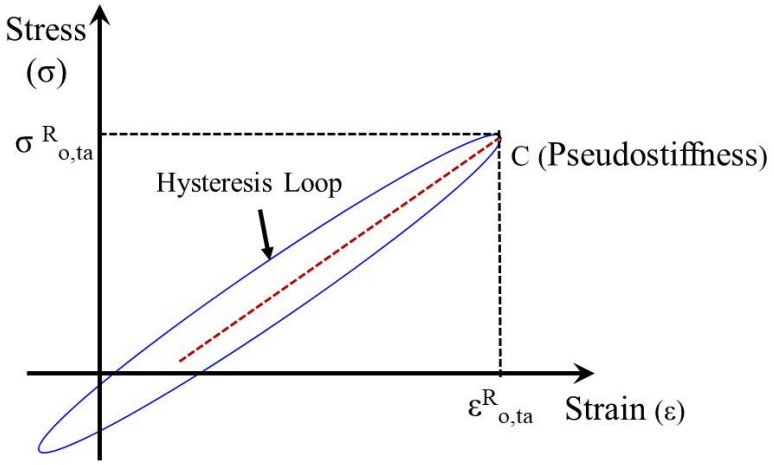

Figure 8. Illustration of representative hysteresis loop that characterizes the stress-strain relationship in asphalt specimen during cyclic tensile loading.

$$\varepsilon^{R}(t) \int_{0}^{t} E(t - \tau) \frac{d\varepsilon}{d\tau} \, d\tau \qquad (4)$$

$$\varepsilon^{R} = \varepsilon = |E*| \varepsilon_i \sin(\omega t + \phi) \qquad (5)$$

Where

ε	Strain amplitude
σ	Stress amplitude
ω	Angular frequency
ϕ	Phase angle
$\varepsilon^{R}(t)$	Pseudostrain during first loading cycle
t, τ	Time
E(t)	Relaxation Modulus
ε_i^R	Pseudostrain during cycle i
$\|E^*\|$	Dynamic modulus

The area enclosed by the hysteresis loop in the stress-pseudostrain domain represents the pseudostrain energy stored in asphalt specimen during a particular loading cycle (W_i^R) [38]. The maximum stored psuedostrain energy (W_{max}^R) during a load cycle is given by (Equation 6). From this equation it can be seen that the W_{max}^R is determined from the maximum pseudostrain and pseudostiffness (C) of the specimen during each cycle (Equation 9). The pseudo-stiffness represents the pseudosecant modulus of the asphalt specimen at maximum pseudostrain during each loading cycle (Figure 8). The potential for specimen to store energy decreases as cyclic tension loading cycles increase. Therefore the total pseudostrain energy released during each loading cycle is defined as the difference between the initial energy stored in the specimen before loading (i.e., undamaged specimen state) and the maximum pseudo-strain stored by the mixture during the current load cycle (Equation 7) [38].

$$W_{max}^R = \frac{1}{2}(\sigma_{o,ta})(\varepsilon_{o,ta}^R) = \frac{1}{2}\,C(\varepsilon_{o,ta}^R)^2 \qquad (6)$$

$$W_C^R = \frac{1}{2}(1 - C)(\varepsilon_{o,ta}^R)^2 \qquad (7)$$

Where

W_{max}^R	Maximum stored pseudostrain energy
W_C^R	Total strain energy released during a loading cycle
$\sigma_{o,ta}$	Maximum stress during loading cycle
$\varepsilon_{o,ta}^R$	Maximum pseudostrain during loading cycle
C	Pseudostiffness

Formulation of S-VECD model. The S-VECD model characterizes fatigue damage accumulation in asphalt mixtures based on the stiffness reduction and damage. The damage (S) assessed in the S-VECD model represents the change in internal state of asphalt specimen due to microstructural changes such as micro-cracking and plastic deformation of localized discontinuities in the mixture [38]. The damage is related to the total dissipated pseudostrain energy and its evolution within an asphalt specimen is defined by (Equation 8). The damage (S) is also related to the pseudo stiffness (C) (Equation 9). Damage characteristic curves for asphalt mixtures can be constructed using this relationship between Damage and pseudostiffness.

$$\cdot \frac{\mathrm{dS}}{\mathrm{st}} = \left(\frac{\partial W^R}{\partial \varepsilon^R}\right)^{\alpha} = \left(\frac{\partial {W_{max}}^R}{\partial \varepsilon^R}\right)^{\alpha} \qquad (8)$$

$$C = 1 - C_{11}S^{C12} \qquad (9)$$

Where

S	Damage
W^R	Psuedostrain energy density function
${W_{max}}^R$	Maximum stored pseudostrain energy
α	Damage growth rate
ε^R	Pseudostrain
C	Pseudostiffness
C_{11} and C_{12}	Damage characteristic curve power function model coefficients

The SVECD model allows for the determination of an apparent damage capacity (S_{app}) parameter for asphalt mixtures. The S_{aap} is a cracking index that can be used to compare the relative propensity of HMA mixtures to resist fatigue cracking. The S_{aap} is

defined by (Equation 11). It accounts for the total input pseudostrain energy and material fatigue life of HMA mixtures due to repeated loading [39]. The S_{app} index incorporates the D^R failure criterion (Equation 10) which, accounts for the toughness of asphalt mixtures. The S_{app} also accounts for time-temperature superposition of asphalt mixtures, which is related to mixture stiffness.

$$D^R = \frac{sum\ (1-C)}{N_f} \qquad (10)$$

$$S_{app} = \frac{1\ (\frac{\alpha_T}{C_{11}} D^R)^{\frac{\frac{C_{12}}{\alpha+1}}{C_{12}}}}{1000\ |E*|^{\frac{\alpha}{4}}} \qquad (11)$$

Where

α_T Time-temperature shift factor at target temperature

$|E^*|$ Dynamic modulus at target temperature and 10Hz, MPa

D^R S-VECD model failure criterion

N_f the number of uniaxial cyclic fatigue cycles to failure

Bending beam fatigue test. The bending beam fatigue test (Figure 9) is a four point bending test that is used to characterize the fatigue performance of HMA mixtures at intermediate temperatures. During the bending beam fatigue test, a cyclic flexural load is applied to the center third of a rectangular beam specimen at a specified loading rate [40]. The evolution of damage in the specimen is then continuously recorded throughout the test. Typically, the stress and strain in the specimen in measured using (Equation 12) and (Equation 13), respectively. The load required to achieve the specified displacement (i.e., on-specimen strain) is also monitored and recorded during the test. The flexural stiffness (Equation 14) of the specimen is computed during each loading cycle. The flexural stiffness

is subsequently used to calculate the normalized stiffness of the specimen (Equation 15). The number of cycles to failure (N_f) of each bending beam fatigue test specimen is determined based on the reduction in normalized stiffness [41].

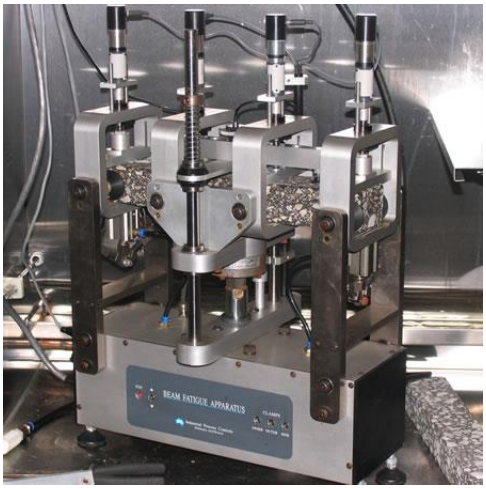

Figure 9. Bending beam fatigue test setup.

$$\sigma_t = \frac{3 \times a \times P}{b \times h^2} \qquad (12)$$

$$\varepsilon_t = \frac{12 \times \delta \times h}{(3 \times L^2) - (4 \times a^2)} \qquad (13)$$

$$S = \frac{\sigma_t}{\varepsilon_t} \qquad (34)$$

$$\text{Normalized Stiffness} = \frac{S_i \times N_i}{S_0 \times N_0} \qquad (15)$$

Where

σ_t Tensile stress, MPa

a Center-to-center load spacing, mm

P Load, N

B Specimen width, mm

h Specimen thickness, mm

ε_t Tensile strain

δ Beam deflection, mm

L Specimen Length, mm

S Flexural stiffness, MPa

S_i Flexural stiffness at cycle i

N_i Number of cycles at cycle i

S_o Flexural stiffness at initial cycle

N_o Number of cycles at initial cycle

Reflection cracking tests performed on HMA overlays. Currently the laboratory reflection cracking performance of HMA overlays is assessed using both standardized and non-standardized tests. These laboratory reflection cracking tests are summarized in Table 1. A major drawback of the majority of the current HMA overlay reflection cracking tests is the fact that very few tests have been validated by field reflection cracking performance data [40]. One of the few standardized tests used to assess the reflection cracking of HMA overlays is the overlay test. The overlay test has been verified using field performance data and the test has shown good agreement between laboratory mixture results and field mixture performance. The overlay test is outlined in detail in the following section.

Table 1

Summary of Laboratory Test used to Evaluate Reflection Cracking Performance of HMA Overlays

Testing Device	Test Type	Failure Mode	Input Load	Test Parameters	Schematic of Test Setup
University of Illinois [40]	Uniaxial Tension	Mode I	• Cyclic triangular uniaxial load	• Strain in HMA Overlay • Crack Length vs. Time	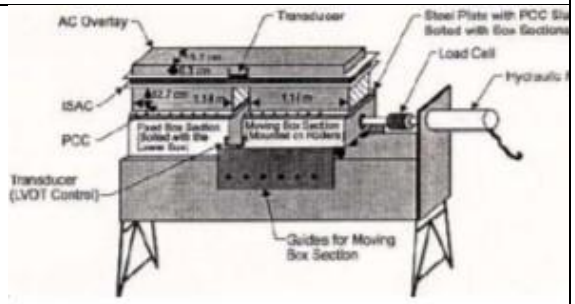
Aeronautical Technological Institute, Brazil [40]	Bending or Shearing	Mode I Mode II	• Sinusoidal load:	• Permanent Strain vs. Number of Cycles • Tensile Stress vs. Crack Length	
Wheel Reflective Cracking Device [40]	Biaxial	Mode I Mode II	• Static traction force • Cyclic wheel load	• Vertical length of crack vs. Time • Vertical Displacement vs. Time • Relative movement between crack edges	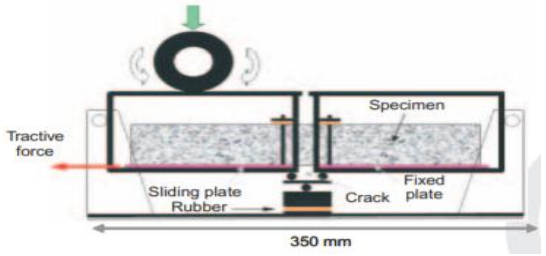
Overlay Tester [40]	Biaxial	Mode I Mode II	• Triangular cyclic tension	• No. of Cycles versus crack length • Fracture energy • Crack Progression Rate	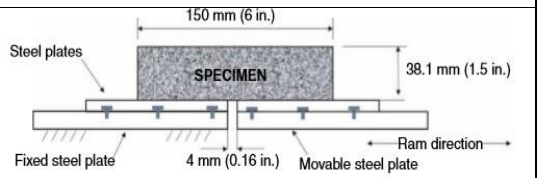

Overlay test. In the overlay test HMA specimens are mounted to two aluminum plates (Figure 10) in an overlay tester, a device which contains an electrohydraulic system that is capable of applying repeated direct tensional displacements on asphalt specimen [41]. During the test, one aluminum plate is fixed in the overlay tester and the other plate is allowed to slide horizontally. This loading mechanism simulates the opening and closing of cracks and joints in the existing layer of composite pavements due to traffic and environmental loads [41].

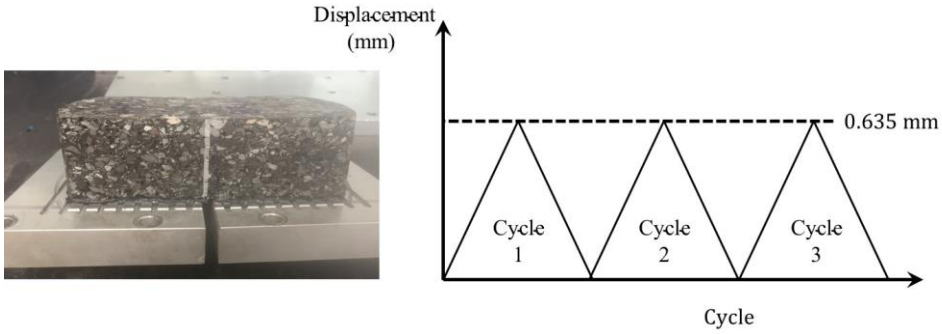

Figure 10. Illustration of overlay test setup and cyclic triangular tensile load.

The overlay test is conducted in displacement controlled mode at a loading rate of one cycle per second. A cyclic, triangular, tensile load is applied to the OT specimens at a constant maximum displacement of 0.635 mm (0.025 in.) [41] (Figure 10). During each loading cycle the aluminum plate reaches its maximum position and the overlay test forces the plate back to its original position. The overlay test is typically performed at 25^{o}C (77^{o}F). The test is terminated when there is a 93% reduction in the original load that caused a displacement of 0.635 mm (0.025 in.) during the first cycle of the overlay test.

New Jersey Specialty Overlay Mixtures

Stone matrix asphalt mixtures. Stone matrix asphalt is a type of gap-graded mixture that has high durability and rutting resistance. SMA mixtures originated in Europe in the 1960's and have been successfully used in the United States (US) since 1991 [42]. Stone matrix asphalt consists of two components: a coarse aggregate skeleton and a rich, asphalt mortar. The coarse aggregate skeleton is the key component of SMA mixtures and it accounts for 70 to 80% of the total aggregate blend [42]. The asphalt mortar, on the other hand; supports the coarse aggregate skeleton and primarily consists of: asphalt binder, fine aggregate, and mineral filler.

The design of SMA mixtures is centered on four main principles. The first principle requires a gap-graded, aggregate blend to be utilized in the mixture which facilitates stone-on-stone contact [42]. Stone-on-stone contact is vital for SMA mixtures because it leads to an increase in aggregate interlock in the coarse aggregate skeleton, which increases the load transfer efficiency and overall rutting resistance of the mixture. The second principle in the design of SMA mixtures requires the voids in the coarse aggregate skeleton to be filled with the asphalt mortar (i.e., asphalt binder, fine aggregate, and mineral filler). The third design principle of SMA mixtures requires the voids in mineral aggregate (VMA) to range between 18% and 20% [42]. Since the void in mineral aggregate refers to the volume of air voids between the aggregates of a compacted HMA mixture (i.e., effective binder content and air voids), it can be interpreted that the third design principle necessitates that SMA mixtures should have a relatively high binder content. This high binder content is required to increase the overall support provided to the coarse aggregate skeleton of the mixture [42].

New Jersey high performance thin overlay. High performance thin overlay mixtures are used as a rut resistant, durable thin-lift mixture for pavement maintenance and preservation. New Jersey HPTO mixtures are dense-graded, HMA mixtures that have a fine gradation. NJ HPTO mixtures are typically designed according to slightly modified Superpave procedures. The design of NJ HPTO mixtures allow for up to five percent 9.5 mm aggregates as opposed to ten percent, the threshold for conventional, coarse-graded HMA mixtures [43]. NJ HPTO mixtures also have a slightly higher voids in mineral aggregate than conventional asphalt mixtures (i.e., 16% compared to 15%) [43]. The required dust to binder ratio of NJ HPTO mixtures is also higher than that of conventional overlay mixtures. The binder selection procedure utilized in NJ HPTO design is similar to the guidelines that are followed for conventional coarse-graded asphalt mixtures. However, polymer modified binder is typically used in NJ HPTO mixtures to improve the reflection cracking resistance of the mixture. NJ HPTO mixtures are typically designed with a higher binder content than conventional, coarse graded mixtures and they are also compacted to a lower air void content than conventional asphalt mixtures.

Binder rich intermediate course mixtures. Binder rich intermediate course mixtures are specially designed New Jersey mixtures that are primarily used at the bottom of HMA overlays to stymie reflection cracking which occurs due to horizontal and vertical movement at cracks or joints in the underlying Portland cement concrete (PCC) layer. These movements in the PCC layer arise due to environmental and vertical loading. The New Jersey BRIC mixture is essentially a modification of the Texas DOT,

crack attenuating mixture (CAM) [44]. BRIC mixtures and crack attenuating mixtures are often defined as a stress relieving asphalt interlayers.

A stress relieving interlayer is a crack mitigation technique that is primarily designed to dissipate energy and absorb a portion of the shear stresses that arise at the HMA overlay-PCC layer interface due to the differential movements at cracks or joints in the PCC layer during loading [44]. Stress relieving interlayers carry-out their main functions by deforming horizontally and vertically. They are typically designed with low stiffness (i.e., high flexibility) to enhance their ability to dissipate energy and absorb stresses. When stress relieving interlayers are placed over joints or cracks in a deteriorated pavement layer, the gauge length (i.e., original length) for strain development increases. This decreases the overall potential for reflection cracking to occur in HMA overlays due to environmental and traffic loading [45].

Types of stress relieving interlayers. There are three types of stress relieving interlayers: stress absorbing membrane interlayers, cushion or crack relief layers, and bond breaker interlayers. Stress absorbing membrane interlayers are defined as interlayers that have a thickness of 50 mm (2 in.) or less [46]. Several materials fall under the category of stress absorbing interlayers. These materials include: chip seals, geo-synthetics, polymer-modified interlayers, asphalt-rubber interlayers, and soft asphalt interlayers. Cushion or crack relief interlayers are defined as interlayers that have a thickness greater than 75 mm (3 in.) [46]. Some examples of cushion interlayers include: crushed stone, unbound aggregates, and open graded HMA. Bond breaker interlayers are placed on the surface of deteriorated rigid pavement adjacent to joints or cracks prior to overlay construction Bond breaker interlayers typically span as wide as 50 to 610 mm (2

to 4) on either side of a joint or crack. Some of the materials used as bond breaker interlayers include: wax paper; aluminum foil; roofing paper, and a thin layer of sand or dust [46].

Reflection cracking mitigation mechanisms in stress relieving interlayers. The mechanism that governs reflection cracking mitigation in the various types of stress relieving interlayers differs. Stress absorbing membrane interlayers strictly dissipate horizontal movements at joint or cracks in the PCC layer [46]. This is because they do not contribute to the overall structural capacity of the pavements. Cushion or crack relief interlayers dissipate both horizontal, and differential, vertical movements at cracks or joints in the PCC layer [46]. Bond breaker interlayers decrease the stress concentrations in HMA overlays by inhibiting the formation of a bond between the existing pavement and HMA overlay; near cracks and joints. This lack of bonding between the two pavement layers increases the area of stress in the HMA overlay directly above the cracks and joints; which reduces the overall strain in the HMA overlay throughout its design life [46].

Characteristics of soft asphalt interlayers. The New Jersey binder rich intermediate course can be classified as a soft asphalt interlayer. Soft asphalt interlayers are extremely flexible HMA mixtures that consist of finely graded aggregates and elastic, polymer-modified binder. The aggregates in soft asphalt interlayers typically have a NMAS of 9.5 mm (0.37 in.); or less, and the mixture usually has a high binder content which ranges between 7% and 7.5% (by weight) [47]. A binder with a softer (i.e., lower) performance grade is used in soft asphalt interlayers because they considerably reduce the elastic modulus of the HMA mixture; thereby decreasing the crack tip stress in HMA

overlays. Soft asphalt interlayers are used in conjunction with HMA overlays because their low viscosity and low elastic modulus allows them to function as a stress relieving medium [47].

Summary of Studies Performed on HMA Overlays

Laboratory studies performed on HMA overlays. Several studies have been carried-out to assess the laboratory reflection cracking performance of HMA overlays. Butler and Gibney [48] conducted one such study which investigated the reflection cracking performance of three HMA mixtures used in Ireland. These mixtures included: a 14 mm (0.6 in.); dense-graded surface course mixture, 20 mm (0.8 in.); dense-graded base course mixture, and a 10 mm (0.4 in.); stone matrix asphalt mixture. Two short term aged (140 mm long, 50 mm wide, and 280 mm thick), specimens and two (140 mm long, 50 mm wide, and 260 mm thick) were evaluated for each mixture in the study. These specimens were compacted using a laboratory-scaled roller compactor. The researchers utilized a test setup similar to a simply supported beam to simulate bottom-up cracking (i.e., reflection cracking). In the test setup, the bottom of the specimens were supported on timber blocks, 10-mm metal plates were placed under the HMA mixture; to mimic a concrete layer, and foam was placed below the metal plates; along the specimen span, to simulate a weak foundation. Butler and Gibney [48] performed wheel tracking tests at 25^{o}C (77^{o}F) on all specimens. These wheel tracking test involved the application of a 520 N (116 lb.) load at a frequency of 21 cycles per minute. Based on the results of the testing, Butler and Gibney [48] reported that the dense-graded surface course mixture showed 1.8 times more resistance to reflection cracking than the stone matrix asphalt

mix. The researchers also determined that a 10 mm (0.4 in.) increase in overlay thickness improved the reflection cracking resistance of the overlay by a factor of 1.3.

Yu et al. [49] carried out a study to evaluate the effectiveness of various stress-absorbing interlayers that are used to retard reflection cracking. The researchers evaluated several stress absorbing interlayers which included: a styrene-butadiene-styrene (SBS) modified; sand concrete interlayer; asphalt rubber-sand concrete interlayer; fiberglass-polyester paving mat and stress absorbing membrane interlayer. Yu et al. assessed four specimens containing each of the stress absorbing interlayers considered in the study. These specimens were 29 cm (11.4 in.) long and 7 cm (2.8 in.) wide and consisted of a 2 cm thick concrete layer, 2 cm (0.8 in.) thick, stress absorbing interlayer, and a 4 cm (1.6 in.) thick HMA surface layer. The control specimen consisted of a 4 cm thick concrete layer and a 4 cm (1.6 in.) HMA surface layer. The researchers subjected each test specimen to a dynamic wheel load of 0.7 MPa (101.5 psi) at temperature of 15^{o}C (59^{o}F) and a loading rate of 52 cycles per minute. This was done to simulate the load induced reflection cracking in the test specimen. Based on the testing results, Yu et al. [49] reported that asphalt rubber, sand concreter interlayer performed the best followed by the fiberglass-polyester mat, SBS asphalt-sand concrete and SAMI interlayer. The researchers also reported that adequate bonding conditions should be emphasized during field construction since deboning occurred between the base and stress-absorbing interlayers.

Montestruque et al. [50] performed a study which compared the reflection cracking performance of conventional HMA overlays to that of overlays which contained a stress relieving asphalt interlayer. The researchers evaluated three overlay systems in

the study. The first overlay system consisted of a 60 mm conventional asphalt mixture overlay. The second overlay system consisted of a 40 mm stone matrix asphalt layer overlaid on a 20 mm crack relief asphalt layer. The third overlay system also contained a 40 mm stone matrix asphalt layer overlaid on a 20 mm crack relief asphalt layer. However, a polyester geogrid was placed between the SMA and crack relief layer in the third overlay system. All overlay systems were supported by a jointed, PCC layer and a thin rubber layer. Montestruque et al. [50] subjected all overlay systems to wheel reflective cracking testing which involved the application of low shear displacement (δc) or vertical movement ($\delta c = 30x10^{-3}$ mm), medium shear displacement ($\delta c = 100x10^{-3}$ mm) and high shear displacement ($\delta c = 500x10^{-3}$ mm). Based on the results of the study, Montestruque et al. [50] reported that the 40 mm stone matrix asphalt plus 20 mm crack relief asphalt layer, proved to be two time more efficient than the 60 mm conventional overlay in terms of reducing the rate of reflection cracking. The researchers also determined that the addition of the polyester geogrid between the SMA and stress relief layer, increased the number of cycles by more than 3 times for medium and high displacements.

A plethora of other laboratory studies [50] – [53] have also compared the effectiveness of various types of stress relieving interlayers in mitigating reflection cracking in HMA overlays. These laboratory studies have analyzed the benefit of using, asphalt membranes, stress absorbing interlayers (SAMI), geogrids and soft asphalt in HMA overlays. A summary of the key findings reported in these studies is provided in Table 2.

Table 2

Summary of Key Findings of Previous Lab Studies on HMA Overlays

Author	**Key Findings**
Dumas and Vecoven [47]	• Paving fabrics such as geosynthetics delay the crack initiation time of HMA overlays (i.e. geosynthetics improve fatigue cracking performance of HMA overlays) • Binder rich HMA mixtures reduces the rate of crack propagation in HMA overlays when used in composite overlays (i.e., stress relieving interlayers improve reflection cracking performance of HMA overlays)
Montestruque et al. [48]	• Fatigue life of HMA overlay reinforced with geogrid .was 6 times higher than HMA overlays with no reinforcement
Bennert [49]	• Dense-graded HMA mixtures are not capable of resisting joint/crack movement greater than 0.25 mm (0.01 in.). • Reflective crack relief interlayer should be placed under asphalt overlay if cracks have movements greater than 0.25 mm 0.01 in.
Blankenship et al. [50]	• Reflective crack interlayer can reduce crack propagation rate of HMA overlays by 50% if they meet required laboratory performance criteria.

Field studies performed on HMA overlays. Bennert and Maher [54] conducted a study which evaluated the impact of a reflection crack relief interlayer on the performance of composite pavements in New Jersey. The researchers monitored the field performance of three sections of Route 34 in New Jersey between mileposts 0.3 and 7.6. The pavement system in this two-lane highway segment assessed consisted of a composite pavement structure which was supported by an uncrushed gravel base layer and silty, sand subgrade. The concrete pavement layer was 228.6 mm (9 in.) thick and it contained 12.2 m (40 ft.) slabs separated by 31.75 mm (1.25 in.) dowel bars and a 19 mm (0.75 in.) expansion joint. The HMA overlay in Section 1 of Route 34 consisted of a 25 mm (1 in.) reflection crack relief interlayer (RCRI) mixture overlaid by a 50 mm (2 in.)

12.5-Superpave mixture and 38.1 mm (1.5 in.) 9.5-Superpave mixture (NJDOT 9.5H76) respectively. The overlay on Section 2 consisted of a 76.2 mm (3 in.) 12.5-Superpave mixture overlaid by a 38.1 (1.5 in.) 9.5-Superpave mixture. The overlay on Section 3 consisted of a 25 mm (1 in.) RCRI mixture overlaid by a 50 mm (2 in.) 12.5-Superpave mixture and 38.1 mm (1.5 in.) 9.5-Superpave mixture (NJDOT 9.5M64) respectively. All highway sections were subjected to an average daily traffic (ADT) of 8,840 vehicles which consisted of 91.6 % automobiles, 2.7% light trucks, and 5.7 % heavy trucks. The researchers conducted visual distress surveys and performed falling weight deflectometer tests all sections. Based on the results of the forensic testing Bennert and Maher [54] determined that Section 1 had the highest average load transfer efficiency while Section 2 and 3 had a similar load transfer efficiency. The researchers also found that 16.4% of the transverse cracks reflected through the overlay on Section 1; 9% of the transverse cracks reflected through the overlay on Section 2; and 2% of the transverse cracks reflected through the overlay on Section 3.

Bennert [20] carried-out a study to compare the field reflection cracking performance of HMA overlays with a crack relief interlayer and HMA overlays produced with a flexible binder. The overlays were constructed on the two southbound lanes of Route 202 between mileposts 13.4 and 17.03. A total of three overlays were evaluated in the study. These overlays were constructed on four different segment of Route 202. The overlay on Test Section 1 consisted of a 50 mm (2 in.) layer of 12.5- Superpave mixture (NJDOT 12.5H76) overlaid by a 2 in. layer of 12.5-Superpave (NJDOT 12.5M64) mixture. The overlay on Test Section 2 consisted of a 76.2 mm (3 in.) layer of 12.5-Superpave (12.5H76) overlaid on a 25.4 mm (1 in.) layer of RCRI mixture. The overlay

on Test Section 3 consisted of a 76.2 mm (3 in.) layer of 12.5-Superpave (12.5H76+) overlaid on a 25.4 mm (1 in.) layer of RCRI mixture. The 12.5-Superpave (12.5H76+) mixture in Test Section 3 was produced using a proprietary, fatigue resistant, flexible binder. Test Section 4 consisted of a 50 mm (2 in.) layer of 12.5- Superpave mixture (NJDOT 12.5H76+) overlaid by a 2 in. layer of 12.5-Superpave (NJDOT 12.5M64+) mixture. The highway segments were subjected to an ADT of 10,178 vehicles which consisted of 94.5 % automobiles, 1.9 % light trucks, and 3.6 % heavy trucks. The researchers conducted falling weight deflectometer tests and visual distress surveys on all sections over a three year period. Based on the results of the study, Bennert [20] determined that the Test Sections 1, 2, and 3 had a similar load transfer efficiency while Test Section 4 had the worst load transfer efficiency (i.e., 69.8%). The researcher also reported that no transverse (i.e. reflection) cracking was observed on all test sections during the study period.

Kim et al. [55] performed a field study which evaluated the reflection cracking performance of HMA overlays which contained conventional asphalt mixtures and premium overlay mixtures respectively. The conducted field distress surveys on six different pavement sections constructed on three different highways: Illinois 29, Illinois 130, and US 136. The supporting structure section on Illinois 29 consisted of a 50 mm (2 in.) thick existing HMA overlay overlaid on a 250 mm (10 in.) thick jointed reinforced concrete pavement (JRCP). A 38 mm (1.5 in.) polymer modified HMA overlay was placed on one segment of the highway and a (38 mm (1.5 in.) conventional HMA overlay was placed on the other segment of the highway. A fabric interlayer was placed over the segment which contained the conventional mixture and a 19 mm (0.75 in) conventional

leveling course was placed over both highway segments. The supporting structure of the highway segment on Illinois 130 consisted of a 200 mm (8 in.) thick JRCP and a 50 mm (2 in.) thick existing overlay. The overlay on the southbound lane of the highway consisted of a 38 mm (1.5 in.) thick, 9.5 mm Superpave mixture overlaid on 19-mm (0.75 in) thick layer of a 4.75 NMAS, sand mix leveling binder course. The overlay on the northbound lane consisted of a 38 mm (1.5 in.) thick, 9.5 mm Superpave mixture overlaid on 19-mm (0.75 in) thick layer of sand mix leveling binder course. The supporting structure of the highway segment on US 136 consisted of a 50 mm (2 in.) existing HMA overlay overlaid on a 9 m (30 ft.) joint concrete pavement (JCP) layer.

Two types of overlays were utilized in the test segment. The first overlay consisted of a 38 mm (1.5 in.) thick, 9.5 mm Superpave conventional mixture overlaid on a 25-mm (0.5 in) thick sand anti-fracture layer. The second overlay consisted of a 38 mm (1.5 in.) thick, 9.5 mm Superpave conventional mixture overlaid on a 25-mm (0.5 in) thick leveling binder course layer. The test sections on Illinois 29, Illinois 130 and US 136 were subjected to 2310 equivalent single axle loads (ESALs), 358 ESALs, and 334 ESALs, respectively. Based on the results of the field distress surveys, the researchers concluded that the HMA overlays which contained interlays (i.e. woven fabric and sand mix crack relief interlayers) generally underwent less reflection cracking than convention overlays.

In addition to the previously outlined studies, many other studies [56] – [59] have assessed the relative field performance of composite pavement systems that contain stress reliving interlayers between the PCC base layer and HMA overlay. The key findings of some of these studies are presented in Table 3.

Table 3

Summary of Key Findings of Previous Field Studies on HMA Overlays

Author	**Key Findings**
Carpenter [56]	• Optimal HMA overlay design to mitigate reflection cracking is a composite overlay with a thin stress reliving interlay. • Thin stress relieving layer should have soft binder with low viscosity and low modulus of elasticity • Surface course layer should contain has soft binder with high modulus of elasticity. • Composite overlay arrangement will accelerate reflection crack initiation (fatigue cracking) but stress relieving layer will slow down reflection crack propagation.
Bennert [57]	• A phenomenon called "crack jumping" periodically occurs in composite overlays in which reflection cracking does not initiate in the stress relieving layer but does so at the bottom of the surface course HMA overlay mixture. • Crack jumping reduces fatigue cracking and reflection cracking resistance of HMA overlays.
Makowski et al. [58]	• Field cores obtained from highway test locations indicated that interlayers did not crack (i.e. remained intact) when transverse cracking was observed in the surface layer. • Intact layer which was compacted to a lower air void content protected pavement system from moisture infiltration.

Chapter 3

Materials Description & Laboratory Experimental Plan

This chapter provides a detailed description of the four specialty, New Jersey HMA mixtures considered in this study. The chapter also summarizes the testing matrix and laboratory tests that were utilized to assess the stiffness characteristics, fatigue cracking, reflection cracking, and rutting performance of laboratory-compacted, specimens of the four specialty, HMA mixtures. Additionally, the chapter presents the laboratory evaluation plan that was employed to assess the laboratory cracking and rutting performance of field-extracted, specimens (i.e., field cores) of the specialty and composite HMA overlays considered in this study.

Materials Description

A total of four, plant-produced, HMA mixtures were evaluated in this study. These mixtures included: a 9.5 ME mixture; stone matrix asphalt mixture; NJ high performance thin overlay mixture; and a binder rich intermediate course mixture. All mixtures consisted of virgin aggregates only. That is, no mixture contained reclaimed asphalt pavement (RAP) aggregates. A discussion of the aggregate gradation, volumetric properties (i.e., air void content), binder type and binder content of each mixture is presented in the following subsections.

9.5ME Superpave mixture. The 9.5 ME Superpave mixture; hereinafter referred to as 9.5-SP, was a conventional, HMA mixture that is typically used in the surface course of flexible and composite pavements in New Jersey (Figure 11) [60]. Therefore, the 9.5-SP mixture was utilized as the control mixture in this study. The 9.5-SP mixture

was prepared using standard Superpave design procedures and volumetric requirements for HMA mixtures. This implied that the mixture was designed with a dense aggregate gradation which fell within the specified control points as shown in Figure 12. The 9.5-SP mixture consisted of: 35.1% coarse aggregates by mass; (i.e., aggregates larger than 4.76 mm (0.187 in.); 64.6% fine aggregates; (i.e., aggregates larger than 0.075 mm (0.003 in.) but smaller than 4.76 mm (0.187 in.); and 0.3% dust or mineral filler; (i.e., aggregates smaller than 0.075 mm (0.003 in.). The nominal maximum aggregate size of the mixture was 9.5 mm (0.37 in.) and a PG 76-22 binder was utilized to produce the mixture. The binder content of the 9.5-SP mixture was 5.7%. The target performance air void content of the mixture was 7.0 ± 0.5%. No RAP was used in the 9.5-SP, as opposed to the common practice in NJ for this mixture. This was done to minimize variability and ensure optimal cracking and rutting performance.

Figure 11. 9.5-SP control HMA mixture evaluated in this study.

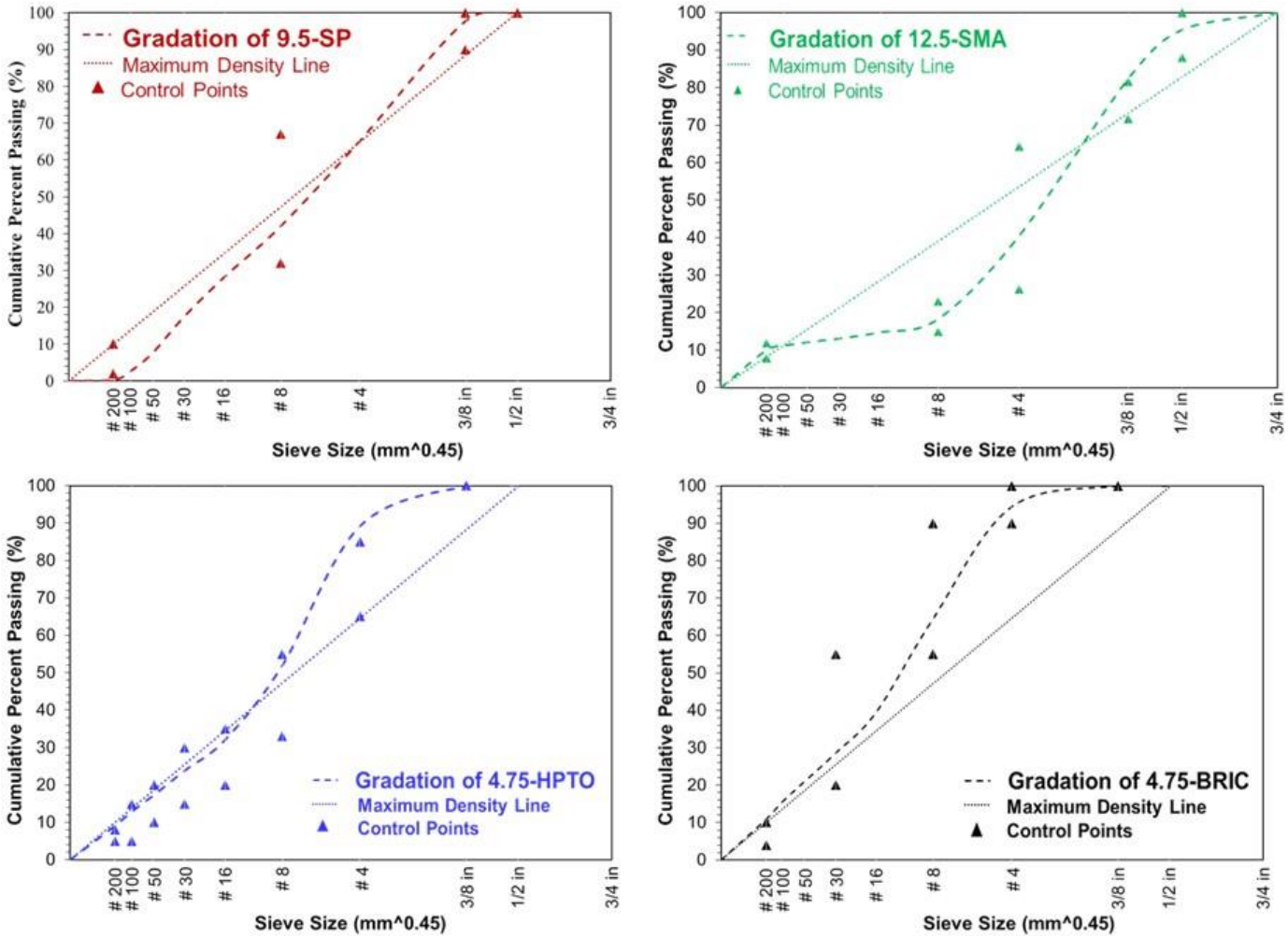

Figure 12. Gradation of the four specialty New Jersey mixtures.

Stone matrix asphalt mixture. The stone matrix asphalt mixture (i.e., 12.5-SMA) evaluated in this study, was a rut resistant, conventional, HMA mixture that is primarily used in surface courses in New Jersey (Figure 13) [61]. The mixture was gap graded: which, implied that it contained a small proportion of intermediate size aggregates (Figure 12). The 12.5-SMA mixture was intentionally designed with a low proportion of intermediate size aggregates to ensure that stone-on-stone contact was maintained between the coarse aggregates in the mixture. This stone-on-stone contact facilitated greater load transfer efficiency between the coarse aggregates and enhanced the mixture's overall resistance to permanent deformation [62].

Figure 13. 12.5-SMA mixture evaluated in this study.

The aggregate gradation of the 12.5-SMA mixture consisted of 59.5% coarse aggregates by mass, 30.4 % fine aggregates, and 10.1% dust or mineral filler (Figure 12). The NMAS of the stone matrix asphalt mixture was 12.5 mm (0.49 in.). The breakpoint sieve size (i.e., finest sieve size to retain at least 10%) of the mixture was 2.36 mm (No. 8

sieve). The type of binder used in the mixture was a polymer-modified, PG 76-22 binder and the binder content was 7.0%. The target performance air void content of the 12.5-SMA mixture was 7.0 ± 0.5%.

New Jersey high performance thin overlay mixture. The New Jersey high performance thin overlay mixture; hereinafter referred to as 4.75-HPTO, was an unconventional, Superpave mixture (Figure 14). This mixture is commonly utilized in New Jersey as a rut resistant, durable, thin-lift surface course for pavement preservation and maintenance applications. It is also used as a superior leveling course when extended staging time is expected for pavement construction [63]. The 4.75-HPTO mixture had a dense gradation (Figure 12). Based on the Superpave definition, the 4.75-HPTO can be described as a finely graded mixture. The NMAS of mixture was 4.75 mm (0.19 in.) and the aggregate gradation was composed of 10.7% coarse aggregate by mass, 80.2% fine aggregate, and 9.1% mineral filler. The 4.75-HPTO mixture was produced using a polymer-modified, PG 76-22 binder. The binder content of the mixture was 7.6% and the target performance air void content was 5.5 ± 0.5%. 3.2%. In New Jersey, 4.75-HPTO mixtures are specifically designed with a higher optimum binder content and finer gradation to improve the mixtures' ability to mitigate cracking. This mixture is also deliberately compacted to a lower air void level than typical Superpave mixtures in order to enhance the mixture's rutting resistance.

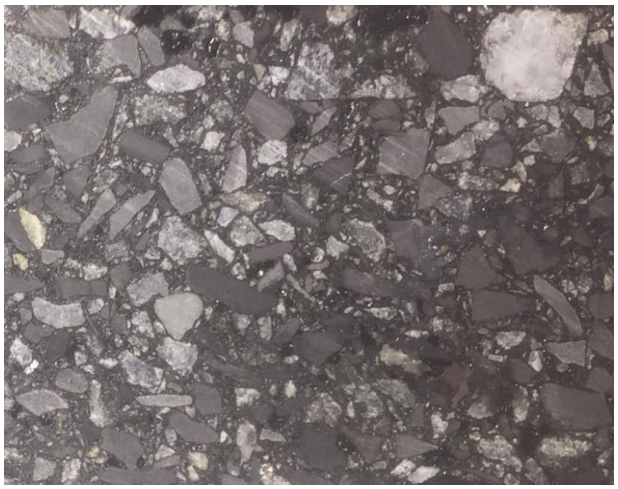

Figure 14. 4.75-HPTO mixture evaluated in this study.

Binder rich intermediate course mixture. The binder rich intermediate course mixture (i.e., 4.75-BRIC) analyzed in this study was an unconventional, HMA mixture (Figure 15). Binder rich intermediate course mixtures are mainly used in New Jersey in crack resistant interlayers between deteriorated, existing and newly, constructed pavements [64]. The 4.75-BRIC mixture assessed in this study was a dense-graded mixture which, had a NMAS of 4.75 mm (0.19 in.). The aggregate gradation of the mixture comprised of 5.5% coarse aggregate by mass, 83.6% fine aggregate, and 10.9% mineral filler. A polymer-modified, PG 70-28 binder was utilized to produce the 4.75-BRIC mixture and the mixture was designed with a 7.4% optimum binder content. The target performance air void of the mixture was 3.5± 0.5%.

The 4.75-BRIC mixture was essentially a finely graded Superpave mixture: intentionally designed with a higher binder content, to allow the mixture to be more crack resistant [64]. The mixture was also compacted to a lower air void content in order to increase its overall stiffness. From Figure 12 it can be observed that the aggregate

gradations of the 4.75-BRIC and 4.75-HPTO were relatively similar. However, the main difference between the mixtures was their respective binder type and performance air void content. A lower binder grade and performance air void content was utilized in the 4.75-BRIC mixture because of its specific application a stress relieving interlayer as opposed to a surface course mixture.

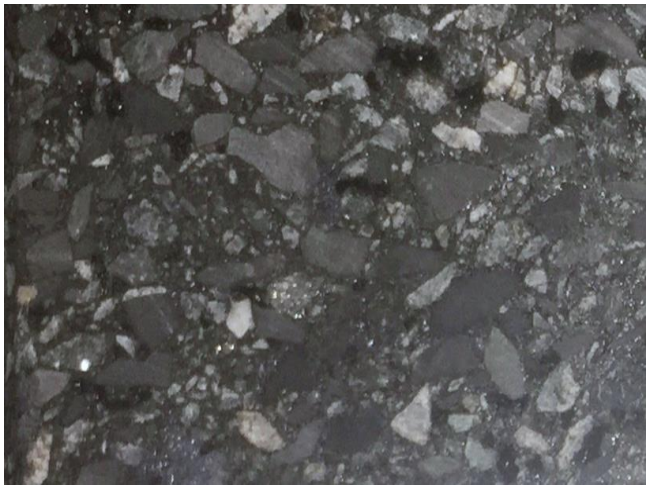

Figure 15. 4.75-BRIC mixture evaluated in this study.

Laboratory Experimental Plan

Laboratory testing was divided into two phases in this study. The first phase of laboratory testing was conducted on laboratory-compacted, specimens of the four specialty, New Jersey mixtures: 9.5-SP, 12.5-SMA, 4.75-HPTO; and 4.75-BRIC. In this phase of laboratory testing: the stiffness characteristics, fatigue cracking performance, reflection cracking performance, and rutting performance of the four specialty mixtures were analyzed. Additionally, the fracture properties of the surface course, HMA mixtures

(i.e., the 9.5-SP, 12.5-SMA, and 4.75-HPTO) were also assessed as part of phase one of the laboratory testing. Phase 1 of laboratory testing

The second phase of laboratory testing was performed on field-compacted specimens extracted from the six full-scale composite pavement sections evaluated during the field testing component of this study. The fatigue cracking performance, reflection cracking performance and rutting performance of these HMA overlay mixtures were analyzed during this phase of laboratory testing. The six HMA overlay mixtures assessed included: the 9.5-SP, 12.5-SMA, 4.75-HPTO mixtures and three composite overlay mixtures which, consisted of the 9.5-SP, 12.5-SMA, 4.75-HPTO mixtures respectively, overlaid on a layer of the 4.75-BRIC mixture. The experimental plan adopted during both phases of laboratory testing is outlined in the following sections.

Laboratory testing: phase 1. The laboratory experimental plan employed during Phase 1 of laboratory testing is shown in Table 4. A total of 60 specimens were evaluated during this phase of laboratory performance testing. The DCM test was used to quantify the stiffness of the 9.5-SP, 12.5-SMA, 4.75-HPTO and 4.75-BRIC mixtures over a range of temperatures and test frequencies. This stiffness quantification allowed conclusions to be drawn about the rutting and cracking potential of the mixtures based on their respective viscoelastic properties.

The uniaxial cyclic fatigue test was carried out in order to assess the fatigue cracking performance of the specialty mixtures. It was essential to evaluate the fatigue performance of the specialty mixtures because HMA overlays are prone to fatigue related damage during the initial stages of repeated loading. This is due to the presence of cracks in the underlying pavement layer which, lead to non-uniform vertical deflections in that

layer during loading. These non-uniform vertical deflections in the underlying layer cause overlays to undergo repeated cycles of flexure (i.e., bending) and relaxation: resulting in micro-crack development [65]. Micro-cracks then coalesce as loading continues and subsequently evolve into macro-cracks (i.e., reflection cracks). It was therefore essential to assess the fatigue performance of the specialty mixtures because the onset of reflection cracking is influenced by their fatigue cracking resistance (i.e., resistant to flexure) [65].

Table 4

Experimental Program Used to Evaluate the Laboratory Performance of the Specialty HMA mixtures during Phase 1 of Laboratory Testing

Laboratory Performance Test	**Number of Specimen**			
	9.5-SP	**12.5-SMA**	**4.75-HPTO**	**4.75-BRIC**
Dynamic Complex Modulus Test	3	3	3	3
Uniaxial Cyclic Test	3	3	3	3
Overlay Test	5	5	5	5
Asphalt Pavement Analyzer Test	4	4	4	4
Total Specimen (per mix)	15	15	15	15
Grand Total	60			

Dynamic complex modulus test. The dynamic complex modulus test was conducted as a prerequisite for the uniaxial cyclic test. That is, the results for the DCM test were essentially utilized as inputs in the uniaxial cyclic fatigue test. The dynamic modulus test was carried out according to AASHTO T378 specifications; without lateral confinement. This is because the uniaxial cyclic fatigue test is typically performed without confinement. The use of no confinement for the DCM test ensured that characteristic, seed moduli values of each mixture were used to determine fingerprint dynamic moduli during the uniaxial cyclic fatigue test. The use of no confinement also

ensured that representative moduli and phase angle values were utilized during subsequent, S-VECD data analyses. Three specimen with a diameter of 38 mm (1.5 in.) and height of 110 mm (4 in.) were evaluated for each mixture. These specimen were cored from gyratory-compacted, cylindrical samples which, had a diameter and height of 150 mm (6 in.) and 180 mm (7 in.), respectively. The dynamic complex modulus tests were conducted at 4, 19, 31, 46, and 58^{o}C (39.2, 66.2, 87.8, 114.8, and 136.4^{o}F) using test frequencies of 25, 10, 1, and 0.1 Hz.

Uniaxial cyclic fatigue ***test.*** The uniaxial cyclic fatigue tests were conducted according to AASHTO TP 133. Three specimens of each specialty mixture were evaluated during the uniaxial cyclic fatigue test. The diameter and height of the uniaxial cyclic fatigue test specimens for all mixtures were 38 mm (1.5 in.) and 110 mm (4 in.), respectively. All specimens were cored from gyratory-compacted, cylindrical samples which, had a diameter and height of 150 mm (6 in.) and 180 mm (7 in.), respectively. The test temperature used for each mixture was defined by Equation 16. Therefore the uniaxial cyclic fatigue test was conducted at 21^{o}C (70^{o}F) for the 9.5-SP. 12.5-SMA, and 4.75-HPTO mixtures while the test temperature used for the 4.75-BRIC mixture was 18^{o}C (64^{o}F).

$$T\ (^{o}C) = \frac{T_H + T_L}{2} - 3 \ \text{ if } T \leq 21^{o}C\text{: else } T = 21^{o}C \qquad (16)$$

Where

T uniaxial cyclic fatigue test temperature, ^{O}C

T_H high temperature performance grade (PG), ^{o}F

T_L low temperature performance grade, ^{o}F

Prior to uniaxial cyclic fatigue testing, fingerprint dynamic moduli tests were conducted at the respective uniaxial cyclic fatigue test temperatures for each mixture; using a frequency of 10 Hz and target strain range of 50 to 70 micro-strains. Cyclic tension tests were then performed on each uniaxial cyclic fatigue test specimen using a peak to peak strain amplitude on the specimens which, ranged from 250 to 500 micro-strains. The peak to peak strain amplitude used for the initial uniaxial cyclic fatigue test on each mixture was based on the range of the dynamic modulus fingerprint values. The subsequent uniaxial cyclic fatigue tests were conducted using strain levels that depended on the number of cycles to failure of the preceding uniaxial cyclic fatigue test specimens. Each uniaxial cyclic fatigue test was terminated when the specimens' phase angle began to decrease.

Overlay test. The overlay tests were conducted according to NJDOT B-10 specifications; a slight variation of the Tex-F-248 specifications. The main difference between the two specifications is specimen mounting process. Sample preparation for the overlay tests entailed two steps: mounting the specimens to the base plates of the overlay tester using 20 g of two-part epoxy and conditioning the specimens in the temperature chamber of the overlay tester at 25^{o}C (77^{o}F) for 1 hour before initiating the test. The overlay tests involved loading the specialty mixture specimens until a 0.6 mm (0.025 in.) displacement was achieved during each test cycle. The termination criterion used for the overlay tests was a 93% reduction of the initial applied load. A total of 20 specimens (i.e., five specimens per HMA overlay mixture) were evaluated during the overlay tests. The thickness, length of width of these specimens were 38 mm, 150 mm, and 76 mm, respectively.

Asphalt pavement analyzer test. The APA tests were conducted according to AASHTO T340 specifications. Four gyratory-compacted, cylindrical specimens of each mixture were evaluated during the APA tests. The diameter and height of each specimen was 150 mm (6 in.) and 76 mm (3 in.), respectively. All APA test specimens were conditioned at 18^{o}C (64^{o}F) for 6 hours and subsequently subjected to 8000 loading cycles of the asphalt pavement analyzer test wheel. During each loading cycle, the test wheel applied a load of 444.8 N (100 lb.) on top of the specimens via a 6.89 kN/m^2 (100 psi) pressurized, rubber hose. The NJDOT specified, rut depth criterion for each mixture was utilized. The rut depth criterion of the 9.5-SP and 12.5-SMA were 5.5 mm (0.22 in.) and 5 mm (0.20 in.), respectively, while that of the 4.75-HPTO and 4.75-BRIC mixtures was 4 mm (0.16 in.).

Phase 1 laboratory testing statistical analysis. Statistical analyses were conducted to quantitatively assess the relative performance of the laboratory compacted, New Jersey HMA mixtures based on their reflection cracking performance and fracture properties. A one-way analysis of variance (ANOVA) was used to test the following null hypotheses: (H_o^1): mean number of number of OT cycles to failure of all mixtures was equal; (H_o^2): mean critical fracture energy of all mixtures was equal; and (H_o^3): mean crack progression rate of all mixtures was equal. This was followed by the Tukey's Honestly Significant Difference (HSD) to identify significant difference in the mean number of OT cycles to failure, critical fracture energy, and crack progression rate between the overlay mixtures at $\alpha = 0.05$. A 95% confidence interval was utilized for all statistical analyses.

***Laboratory testing: phase 1 summary*.** All specimens of the four specialty New Jersey overlay mixtures were prepared using the NJDOT sample air void requirements for performance testing: 7.0 ± 0.5% for 9.5-SP and 12.5-SMA specimens, 5.5 ± 0.5% for 4.75-HPTO specimens, and 3.5 ± 0.5%, for 4.75-BRIC specimens. The overall experimental program utilized in Phase 1 of laboratory testing facilitated a laboratory performance comparison of the specialty New Jersey mixtures considered in the study

Laboratory testing: phase 2. The laboratory experimental program utilized during Phase 2 of laboratory testing is shown in Table 5. A total of 90 specimens were evaluated during the second phase of laboratory performance testing. The bending beam fatigue test was used to assess laboratory fatigue cracking performance of the field-extracted, HMA overlay specimen. This is because the BBF test replicated the fatigue cracking mechanism the overlays experienced during the initial stages of accelerated pavement testing (i.e., flexure) [66]. The overlay test was utilized to evaluate the laboratory reflection cracking performance of the HMA overlay field cores because the test replicated the cracking mechanism in the overlays during the later stages of APT (i.e., after crack initiation) [66]. The asphalt pavement analyzer test was employed to determine the laboratory rutting performance of the field-extracted, HMA overlay mixtures. Statistical analyses were also conducted to quantitatively assess and compare the relative laboratory performance of the field-extracted overlay mixtures.

Table 5

Experimental Program Used to Evaluate the Laboratory Performance of the HMA Overlay Field Cores during Phase 2 of Laboratory Testing

Laboratory Performance Test	**Number of Specimen**					
	9.5-SP	**12.5-SMA**	**4.75-HPTO**	**9.5-SP & 4.75-BRIC**	**12.5-SMA & 4.75-BRIC**	**4.75-HPTO & 4.75-BRIC**
Bending Beam Fatigue Test	6	6	6	6	6	6
Overlay Test	5	5	5	5	5	5
Asphalt Pavement Analyzer Test	4	4	4	4	4	4
Total Specimen (per mix)	15	15	15	15	15	15
Grand Total	90					

Bending beam fatigue test. The bending beam fatigue tests were conducted according to AASHTO T321 specifications. Six beam specimens of each field-extracted HMA overlay mixture were assessed during the BBF tests. The dimensions of the beam specimens were as follows: 380 mm (15 in.) length, 63 mm (2.5 in) width; and 50 mm (2 in.) height. For the composite overlay specimens, the thickness ratio utilized in the field overlays between the 4.75-BRIC mixture and 9.5-SP, 12.5-SMA, and 4.75-HPTO mixtures was maintained. All BBF specimens were conditioned at 25^{o}C (77^{o}F) for 2 hours and subsequently subjected to haversine loading at a constant strain of 725 micro-strain. Haversine loading was utilized for the BBF testing because it replicated the triangular, loading mechanism the HMA overlays experienced during field evaluation. All BBF tests were terminated when there was a 15% reduction in normalized stiffness.

Phase 2 laboratory testing statistical analysis. Three statistical tests were performed: to compare the performance of the field-extracted overlay mixtures; obtained

from the full-scale test sections. In the first statistical test the fatigue cracking performance of the HMA overlays; with a layer 4.75-BRIC, and overlays without a layer of 4.75-BRIC were compared. This statistical test was based on a two-way analysis of variance (ANOVA); with replication. To achieve the objective of this test F-ratios were used to test the following null hypotheses: (H_o^1) - all the means of HMA overlays without 4.75-BRIC are equal; (H_o^2) -all the means of HMA overlays with 4.75-BRIC are equal; (H_o^3) - there are no interactions between HMA overlays without 4.75-BRIC and HMA overlays with 4.75-BRIC. A similar testing procedure was used to compare the reflection cracking and rutting performance of the field extracted HMA overlay mixtures; using the three hypotheses outlined previously. A Bonferroni, test was performed to identify the combination of field-extracted overlay mixtures that showed significant statistical differences. A 95% confidence interval was utilized for all statistical tests.

Laboratory testing: phase 2 summary. The overlay and APA tests performed during Phase 2 of laboratory testing were conducted in using the same sample preparation and test procedures adopted in Phase 1 of laboratory testing. The overall texting matrix utilized during Phase 2 of laboratory testing facilitated the quantification of the fatigue life and laboratory reflection cracking performance of the 9.5-SP, 12.5-SMA, 4.75-HPTO, and composite overlay field cores. This allowed for the relative laboratory cracking performance of the field-extracted, overlay mixtures to be directly compared. The testing matrix also facilitated the laboratory performance comparison between the specialty overlay mixtures and the composite overlay mixtures.

Chapter 4

Laboratory Testing Results

This chapter presents the results of the laboratory testing that was conducted during Phases 1 and 2 of laboratory testing. During Phase 1 of laboratory testing the laboratory fatigue cracking, reflection cracking and rutting performance of four specialty New Jersey mixtures were assessed. During Phase 2 of laboratory testing the cracking and rutting performance of field-extracted specimens of the three specialty and composite overlay mixtures assessed during field testing were evaluated. Interpretation of all laboratory testing results is provided in this chapter.

Laboratory Testing: Phase 1 Results

This section presents the results of the mixture performance testing that was conducted during phase 1 of laboratory testing. In this phase of laboratory testing the performance of the 9.5-SP, 12.5-SMA, 4.75-HPTO and 4.75-BRIC specialty New Jersey mixtures was assessed. Phase 1 of laboratory testing allowed for performance comparisons to be made between the four specialty New Jersey mixtures. A discussion and interpretation of the results obtained during Phase 1 of laboratory testing is outlined in following sections.

Dynamic complex modulus tests results. The dynamic complex modulus test was conducted as a prerequisite for the uniaxial cyclic fatigue test; as mentioned previously. That is, the results for the DCM test were utilized as inputs in the uniaxial cyclic fatigue test. Dynamic modulus master curves of the laboratory-compacted specialty New Jersey mixtures (i.e., 9.5-SP, 12.5-SMA, 4.75-HPTO and 4.75-BRIC

mixtures) were developed by shifting measured dynamic modulus data using nonlinear optimization. The nonlinear optimization process involved: computing the dynamic modulus shift factors simultaneously (Equation 17) and fitting the shifted dynamic modulus data using the sigmoidal function presented in (Equation 18). The FlexMAT software was used to carry-out this process. The FlexMAT software is a Microsoft Excel based analysis tool; developed by the Federal Highway Administration (FHWA) to: characterize the dynamic modulus of HMA mixtures; determine master curve coefficients and time-temperature shift factors; and analyze cyclic fatigue test results. The accuracy of the predicted dynamic modulus values (i.e., sigmoidal function prediction) was measured by the sum of the squared differences between the predicted and measured moduli values (i.e., error sum of squares (SSE)). The reference temperature used to construct the dynamic modulus master curves of the asphalt overlay mixtures was 21°C (70°F).

$$\alpha\,(T_i) = a_1T^2 + a_2T + a_1T_{ref}^2 - a_3T_{ref} \qquad (17)$$

$$\log|E^*| = \delta + \frac{\log[\mathrm{Max}|E^*|] - \delta}{1 + e^{\beta+\gamma\log f_r}}$$

$$\mathrm{Max}\,|E^*| = \left[\frac{\left(20+435{,}000\frac{VFA}{VMA}\right)^{0.58}}{\left(650+435{,}000\frac{VFA}{VMA}\right)^{0.58}}\left[29{,}000{,}000\left(\frac{1-VMA}{100}\right) + \frac{3{,}000{,}000*VMA*VFA}{1000} + \left(1 - \frac{\left(20+435{,}000\frac{VFA}{VMA}\right)^{0.58}}{\left(650+435{,}000\frac{VFA}{VMA}\right)^{0.58}}\right)\right]\right] \qquad (18)$$

Where: -

$\alpha\,(T_i)$	Shift factor for a given temperature
T	Temperature at which dynamic modulus is measured
T_{ref}	Reference temperature

a_1, a_2 and a_3	Shift factor parameters
$\lvert E^* \rvert$	Dynamic modulus
f_R	Reduced frequency
δ	Minimum value of $\lvert E^* \rvert$
Max $\lvert E^* \rvert$	Maximum limiting value of $\lvert E^* \rvert$
β and γ	Parameter that describe the shape of the sigmoidal function
VMA	Voids is mineral aggregate
VFA	Percentage of voids filled with asphalt in a compacted HMA sample

The dynamic modulus master curves of the four New Jersey mixtures evaluated in this phase of laboratory testing are illustrated in Figure 16.The shift factor parameters, dynamic modulus master curve parameters, and mean absolute percent error between the predicted and measured dynamic modulus values of the specialty mixtures are presented in Table 6. As can be seen from Figure 16, the dynamic modulus values of the 4.75-HPTO and 12.5-SMA mixtures had an almost identical shape and generally were higher than that of 9.5-SP control mixture. This result was expected despite the fact that the 9.5-SP contained no RAP aggregates. This is because the 4.75-BRIC mixture was compacted to a lower performance air void content than that of the 9.5-SP (i.e., 5.5% compared to 7%) while the 12.5-SMA contained a larger proportion of coarse aggregate sizes in comparison to the 9.5-SP mixture. Additionally, it can be observed from Figure 16 that the dynamic modulus of the 4.75-BRIC mixture was generally lower than that of the 9.5-SP mixture. Hence, the overall stiffness of the 4.75-BRIC mixture was lower than that of the control mixture; and all other mixtures. This trend was also expected because the

4.75- BRIC contained a softer binder (PG 70-28) than the other mixtures which contained PG 76-22 binder.

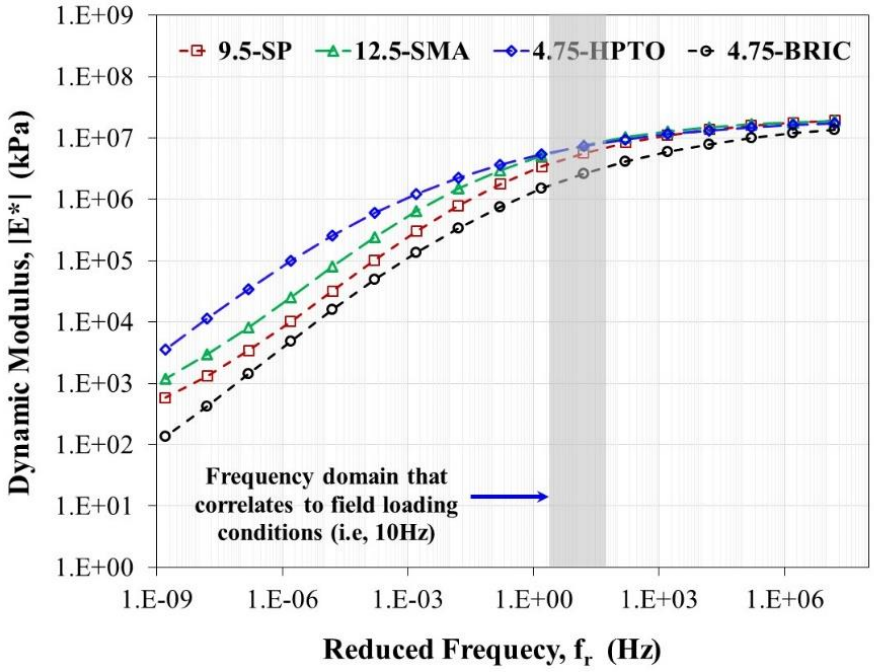

Figure 16. Fitted dynamic modulus master curves of specialty New Jersey mixtures.

Table 6

Dynamic Modulus Master Curve Parameters of the Specialty New Jersey HMA Mixtures

Mixture Type	Shift Factor Parameters			Dynamic Modulus Parameters			Error Sum (SSE)
	a_1	a_2	a_3	δ	β	γ	
9.5-SP	-0.0024	0.0489	0.0473	1.661	-1.702	-0.355	5.6
12.5-SMA	-0.0013	-0.0490	1.6005	1.817	-1.976	-0.363	1.2
4.75-HPTO	-0.0018	-0.0398	1.6330	0.2546	-2.3358	-0.2809	1.8
4.75-BRIC	-0.0010	-0.0447	1.3877	-0.6256	-1.7025	-0.2661	10.3

Based on the dynamic modulus master curves inferences were made about the cracking susceptibility of the asphalt mixtures at intermediate temperatures. This is because a frequency and temperature combination of 10 Hz and of 21^{o}C, typically correlates to field loading conditions of asphalt mixtures [64]. Therefore, the overall stiffness and shape (i.e., slope) of the dynamic modulus master curve of the mixtures at 10 Hz was used to gain some insight about the relative fatigue and reflection cracking susceptibility of the mixtures. Since the stiffness of the 4.75-BRIC and 12.5-SMA were higher than that of the 9.5-SP mixture (particularly in the 10 Hz frequency domain), it was determined that the 4.75-HPTO and 12.5-SMA mixture may have a higher fatigue cracking susceptibility than the less stiff 9.5-SP mixture. Additionally, since the slope of the dynamic modulus master curve of the 4.75-BRIC mixture was generally steeper than that of the 9.5-SP mixture (especially in the 10 Hz frequency domain) it was determined that the 4.75-BRIC had a higher sensitivity to an increase in loading rate. Hence, the 4.75-BRIC may be more susceptible to fatigue cracking than the 9.5-SP mixture. The dynamic modulus values of all mixtures were almost identical at high loading frequencies. Therefore, it was determined that the low temperature cracking performance of all mixtures may be similar because the high loading frequencies generally coincide with low temperature cracking performance.

The relative rutting potential of the specialty mixtures was also interpreted from the dynamic modulus master curves. This is due to the fact that the dynamic modulus of mixtures at low frequencies generally correlates to mixture stiffness at high temperature (i.e., rutting performance). From Figure 16 it can be observed that the stiffness of the 4.75-BRIC and 12.5-SMA were higher than that of the 9.5-SP mixture at low test

frequencies while the 4.75-BRIC had a lower stiffness than the control mixture at low test frequencies. These results implied that the 4.75-BRIC may have the highest susceptibility to rutting, followed by the 9.5-SP, 12.5-SMA, and 4.75-HPTO mixtures, respectively. This result was expected because the 4.75-BRIC had the highest binder content of all the mixtures while the 4.75-HPTO and 12.5-SMA mixtures were specifically designed to be rut resistant.

Uniaxial cyclic fatigue tests results. The uniaxial cyclic fatigue test was performed in order to assess the fatigue cracking resistance of the four laboratory-compacted, specialty New Jersey mixtures evaluated during phase 1 of laboratory testing. Figure 17 presents analyzed results (i.e., damage characteristic curves) obtained from the uniaxial cyclic fatigue tests that were performed on the four specialty New Jersey HMA mixtures. The damage characteristic curves quantified the reduction in mixture stiffness as fatigue damage increased in the mixtures due to repeated cycles of tension-compression loading. The damage characteristic curve of all mixtures followed a similar trend. That is, the pseudostiffness of all the mixtures started at a value of 1 (when no damage was applied) and subsequently decreased as damage accumulated in the mixture during cyclic loading. A logarithmic decay function is typically fitted to the data set to evaluate the HMA mixture damage characteristic curves and damage accumulation [36, 37, 63]. It can be observed from Figure 17 that the values of the 9.5-SP damage characteristic curve were generally higher than that of the 12.5-SMA, 4.75-HPTO and 4.75-BRIC mixtures, respectively, as damage accumulated in the mixtures. However, when after a damage value of 48,000 was reached, the values of the 9.5-SP damage characteristic was lower than that of the 12.5-SMA and 4.75-HPTO mixtures,

respectively. These observations; along with the results of the DCM tests, implied that the 12.5-SMA and 4.75-HPTO may be more crack resistant after experiencing damage compared to the 9.5-SP mix. It can also be observed from Figure 17 that generally mixtures with higher stiffness (i.e. 9.5-SP) typically appeared higher on the (C vs S) plot than those with a lower stiffness (i.e. 4.75-BRIC). It is noted that other studies [36] and [37] reported a similar trend with respect to mixture stiffness and position of mixture damage characteristic curves on the (C vs S) plot.

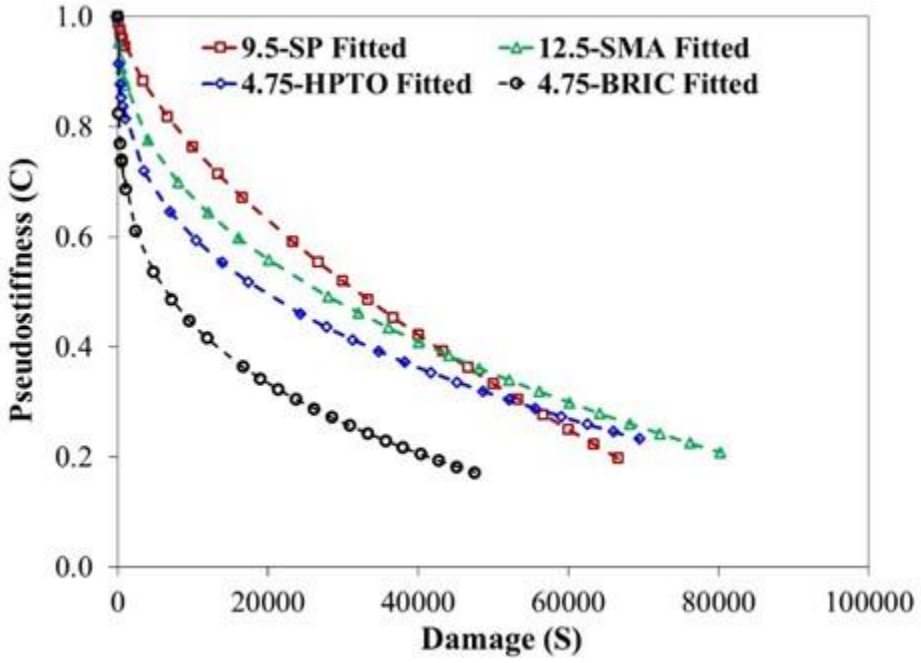

Figure 17. Damage characteristic curves obtained from the uniaxial cyclic fatigue tests performed on the specialty New Jersey HMA mixtures.

Table 7 summarizes the results of the uniaxial axial fatigue test parameters computed from the damage characteristics curves of the mixtures evaluated in the study. These parameters include: the C_{11} and C_{12} damage characteristic curve model

coefficients, the D^R failure criterion, and the apparent damage capacity (S_{app}). Based on the damage characteristic curves presented in Figure 17 and damage characteristic curve model coefficients presented in Table 7, it can be seen that the rate of reduction in pseudostiffness of the mixtures was strongly influenced by the C_{11} model coefficient. This is because the damage characteristic curve of the 9.5-SP mixture had the lowest C_{11} coefficient (i.e., 0.0006) and the lowest rate of reduction in pseudostiffness. Similarly the damage characteristic curve of the 12.5-SMA had the next lowest rate of reduction in pseudostiffness and next lowest C_{11} coefficient (i.e., 0.007). On the other hand, the damage characteristic curve of the 4.75-BRIC had the highest rate of reduction and the highest C_{11} model coefficient (i.e., 0.055).

Table 7

Uniaxial Cyclic Fatigue Test Parameters Computed from Damage Characteristic Curve of the Specialty New Jersey Mixtures

Mixture Type	**C vs S Curve Coefficients**		**Average D^R**	**R^2**	**Standard Deviation**	**Apparent Damage Capacity (S_{app})**
	C_{11}	**C_{12}**				
9.5-SP	0.0006	0.36	0.94	0.059	0.94	7.4
12.5-SMA	0.007	0.53	0.97	0.050	0.97	9.8
4.75-HPTO	0.018	0.47	1.00	0.074	1.00	6.3
4.75-BRIC	0.055	0.64	1.00	0.027	1.00	15.3

The D^R failure criterion parameter represents the average reduction in mixture pseudostiffness during each loading cycle; based on its definition. From Table 7 it can be observed that the average D^R failure criterion value obtained for the 9.5-SP, 12.5-SMA,

4.75-HPTO, and 4.75-BRIC mixtures was 0.36, 0.53, 0.47, and 0.64, respectively. These results suggested that the 9.5-SP had the lowest average reduction in pseudostiffness per unit cycle followed by the 4.75-HPTO and 12.5-SMA mixtures. The results also indicated that the 4.75-BRIC mixture had the highest average reduction in pseudostiffness per unit cycle. The results obtained for the D^R failure criterion implied that damage accumulation occurred at a more rapid rate in the 4.75-BRIC mixture followed by the 12.5-SMA, 4.75-HPTO and 9.5-SP mixtures. It is noted that; with the exception of the 12.5-SMA ranking, the D^R failure criterion results generally coincided with the damage characteristic curves presented in Figure 17. Since the D^R failure criterion is also indicative of a mixture's capacity to failure (i.e. can accumulate greater reduction in pseudostiffness before failure), the average D^R failure criterion values suggested that the 4.75-BRIC mixture had the highest capacity to failure followed by the 12.5-SMA, 4.75-HPTO and 9.5-SP mixtures respectively. These results were generally in agreement with other studies [23, 24] which, found that softer, polymer modified binders and smaller NMAS increased D^R values. It should be noted, that higher capacity to failure does not necessarily reflect good fatigue cracking resistance because mixtures the mixture may reach the failure criterion faster than other mixes (even with a greater D^R) as was seen in the case with the 4.75-BRIC (Figure 17) and in literature [36].

The S_{app} cracking index of the 9.5-SP, 12.5-SMA, 4.75-HPTO, and 4.75-BRIC were 7.4, 9.8, 6.3, and 15.3, respectively. Based on its definition, the Sapp results indicated that the 4.75-BRIC mixture had the highest resistance to fatigue cracking followed by the 12.5-SMA, 9.5-SP and 4.75-HPTO. This is because higher S_{app} values represented higher resistance to fatigue cracking [36]. Since the 4.75-BRIC and 12.5-

SMA had a higher binder content than the 9.5-SP, and the 4.75-BRIC contained a softer, polymer modified binder, it was determined that the general trend with respect to the S_{app} coincided with the findings of another study [63]. This study determined that S_{app} values increased as mixture binder content increased and lower binder grade (i.e., softer binder) was used to produce the mixture. It should be noted however, the S_{app} results contradicted the observed trends with respect to the damage characteristic curves of the mixtures and the average D^R failure criterion value of the mixtures.

Overlay tests results. The overlay tests were conducted to assess the reflection cracking performance of the four specialty New Jersey mixtures evaluated during Phase 1 of laboratory testing. The average number of OT cycles to failure for all mixtures is presented in Figure 18a. As illustrated in this figure, the average number of OT cycles to failure obtained for the 9.5-SP, 12.5-SMA, 4.75-HPTO, and 4.75-BRIC were 783, 217, 760, and 1880 cycles, respectively. These results suggested that 9.5-SP and 4.75-HPTO mixtures had a similar resistance to reflective cracking. The average number OT cycles to failure results also indicated that the 4.75-BRIC mixture had a higher resistance to reflective cracking than the control mixture while the 12.5-SMA was more susceptible to reflective cracking than the 9.5-SP mixture. The trend with respect to the relative reflection cracking susceptibility of the 4.75-BRIC and 9.5-SP mixtures was expected because the 4.75-BRIC mixture was specifically designed with a fine gradation, low air void content, and softer, polymer modified binder in order to enhance its overall cracking resistance and facilitate its role as an interlayer. Previous studies [31, 33] have reported that mixtures designed with softer, binder, high binder content, and finer aggregate

gradation tend to be more resistant to macro-crack propagation than mixtures that contain stiffer binder, lower binder content, and coarser gradation.

The trend in regard to the relative reflection cracking performance of the control (i.e. 9.5-SP), 4.75-HPTO and 12.5-SMA mixtures was not expected. This is because 4.75-HPTO mixtures are intentionally designed to resist cracking and 12.5-SMA has been reported to have better cracking performance than 9.5-SP mixtures [34, 35]. However, it should be noted that the 9.5-SP mixture considered in this study contained only virgin aggregates while the typical 9.5-SP (i.e. Superpave) mixtures in New Jersey can contain up to 15% RAP aggregates by total mixture weight. Therefore, the reflection cracking results based on the average number of OT cycles to failure was thought to be reasonable since the control mixture was expected to perform better than usual New Jersey Superpave mixtures.

Investigation of mixture fracture properties. The fracture properties of the four specialty New Jersey mixtures were analyzed to further investigate their relative reflection cracking susceptibility. These fracture properties included: critical fracture energy (Gc) and the crack progression rate. The G_C and crack progression rate accounted for the asphalt mixtures' behavior during the two stages of the OT test: crack initiation and crack propagation. The G_C characterized the toughness of the HMA mixtures (i.e., their resistance to macro-crack initiation). The crack progression rate quantified the asphalt mixtures' ability to withstand the crack driving force and attenuate the rate of macro-crack propagation, after a crack is initiated [68].

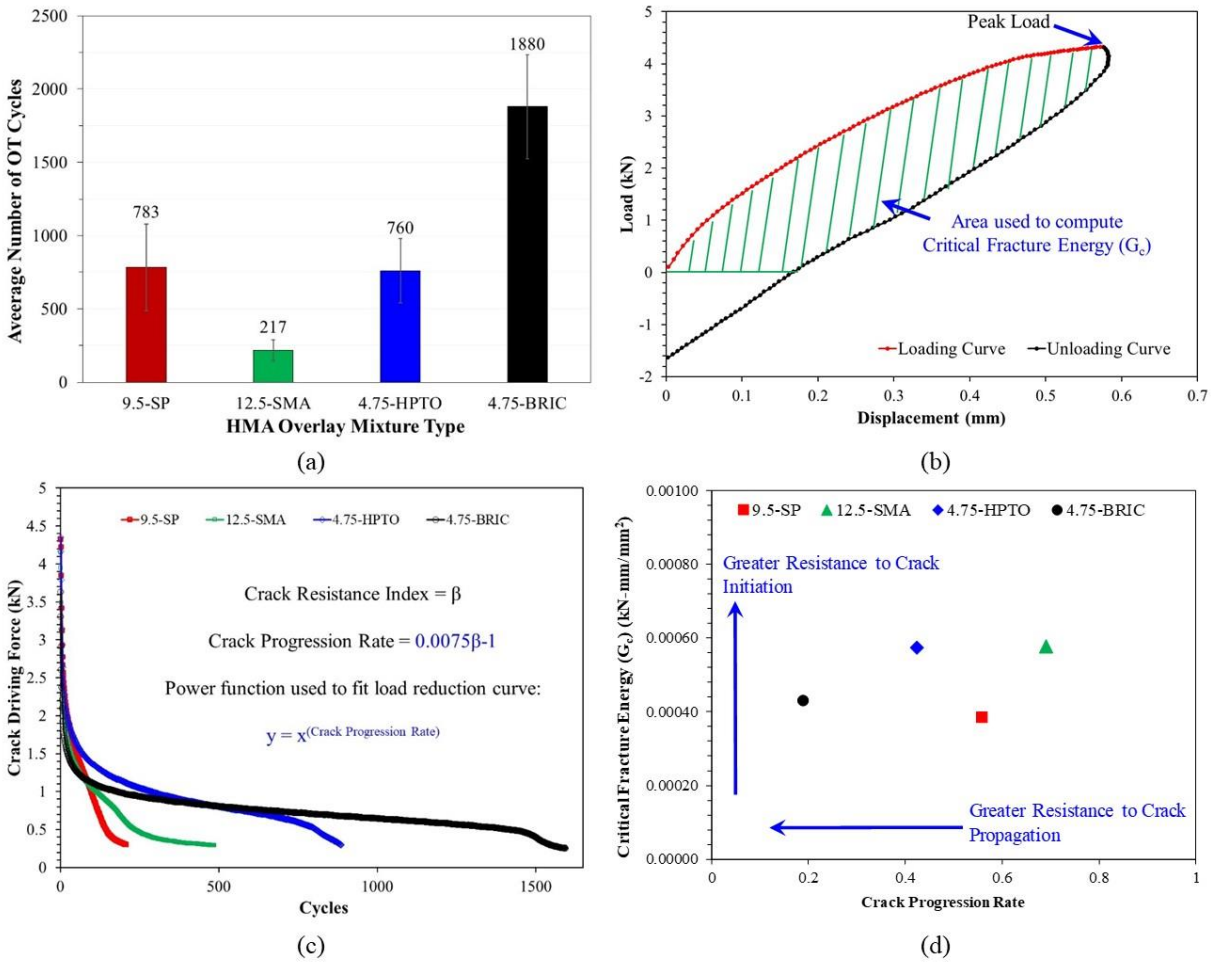

Figure 18. Overlay test results of specialty New Jersey mixtures: (a) average number of cycles to failure (b) critical fracture energy computation (c) crack resistance index and crack progression rate calculation (d) interaction plot of critical fracture energy and crack progression rate.

The area under the loading curve of the hysteresis loop of the initial OT loading cycle was used to determine the G_C. Figure 18b illustrates a hysteresis loop that is representative of those obtained for the asphalt mixtures evaluated in this study. The area used to compute G_C spanned up until the displacement related to the peak load as shown in Figure 18b. The crack progression rate of the asphalt mixtures was calculated from the crack resistance index parameter, as demonstrated in Figure 18c. The crack resistance index of the HMA mixtures was determined by performing a least squares fit of the load reduction curve using a power function. Figure 18c presents a representative load reduction curve for each of the mixtures considered in phase 1 of laboratory testing. The power function used to fit the load reduction curves is also indicated in Figure 18c.

The average G_C, and crack progression rates obtained for the 9.5-SP, 12.5-SMA, 4.75-HPTO, and 4.75-BRIC are presented in Table 8. The 12.5-SMA and 4.75-HPTO mixtures had the highest average G_C followed by the 4.75-BRIC and 9.5-SP mixtures, respectively. These results indicated that 12.5-SMA, 4.75-HPTO, 4.75-BRIC mixtures were more resistant to macro-crack initiation than the 9.5-SP control mixture. These results also suggested that the 12.5-SMA, 4.75-HPTO, and 4.75-BRIC mixtures had a higher fracture toughness than that of the control during macro-crack initiation, respectively. It is noted that the results obtained for G_C generally coincided with the results obtained for the uniaxial cyclic fatigue test parameter, D^R. That is, the 4.75-BRIC, 12.5-SMA and 4.75-HPTO mixtures had a comparatively higher fracture toughness during macro-crack initiation and the control mixture.

Table 8

Computed Fracture Properties of Specialty New Jersey Overlay Mixtures

Mixture Type		9.5-SP	12.5-SMA	4.75-HPTO	4.75-BRIC
Critical Fracture Energy (G_C)	Average (kN-mm/mm^2)	0.00038	0.00058	0.00057	0.00043
	Std. Deviation (kN-mm/mm^2)	0.00018	0.00003	0.00002	0.00011
Crack Progression Rate	Average	0.56	0.69	0.42	0.19
	Std. Deviation	0.09	0.07	0.17	0.17

In regard to the crack progression rate of the mixtures, the 4.75-BRIC had the lowest crack progression rate, which was 98% lower than the 9.5-SP control mixture. The 4.75-HPTO mixture had the next lowest crack progression rate which was 28% lower than that of the control mixture. The 12.5-SMA mixture had the highest crack progression rate of all mixtures which, was 20% higher than that of the 9.5-SP mixture. The crack progression rate results indicated the 4.75-HPTO and 4.75-BRIC were more resistant to macro-crack propagation than the control (9.5-SP mixture) and 12.5-SMA. This was due to the fact that the 4.75-HPTO and 4.75-BRIC mixtures had a higher binder content, lower air void content, and lower NMAS than the 9.5-SP and 12.5-SMA mixtures.

The crack progression rate of the 4.75-BRIC was 75% lower than that of the 4.75-HPTO despite the fact that the mixtures had an almost identical gradation and binder content. Therefore the binder type of the mixtures accounted for the discrepancy in crack progression rate. Since a softer binder, PG 70-28 binder was used in the 4.75-BRIC, the crack progression rate results indicated that a softer, more flexible, polymer-modified binder substantially decreased the rate of macro-crack propagation in the HMA mixtures. This trend was observed in other studies [54] and [55]. It should be noted that the overall

trend obtained for crack progression rate coincided with that of the average number of OT cycles to failure. This implied that the number of OT cycles to failure is more dependent on mixtures' resistance to crack propagation rather than their resistance to macro-crack initiation.

Figure 18d presents an interaction plot that was developed to qualitatively illustrate the reflection cracking susceptibility of the 9.5-SP, 12.5-SMA, 4.75-HPTO, and 4.75-BRIC mixtures based on their respective fracture properties. This interaction plot accounted for the G_C and crack progression rate of the mixtures. Generally, reflective cracking resistance of HMA mixtures can be classified as: tough-crack resistant, tough-crack susceptible, soft-crack resistant, and soft-crack susceptible [68]. Tough-crack resistant mixtures are most favorable because it implies that the mixtures have a high resistance to crack initiation and are flexible during crack propagation. Soft-crack susceptible mixtures are the least favorable is because they have an extremely low resistance to crack initiation and are brittle during crack propagation [68]. By comparing the interaction plots of the 9.5-SP, 12.5-SMA, 4.75-HPTO, and 4.75-BRIC, it can be observed that the specialty New Jersey mixtures (4.75-HPTO and 4.75-BRIC) were generally more tough-crack resistant than the 9.5-SP, control mixture. It can also be observed from Figure 4d that the 12.5-SMA was the more tough-crack susceptible than the control mixture. Therefore, this suggests that the 12.5-SMA mixture may not be ideal for HMA overlay applications because overlays have a high propensity to undergo reflection cracking.

Asphalt pavement analyzer tests results. The rutting performance of the mixtures was evaluated to ensure that the specialty HMA mixtures maintained good

rutting resistance even though they were specifically designed to mitigate cracking. Figure 19 presents the results of the APA tests that were conducted on the four specialty mixtures. The average rut depth of the 9.5-SP, 12.5-SMA, 4.75-HPTO, and 4.75-BRIC after 8000 APA cycles, were 0.8 mm (0.03 in), 1.9 mm (0.07 in), 2.0 mm (0.08 in), and 0.6 mm (0.02 in), respectively. The results indicated that the 4.75-HPTO and 12.5-SMA mixtures experienced the most rutting followed by the 9.5-SP and 4.75-BRIC mixtures respectively. These results were logical because the 12.5-SMA and 4.75-HPTO had a higher binder content than the 9.5-SP, control mixture while the 4.75-BRIC was compacted to a lower air void content than the control mixture. In addition it can be observed from Figure 19 that the NJDOT rut depth thresholds of the 9.5-SP, 12.5-SMA, 4.75-HPTO, and 4.75-BRIC were 5.5 mm (0.22 in), 5 mm (0.20 in), and 4 mm (0.16 in), respectively. Therefore, the average rut depth of all the conventional and specialty New Jersey HMA mixtures fell well below their respective rut depth thresholds. This implied that the conventional 12.5-SMA mixture and specialty mixtures (4.75-HPTO and 4.75-BRIC) evaluated in this study maintained good rutting resistance even though they were specifically designed to mitigate cracking.

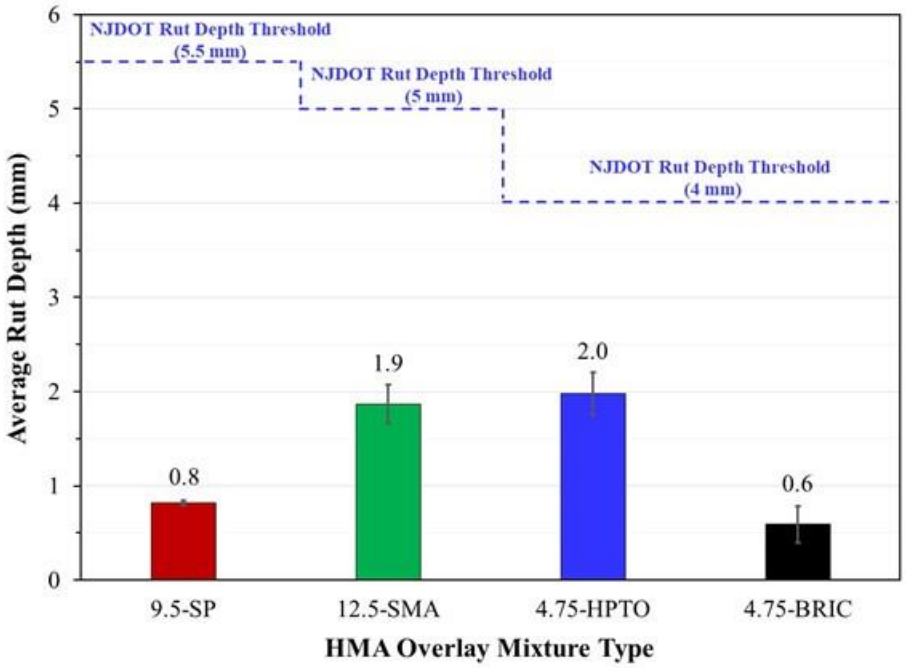

Figure 19. Average rut depth of specialty New Jersey mixtures after 8000 APA loading cycles.

Phase 1 laboratory testing statistical analysis results. Table 9 shows the results of the statistical analysis that was conducted to determine whether there was a significant difference in the reflection cracking performance of the four HMA mixtures evaluated in this study. The dynamic complex modulus and uniaxial cyclic fatigue test results were not included in the statistical analysis because of the inherent fitting process for both laboratory tests. The rutting results were also omitted because all mixes were sufficiently below their respective NJDOT rutting thresholds. The average number of OT cycles to failure, critical fracture energy, and crack progression rate of the mixtures were compared in the statistical analysis. This is because these parameters are closely related to HMA reflection cracking performance; the primary distress of concern for HMA overlays.

Based on the results presented in Table 9, it was determined that the average number of OT cycles to failure of the 12.5-SMA, and 4.75-HPTO was statistically similar to the 9.5-SP control mixture. The average number of OT cycles to failure of the 4.75-BRIC was found to significantly higher than the 9.5-SP and 4.75-HPTO. These results suggested that the 4.75-BRIC mixture was more capable of resisting reflection cracking than the control mixture. The results of the statistical tests also indicated that the use of a softer, more flexible binder in the 4.75-BRIC mixture made the mixture more resistant to reflection crack propagation. This is because the 4.75-BRIC and 4.75-HPTO mixtures had similar gradation and binder content but different binder type.

The critical fracture energy of the 12.5-SMA and 4.75-HPTO mixtures was found to be significantly higher than that of the 9.5-SP control mixture. This indicated that the toughness of the 12.5-SMA and 4.75-HPTO mixtures was generally higher than that of the 9.5-SP control mixture. On the other hand, the crack progression rate of the 4.75-BRIC mixture was found to be significantly lower than that of the 9.5-SP control mixture, 12.5-SMA and 4.75-HPTO mixtures. This result suggested that the rate of reflection crack propagation in asphalt overlays can be reduced by using a layer of the 4.75-BRIC in conjunction with the 9.5-SP, 12.5-SMA, 4.75-HPTO surface course mixture.

Table 9

Tukey's Honest Significant Difference (HSD) Pairwise Comparisons of Computed Fracture Properties of Specialty New Jersey Mixtures at α = 0.05

Test Parameter	Mixture Type		ANOVA		Tukey's HSD	
			F value	P	Mean Difference	P Adjusted
No. of OT Cycles to Failure	9.5-SP	12.5-SMA	7.347	0.004	565.8	0.42
		4.75-HPTO			22.83	1.00
		4.75-BRIC			-1097	**0.05**
	4.75-HPTO	4.75-BRIC			-1120	**0.03**
Critical Fracture Energy (G_C)	9.5-SP	12.5-SMA	5.166	0.014	-0.00020	**0.04**
		4.75-HPTO			-0.00019	**0.03**
		4.75-BRIC			-0.00005	0.89
	4.75-HPTO	4.75-HPTO			0.000143	0.14
Crack Progression Rate	9.5-SP	12.5-SMA	10.688	0.001	-0.13	0.51
		4.75-HPTO			0.14	0.45
		4.75-BRIC			0.37	**0.02**
	4.75-HPTO	4.75-HPTO			0.23	0.09

Laboratory Testing: Phase 2 Results

This section presents the results of the laboratory performance testing that was carried-out on the field-compacted HMA overlays samples extracted from the field sections (i.e., field cores). Phase 2 of laboratory testing allowed for a performance comparison to be made between the specialty overlay mixtures (9.5-SP, 12.5-SMA, and 4.75-HPTO) and composite overlay mixtures (9.5-SP & 4.75-BRIC, 12.5-SMA & 4.75-BRIC, and 4.75-HPTO & 4.75-BRIC). A discussion and interpretation of the results obtained during phase 2 of laboratory testing is outlined in following sections.

Bending beam fatigue tests results. The results of the bending beam fatigue tests is presented in Figure 20. By considering the performance of the surface course overlay

mixtures it can be observed that the 9.5-SP overlay mixture had the highest average number of BBF cycles to failure followed by the 4.75-HPTO, 12.5-SMA. In general, these results of the beam fatigue testing results coincided with the results of the uniaxial cyclic fatigue tests that were performed on the laboratory-compacted mixtures during Phase 1 of laboratory testing. This is because the damage characteristic curves of the mixtures indicated that fatigue damage accumulated at a faster rate in the 4.75-HPTO mixture than in the 12.5-SMA and 9.5-SP mixtures respectively (Figure 20).

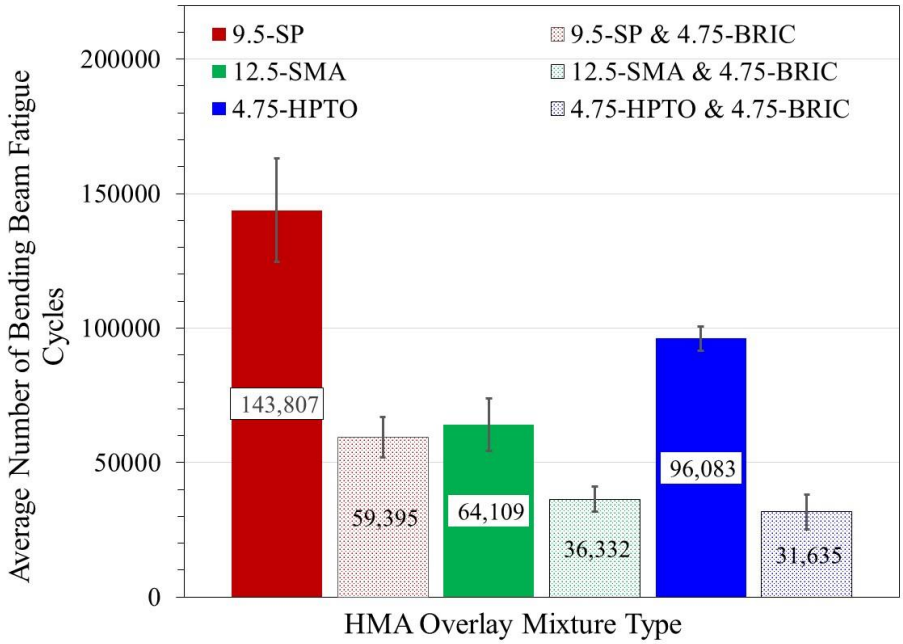

Figure 20. Average number of bending beam fatigue cycles to failure of field-extracted specialty and composite New Jersey mixtures.

By comparing the results of the surface course and composite overlay mixtures it can be observed that the average number of cycles to failure for the 9.5-SP, 12.5-SMA, and 4.75-HPTO mixtures decreased by 60%, 40% and 67% respectively when a layer of

4.75-BRIC was added to the mixtures. This implied that the use of a 4.75-BRIC mixture in conjunction with the 9.5-SP, 12-SMA, and 4.75-HPTO made the mixtures more susceptible to fatigue cracking. This finding was reasonable because the damage characteristics curves obtained from uniaxial cyclic fatigue testing showed that the rate of damage accumulation due to repeated loading was highest in the 4.75-BRIC mixture (Figure 20). Additionally, it was likely that the relatively low thickness of the 4.75-BRIC layer in the composite overlays caused the tensile strains in that layer to be heightened, which in turn made the reduced the overall fatigue cracking resistance of the overlay.

Overlay tests results. The overlay test results obtained for the field extracted specimen is shown in Figure 21. From Figure 21a, it can be observed that the average number of OT cycles to failure of the 4.75-HPTO mixture was larger than that of the 12.5-SMA and 9.5-SP mixtures, respectively. These results suggested that the reflection cracking resistance of the HMA overlays increased as the binder content of the mixtures increased. This is because the binder content of the 9.5-SP, 12.5-SMA, and 4.75-HPTO mixtures was: 4.7%, 7.0%; and 7.6%; respectively. A similar trend was observed when the reflection cracking performance of the composite mixtures were compared. That is, the average number of OT cycles to failure of the 4.75-HPTO & 4.75-BRIC was approximately 3 times larger than that of the 12.5-SMA & 4.75-BRIC overlay mixture and the 9.5-SP & 4.75 BRIC overlay mixture. The reflection cracking performance of the surface course mixtures generally improved when a layer of 4.75-BRIC was added as a stress relieving interlayer. This is because the average number of OT cycles to failure increased by 60%, 50%, and 18% of the 9.5-SP, 12.5-SMA, and 4.75-HPTO.

The crack progression rates (Figure 21b) mirrored the trends observed with respect to average number of OT cycles to failure. That is, the crack progression rates of the HMA overlays decreased when a layer of 4.75-BRIC was placed at the bottom of the surface course mixtures. This implied that the 4.75-BRIC layer retarded the rate of reflection crack propagation in the overlays. This finding was reasonable because the 4.75-BRIC contained a softer, more flexible binder than the surface course overlays (i.e., 9.5-SP, 12.5-SMA, and 4.75-HPTO).

Asphalt pavement analyzer tests results. The results of the APA rut test performed on the field extracted mixtures is shown in (Figure 22). The average rut depth of the 9.5-SP, 12.5-SMA, and 4.75-HPTO, after 8000 APA cycles, was 2.2 mm (0.08 in), 4.5 mm (0.18 in), and 6.0 mm (0.24 in.) respectively. The average rut depth of the 9.5-SP & 4.75-BRIC, 12.5-& 4.75-BRIC, and 4.75-HPTO & 4.75-BRIC was 3 mm (0.12 in.), 4.7 mm (0.19 in.) and 5.5mm (0.22 in.) respectively. These results implied that the average rut depth of the mixtures increased as binder content increased. This trend observed was logical because the stability and load transfer efficiency of mixtures with higher binder contents decreases at high temperatures. This is due to the viscoelastic nature of asphalt binder. The addition of the 4.75-BRIC layer at the bottom of the HMA surface course mixtures appeared to have little to no effect on mixture rutting performance since the average rut depth for the composite overlays were similar to the average rut depth of surface course overlays.

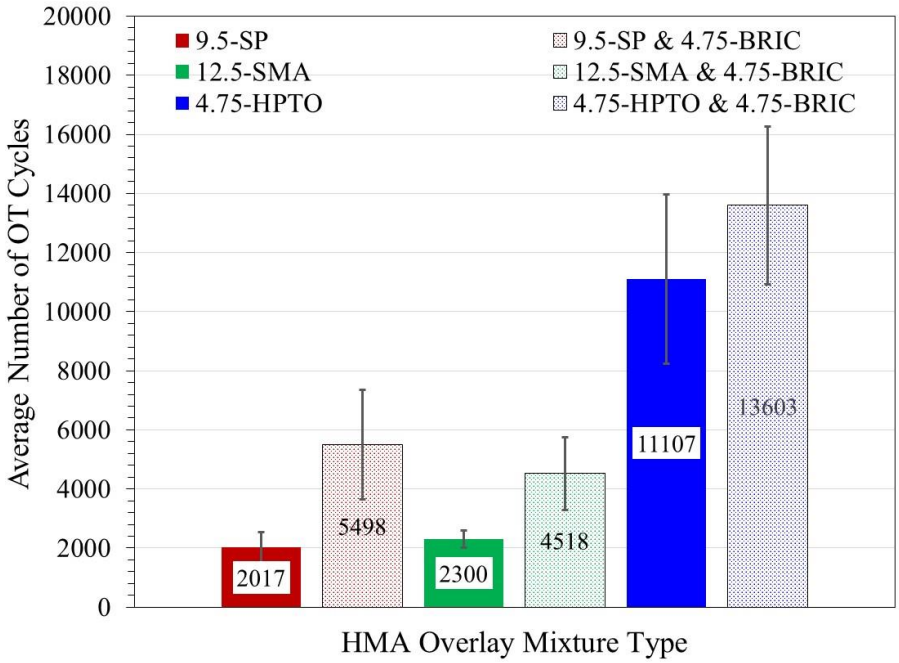

(a)

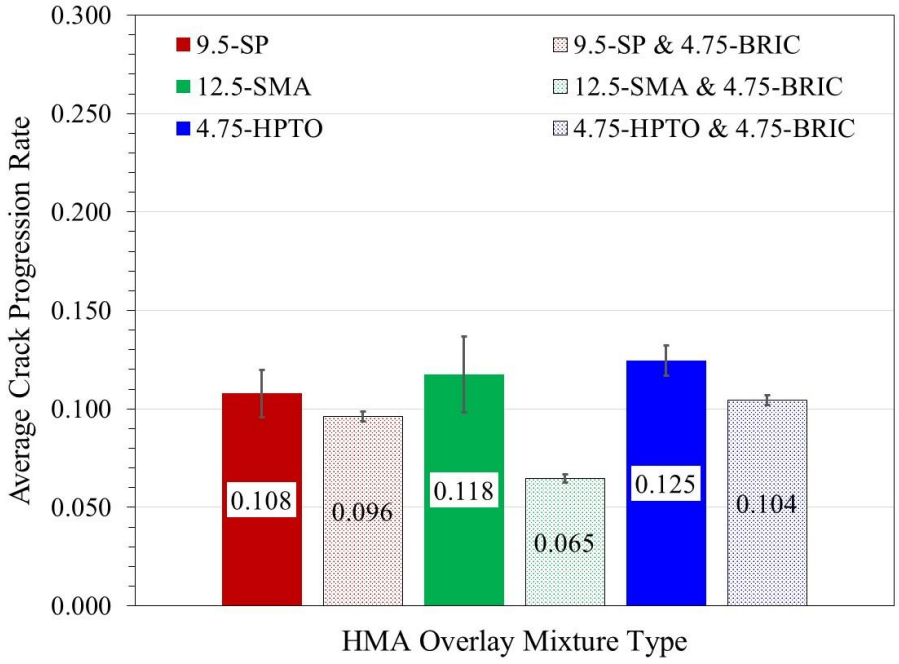

(b)

Figure 21. Overlay test results obtained for field-extracted specialty and composite New Jersey mixtures: (a) average number of cycles to failure (b) crack progression rate.

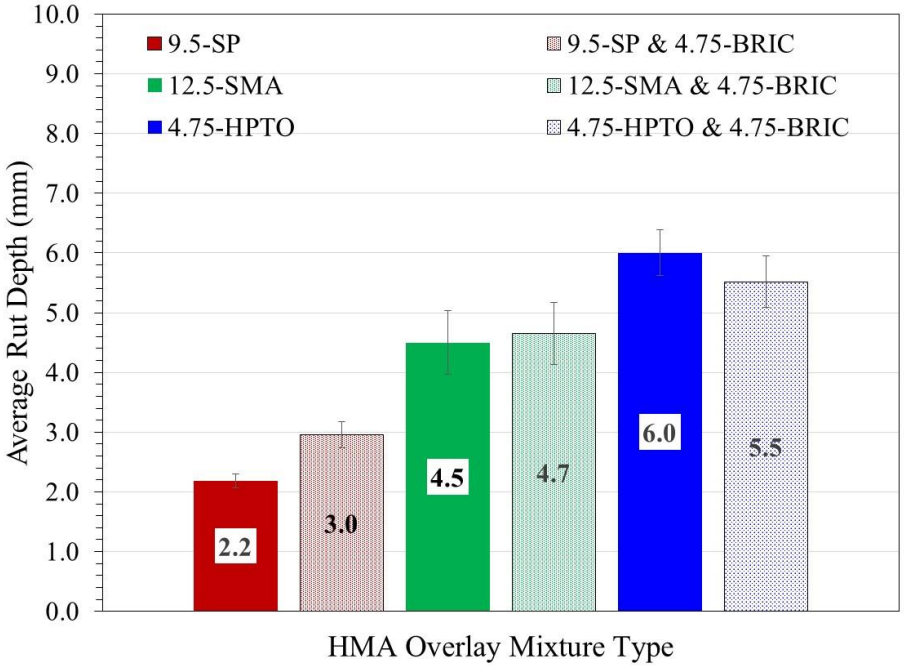

Figure 22. Average APA rut depth obtained for the field–extracted specialty and composite New Jersey mixtures.

Phase 2 laboratory testing statistical analysis results. Appendix A shows the results of the statistical analyses that were conducted to determine whether there was a significant difference in the fatigue cracking, reflection cracking and rutting performance of the three specialty and three composite mixtures evaluated in phase 2 of laboratory testing. Based on the results presented in Appendix A, it was determined that the average bending beam fatigue cycles to failure of the field-extracted, 9.5-SP mixture was significantly higher than that of 12.5-SMA, and 4.75-HPTO mixtures. This suggested that the control specialty mixture (9.5-SP) was more resistant to fatigue cracking than the 12.5-SMA and 4.75-HPTO specialty mixtures. The average number of OT cycles to failure of the field-extracted, 12.5-SMA mixture was statistically similar to that of the 9.5-SP mixture while the number of OT cycles to failure of 4.75-HPTO was found to be

significantly higher than the 9.5-SP (Appendix A). Additionally, the crack progression rates of all three specialty mixtures were similar. Overall, these results implied that the 4.75-HPTO was more capable of resisting reflection cracking than the control and 12.5-SMA mixtures. With respect to the rutting performance of the field-extracted specialty mixtures: the 12.5-SMA and 4.75-HPTO experienced a significantly higher amount of rutting than the control mixture. This result was expected because the 12.5-SMA and 4.75-HPTO had a higher binder content than the control mixture.

The statistical analysis with respect to the field extracted composite overlay mixtures is also presented in Appendix A. According to the results presented in Appendix A, the average bending beam fatigue cycles to failure of the field-extracted, 9.5-SP & 4.75-BRIC mixture was significantly higher than that of the 12.5-SMA & 4.75-BRIC and 4.75-HPTO& 4.75-BRIC mixtures. This suggested that the 9.5-SP & 4.75-BRIC mixture composite mixture was more resistant to fatigue cracking than the 12.5-SMA & 4.75-BRIC and 4.75-HPTO& 4.75-BRIC mixtures. The average number of OT cycles to failure of the field-extracted, 12.5-SMA & 4.75-BRIC mixture was statistically similar to that of the 9.5-SP & 4.75-BRIC mixture. However, the number of OT cycles to failure of 4.75-HPTO & 4.75 BRIC mixture was found to be significantly higher than the 9.5-SP & 4.75-BRIC mixture (Appendix A). The crack progression rates of all three composite mixtures were found to be statistically similar. With respect to the rutting performance of the field-extracted composite mixtures: the 12.5-SMA & 4.75-BRIC and 4.75-HPTO & 4.75-BRIC experienced a significantly higher amount of rutting than the 9.5-SP & 4.75-BRIC mixture. The statistical analysis results with respect to the composite mixtures showed a similar overall trend to that of the specialty mixtures. That is, the overlay

mixture (specialty or composite) that contained the 9.5-SP displayed significantly higher fatigue cracking and rutting resistance while the overlay mixture that contained the 4.75-HPTO exhibited significantly higher reflection cracking resistance.

Chapter 5

Field Sections Description, Construction & Field Experimental Program

This chapter outlines a comprehensive description of the six composite pavement field sections evaluated during the field testing component of this study. The chapter also provides a summary of the construction process and sensor installation procedure implemented during the construction of the composite pavement sections. Lastly, the chapter discusses the field experimental program and accelerated pavement testing scheme that was utilized to evaluate the field cracking and rutting performance of the HMA overlays.

Composite Pavement Field Section Description

A total of six full scale, composite pavement sections were evaluated in this study. These pavement sections were 9 m (30 ft.) long and 3.7 m (12 ft.) wide (Figure 23). All six field sections contained a similar substructure (i.e., base, subbase, and subgrade layer). The base layer of each composite pavement section was 203 mm. (8 in.), thick and consisted of Portland cement concrete (PCC). The subbase layer of each field section was 152 mm (16 in.), thick and was composed of granular, New Jersey I-3 (A-1-a) aggregates. The subgrade layer in all test sections consisted of a 305 mm (12 in.), of compacted, natural soil. It should be noted that the PCC, base layer in each test section consisted of two 4.6 m (15 ft.) long and 3.7 m (12 ft.) wide PCC slabs that were separated by a 25.4 mm (1 in.), un-doweled joint (Figure 12). The base layer of the field sections was intentionally designed in this manner to simulate the cracking mechanism that occurs

during loading in HMA overlays that are placed on deteriorated rigid pavements (i.e., rigid pavements with severe cracking).

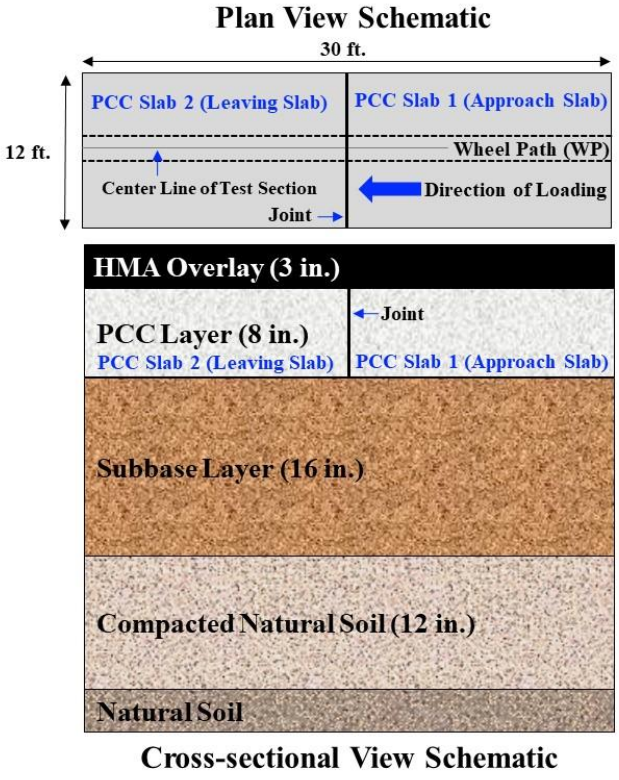

Figure 23. Overall layout of test sections evaluated in this study.

The type of HMA overlay utilized in each test section was different. The overlays used on Test Section 1, 2, and 3 were a 76.2 mm (3 in.) thick, 9.5-SP overlay, 12.5-SMA overlay and 4.75-HPTO overlay, respectively. Test Sections 4, 5, and 6 contained 76.2 mm (3 in.) thick composite overlays. The composite overlays utilized on Test Sections 4, 5, and 6 consisted of a combination of a 50.8 mm (2 in.) thick 9.5-SP mixture, placed over a 25.4 mm (1 in.) thick layer of 4.75-BRIC mixture, 50.8 mm (2 in.) thick 12.5-

SMA mixture placed over a 25.4 mm (1 in.) thick layer of 4.75-BRIC mixture and 50.8 mm (2 in.) thick, 4.75-HPTO mixture placed over a 25.4 mm (1 in.) thick layer of 4.75-BRIC mixture, respectively. The overall design and layout of the field sections facilitated the evaluation of the relative cracking performance of the HMA overlays.

Construction of Field Sections

The construction of the six full scale field sections was conducted in several phases. The first phase of field section construction involved preparing the subgrade and subbase layers. The second stage of test section construction entailed instrumenting the field sections with embedded sensors. The third phase of field section construction involved installing the Portland cement concrete slabs (i.e., base layer). The fourth and final stage of test section construction entailed placing the six HMA overlays evaluated in this study.

The construction of the field sections began with the compaction of 305 mm (12 in.) of the natural soil (Figure 24). This was then followed by the placement and compaction of 203 mm (8 in.) of New Jersey I-3 granular subbase material. Following this step, temperature sensors (i.e., thermocouples and pressure cells) were embedded in the 203 mm (8 in.), layer of NJ I-3 granular material (Figures 24). A second 203 mm (8 in.) layer of NJ I-3 soil was then placed and compacted over the existing 203 mm (8 in.), layer of NJ I-3, granular material (Figure 24).

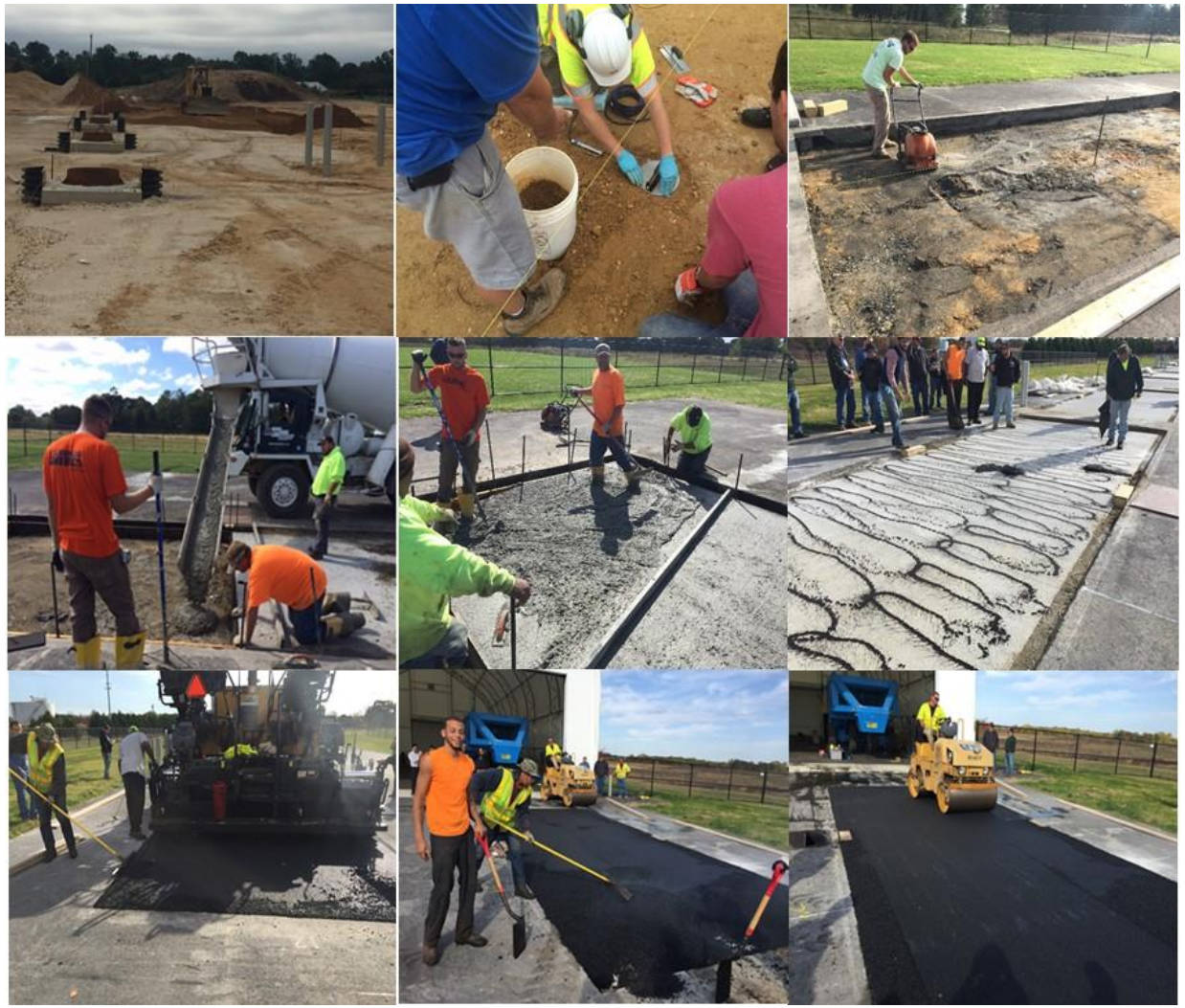

Figure 24. Overall construction process of full-scale, composite pavement test sections evaluated in this study.

In the next phase of construction, two 4.5 m (15 ft.) long by 3.65 m (12 ft.) wide PCC slabs were placed over the granular subbase layers in each test section (Figure24). The HMA overlays were then constructed on top of the PCC slabs and compacted to the NJDOT specified air void content level after the PCC slabs were fully cured (i.e., 28 days after PCC slab placement) (Figures 24). During the construction of the HMA overlays two asphalt strain gauges and three T-type thermocouples were embedded in the HMA overlay layer of each test section. Two linear variable displacement transducers (LVDTs) were also installed at the joint in the base layer of each test section after the sections were fully constructed. The detailed construction procedure utilized for the PCC slabs and HMA overlays is outlined in the following subsections.

Construction of Portland cement concrete slabs. The construction of the PCC slabs in all test sections began with initial preparation of the NJ I-3, granular subbase, (i.e., smoothening and leveling the surface of the sub-base layer using a vibratory compactor) (Figure 24). Two rectangular, 4.5 m (15 ft.) long by 3.7 m (12 ft.) wide wooden forms were then staked into the NJ I-3, sub-base layer in each test section. These wooden forms were utilized as molds for the PCC slabs in the test sections. The interface between the two rectangular wooden forms were separated by a 25.4 mm (1 in.) fiber-impregnated spacer. This spacer facilitated joint construction in the PCC base layer.

After the wooden forms were installed, cement mixture was poured into each rectangular mold using a concrete mixer (Figure 24). Cement mixture samples from each test section were taken for quality assurance testing during the construction of the PCC slabs. After these samples were obtained, the cement mixes in each wooden form were

consolidated and finished using a bull and hand-held floats (Figure 24). The concrete slabs were then covered and left to cure for 30 days in the wooden forms.

Quality assurance of PCC slabs. Quality assurance testing was performed on 27 cement mixture samples obtained during PCC slab construction. This testing involved evaluating the compressive strength of the concrete mixture samples after 7 days, 14 days, and 28 days, respectively. Seven cylindrical, concrete mixture, specimens were evaluated after 7 days. Seven specimens were assessed after 14 days. Thirteen specimens were tested after 28 days. The results of the quality assurance testing is shown in Appendix B. From this figure it can be observed that the average compressive strength of the concrete specimen progressively increased during each 7 day interval as expected. The average 28-day compressive strength of the concrete samples was 30,358 kPa (4403 psi), which exceeded the 25,510 kPa (3700 psi) minimum 28-day compressive strength NJDOT requirement.

Construction of HMA overlays. The construction of the HMA overlays began with the installation of two asphalt strain gauges on top of a 12.7 mm (0.5 in.) thick, HMA bed and three T-type thermocouples at 12.7 mm (0.5 in.) intervals (starting from the top of the PCC slabs). A detailed description of the installation procedure for the asphalt strain gauges and T-type thermocouples is provided in the following subsection. After the sensors were installed, a tack coat was applied on top the PCC slabs in preparation for the placement of the HMA overlays. The plant-produced, HMA overlay mixtures were then placed over the PCC slabs in each test section using a paver as shown in (Figure 24). Following the placement of the HMA by the paver, the HMA was spread evenly across the width of the test sections using shovels and lutes (Figure 24). The HMA

was then compacted using a steel vibratory roller (Figure 24). The Field density of the HMA overlays on each test section was then measured at ten random locations using a nuclear density gauge to ensure that the compaction quality of the HMA overlays was sufficient.

Instrumentation of field sections. The composite pavement sections were instrumented in order to obtain insights about how the HMA overlays responded to the application of full-scale loading. In particular, sensors were installed within each pavement section in order to: measure the tensile strains at the bottom of the HMA overlay layers; measure the change in joint spacing (joint opening/closing) between the two PCC slabs in each test section; and monitor the temperature within the pavement structure (specifically the HMA overlays). The tensile strains at the bottom of HMA overlays were measured because they directly influence the fatigue life of the HMA overlays. Measurement of these tensile strains therefore facilitated the estimation of the fatigue life of the HMA overlays. Similar to tensile strains, the presence of a crack (i.e., joint) underneath an HMA overlay may increase the rate of deterioration of the overlay and increase the potential for reflection cracking to occur. Therefore the measurement of joint opening and closing was essential in order to quantify its effect, if any. The temperature of within the HMA overlays was monitored in order to ensure that all HMA overlays were tested at a similar temperature.

The instrumentation plan used to monitor the responses of the composite sections to full-scale loading is presented in Figure 25. All six sections full-scale sections contained two linear variable displacement transducers, three T-type, thermocouples, and one H-type, asphalt strain gauges (ASG). The linear variable displacement transducers

were installed at the joint; on either side of the test sections. These LVDTs were placed within the PCC base layer at a depth 177.8 mm (7 in.). The thermocouples were installed within the HMA overlays at depths of 12.7 mm (0.5 in.), 38.1 mm (1.5 in.), and 76.2 mm (3 in.), respectively. The ASG was placed directly over the joint within the HMA overlays in each test section. These ASGs were placed at a depth of 63.5 mm (2.5 in.) (i.e., 12.7 mm (0.5 in.) from the bottom of the HMA overlay in each test section.

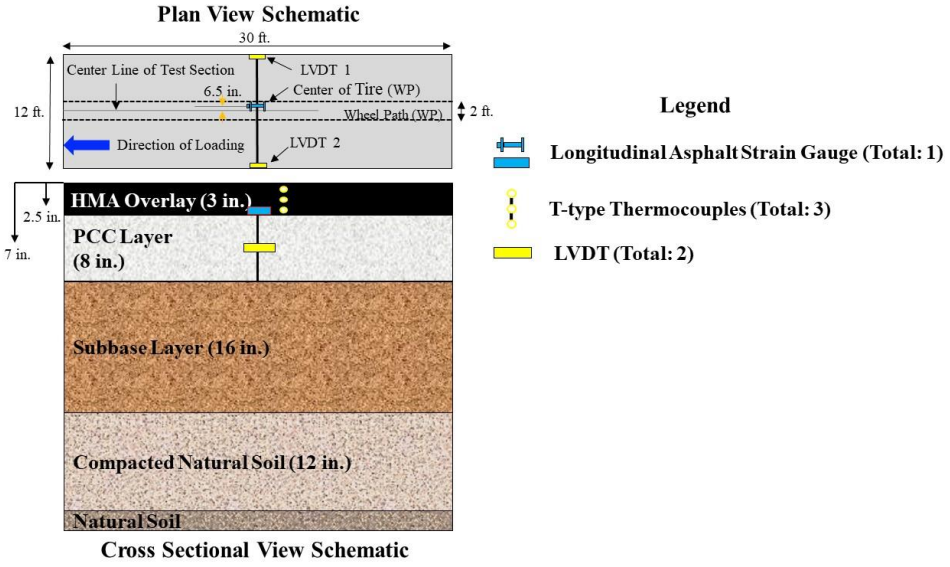

Figure 25. Instrumentation plan for all six composite pavement sections.

Linear variable displacement transducer installation procedure. Linear variable displacement transducers, are electrical transformers used to measure displacements or position. The type of LVDTs utilized in the full-scale test sections were Macro Sensor GHS 750-100 LVDTs (Figure 26). These LVDTs consisted of a spring loaded probe shaft which, was connected to a 19 mm (0.75 in.), diameter stainless steel core. The range of

the LVDTs was 25.4 mm (1 in.) and the maximum linearity of the sensors was -0.038%. Two LVDTs were mounted on either side of each test section in order to measure the joint opening/closing (horizontal displacement) between the two PCC slabs during accelerated pavement testing.

Figure 26. Picture of macro sensor GHS 750-100 LVDT.

The LVDTs were mounted to two steel bars that were inserted into the sides of the PCC base layer; on either side of the 25.4 mm (1 in.) joint (Figure 27). These steel bars were placed at a depth of 101.6 mm (4 in.) in the PCC base layer during the construction of the PCC slabs (i.e. before the cement mixture hardened). The steel bars were utilized with mounting blocks, to mount the LVDTs. The assembly of the steel bars and mounting blocks were covered by a sealed, prefabricated, wooden box in order to protect the LVDTs from moisture damage (Figure 27). This process was found to be sufficient as the measurements from the LVDTs yielded expected horizontal displacement responses (per loading cycle).

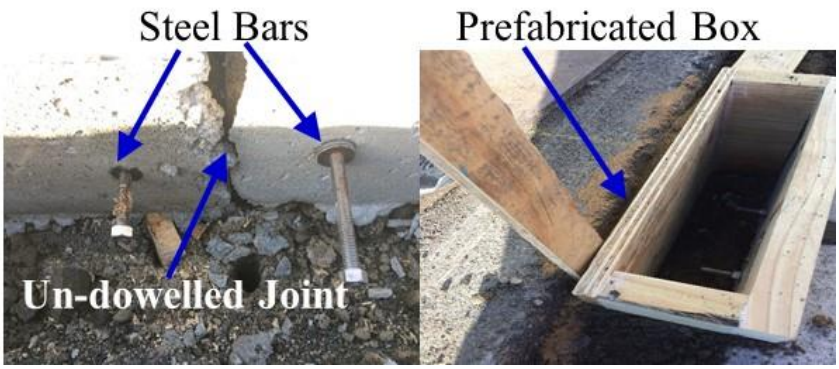

Figure 27. Steel bars used to attach LVDTs to PCC base and prefabricated wooden box enclosure to protect LVDTs from moisture damage.

T-type thermocouple installation procedure. Thermocouples were utilized as temperature sensors in the HMA overlays for several reasons which include: their ability to measure a wide range of temperatures; ease of installation; and cost effectiveness. The type of thermocouples installed in the HMA overlays were T-type thermocouples. T-type thermocouples consist of a pair of copper and constantan wires that are welded together at one end to create a junction. When this junction experiences a change in temperature, an electrical voltage is generated and this electrical signal is converted to temperature measurements using reference tables or a digital thermometer. The step by step procedure employed to install the T-type, thermocouples in the HMA overlays is outlined in this section.

The thermocouple installation procedure consisted of three stages: thermocouple assembly, verification of thermocouple functionality, and placement of thermocouples in full-scale field sections. The thermocouple assembly involved cutting the copper and constantan wires at 203 mm (8 in.) intervals, labelling both sets of wires numerically in ascending order, and pairing the copper and constantan wires based on their respective

labels (i.e., 1-1, 2-2, etc.). Using numerical labels to pair the copper and constantan wires was critical because pairing the wrong sets of wires could have led to erratic temperature measurements in the field sections. Quick tip connectors were then used to connect the copper and constantan wire pairs. Shrink tubing was placed over the Quick tip connectors and heat was applied to the shrink tubing in order to hold the quick tip connections in place and seal the end of the thermocouple, where the wires were connected.

A digital thermometer was used to verify the functionality of the T-type thermocouples. The copper and constantan thermocouple wire pairs were inserted into the digital thermometer and it was verified whether the temperature readings fell within the 24^{o}C and 27^{o}C (75^{o}F and 80^{o}F). This is because the verification process was conducted at room temperature. After the accuracy of the thermocouples' measurements were verified, the thermocouples were installed in the HMA overlays.

A total of three thermocouples were embedded in the HMA overlay on each test section. The first thermocouple was placed directly on the PCC slab at a predetermined location and loose HMA was placed over the installed thermocouple (Figure 28). The loose HMA was then compacted by hand to a height of 38 mm (1.5-in.). The second thermocouple was placed on top of the compacted HMA (Figure 17). Additional loose HMA was placed over the second thermocouple and the mound of HMA was compacted to a height of 63.5 mm (2.5-in.) (Figure 28). The third thermocouple was placed over the 63.5 mm (2.5-in.) mound of compacted HMA and was subsequently covered with loose HMA. This loose HMA was compacted until the total thickness of the HMA mound was 76.2 mm (3-in.).

Figure 28. T-type thermocouple installation procedure.

Asphalt strain gauge installation procedure. The H-type, asphalt strain gauge was used to simultaneously measure the longitudinal and transverse strains within the HMA overlays during full-scale loading. The H-type strain gauge contained an electrical resistance strain gauge embedded within a strip of glass-fiber reinforced epoxy. The strain gauge also contained two transverse stainless steel anchors that were placed on each end of the strip to form an H-type shape (Figure 29). An H-type, strain gauge was used to measure the strain response of the HMA overlays for two main reasons: the stiffness of the reinforced strip was approximately the same as HMA overlays and the gauges were able to withstand the high temperature and loads associated with pavement construction. Therefore, this allowed for accurate pavement responses to be measured.

Figure 29. Picture of H-type, asphalt strain gauge installed in composite pavement sections.

The step by step procedure employed to install the ASG in all six test sections involved several steps. The first step entailed checking the functionality of the ASGs; prior to their installation in the test sections, to ensure that they were working. The second step involved preparing the placement location of the ASG in each test sections. This preparation entailed carefully marking the predetermined locations of the ASG in each test section (i.e., in the wheel path of the right tire of the loading wheel) (Figure 25). Trenches were then saw cut in the PCC slabs to prepare the test sections to receive the ASGs. These trenches were important because the cords of the ASG were placed in the trenches in order to prevent damage to the cords of the ASG. (Figure 30). The third step in the installation procedure involved applying an asphalt emulsion tack coat on the PCC slabs at the demarcated ASG locations and manually compacting a 12.7 mm (0.5 in.) bed of loose HMA at these locations using a tamping rod (Figure 30). In the fourth step, the ASGs were placed on the compacted bed of HMA and were covered by another layer of loose HMA (Figure 16). The loose HMA was then manually compacted to a height less than the thickness of the HMA overlay. The final step in the ASG installation procedure involved constructing the HMA overlay and indicating the location of the embedded ASG on top of the paved surface (Figure 30).

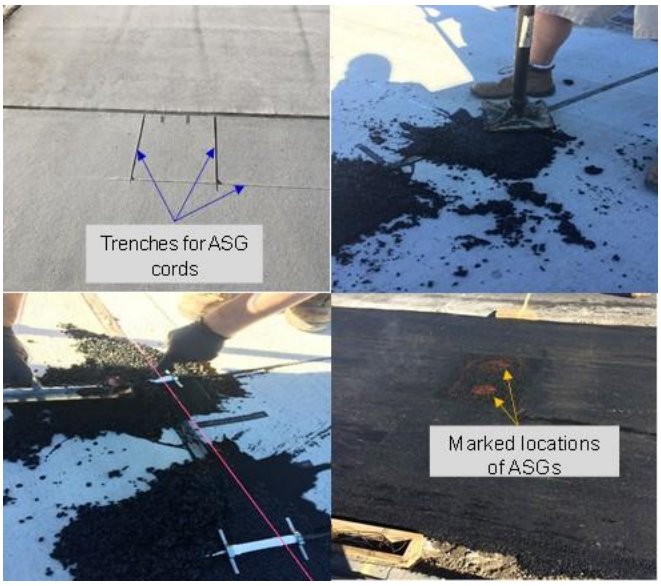

Figure 30. Asphalt strain gauge installation procedure.

Instrumentation of field sections summary. All the sensors embedded in the six full-scale, composite pavement sections were checked after the entire construction process to verify whether they were damage during the test section construction. The success of the sensor installation process was measured by the sensor survival rate. The sensor survival rate (S_{rate}) was defined by (Equation 19). The sensor survival rate was computed for each type of sensor installed in the composite pavement test sections. The sensor survival rate of the ASGs, LVDTs, and thermocouples is presented in Appendix B. All LVDTs and thermocouples were unaffected by test section construction. However, one ASG (i.e., the ASG installed in Test Section 1) was damaged by the test section construction process.

$$S_{rate} = \left(1 - \frac{\sum S_{DAMA}}{\sum S}\right) \times 100 \qquad (19)$$

Where

S_{rate} Sensor survival rate

S_{DAMA} Total amount of sensors (of a specific type) that did not record reasonable measurements after test section construction

S Total amount of sensors (of a specific type)

Field Experimental Program

The field evaluation program adopted in this study consisted of two components: accelerated pavement testing and transverse pavement profile evaluation. The description of each component of the field experimental program is provided in the following subsections.

Accelerated pavement testing. Accelerated pavement testing was carried-out on all six full-scale, field sections using a heavy vehicle simulator. A heavy vehicle simulator is a fully automated, electrically powered, mobile loading machine that accelerates the deterioration of pavements by simulating several years of traffic in a condensed period of time [70]. The accelerated pavement testing involved the application of a 60 kN (13.5 kips), dual-wheel, single axle, truck tire load in a unidirectional manner at a speed of 2.2 m/s (5 mph). A tire pressure of 758kPa (110 psi.) was utilized for the HVS testing. The accelerated pavement testing was conducted at a constant temperature of 25^{o}C (77^{o}F) (i.e., intermediate temperature). Each composite pavement test section was subjected to approximately 200,000 HVS wheel repetitions during accelerated pavement testing.

***Accelerated pavement testing data collection*.** The pavement responses of the full-scale sections were measured by the embedded sensors in each test section (i.e., asphalt strain gauges, LVDTs, and thermocouples). These measurements were recorded using a National Instruments cDAQ, data acquisition system. The HVS and embedded sensors were connected to the data acquisition system in order to collect data from the embedded sensors and synchronize data collection in relation to the loading pass (i.e., wheel repetition) of the HVS. The pavement response data collected during each HVS wheel pass was captured at a frequency of 2,000 data points per second by the data acquisition system. The data sampling frequency (i.e., data recorded by the data acquisition system) was high during the initial stages of APT and decreased as HVS loading progressed on each test section. This type of data sampling frequency was selected because of the typical response of pavements to repeated loading. That is, a rapid change (reduction) in HMA layer stiffness during the initial stages of repeated loading and a lower rate of reduction in stiffness as repeated loading continues. Table 10 presents the loading passes at which data obtained from the embedded sensors was recorded.

Table 10

HVS Loading Passes at which Embedded Sensor Measurements were Recorded (Sampling Frequency)

Stage of Data Sampling	Sampling Frequency
Below 1000 HVS passes	Every 100th pass
1000 to 10,000 HVS passes	Every 500th pass
10,000 to 20,000 HVS passes	Every 1,000th pass
20,000 to 50,000 HVS passes	Every 2,250th pass
50,000 to 100,000 HVS passes	Every 10,000th pass
100,000 to 200,000 HVS passes	Every 20,000th pass

Transverse pavement profile evaluation. Transverse pavement profile evaluation was conducted to assess the amount of permanent deformation that occurred in the HMA overlay due to accelerated pavement testing. Pavement profile evaluation was performed using a manual laser profilometer (Figure 31). The laser profilometer measured the distance from a reference point on the device to the HMA overlay surface at 1,000 points across the pavement width. The measured data was then used to compute and estimate the permanent deformation on the HMA overlay surface in each test section.

Figure 31. Picture of manual laser profilometer.

Transverse pavement profiles were obtained from each test section at seven different locations (Figure 32). The pavement profile data measured at these seven locations provided comprehensive information related to the field rutting potential of the HMA overlays evaluated in this study. Initial pavement profiles were obtained from the test sections before HVS testing. Pavement profiles were also obtained from the test sections after HVS testing. The initial pavement profiles were utilized as a baseline to compute the amount of permanent deformation that occurred in each HMA overlay during APT. This pavement profile evaluation scheme allowed for the field rutting potential of the HMA overlays to be evaluated.

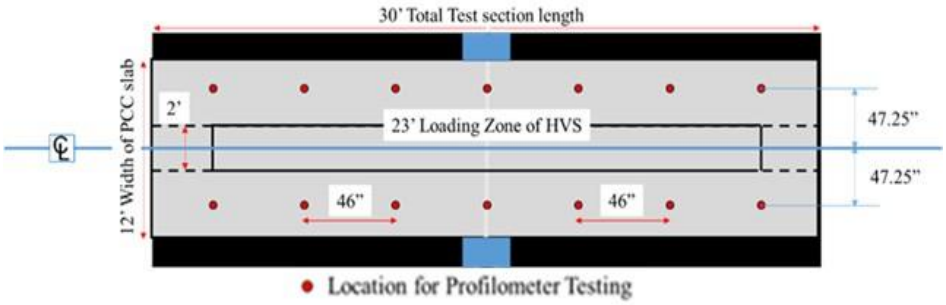

Figure 32. Transverse manual laser profileometer test locations on each test section.

Chapter 6

Field Testing Results

This chapter presents the results of the accelerated pavement testing that was carried-out on the six full-scaled, field sections in order to assess their relative cracking and rutting performance. This chapter also provides a detailed discussion about the procedures adopted to process and analyze the data obtained from the embedded sensors in the test sections. The interpretation of the field results is also included in this chapter.

Linear Variable Displacement Traducer Results

The joint movements in the test sections were measured by the LVDTs during each loading cycle of the HVS. These movements gave insight about the HMA overlays' ability to effectively transfer load across the joint since all full-scale test sections contained a similar supporting structure. The joint movements recorded during APT also gave an indication of the relative reflection cracking susceptibility of the HMA overlays. This is because larger joint displacements implied that the HMA overlays were more likely to experience reflective cracking. This section presents the results (i.e., sensor data) obtained from the LVDTs installed in each full scale test section. The overall approach adopted to analyze the LVDT data and compute joint displacement is also outlined in this section.

LVDT data analysis procedure. The procedure that was utilized to process and analyze LVDT data in this study involved two steps. The first step involved processing the raw LVDT data obtained from the test sections. In order to process the raw LVDT data: voltage signals recorded by the LVDTs during APT were converted to displacement

measurements using manufacturer provided calibration factors. The displacement measurements obtained for each loading pass were then filtered using a signal processing technique (i.e., moving average) to remove any noise that was present in the data. A 25-point data-point of 10,000 data points was utilized to reduce the number of data points required to capture the overall trend in joint displacement during a particular loading pass. This process used to reduce the amount of joint displacement measurements per loading pass was found to be optimal because it accurately captured the trend in measured joint displacement as illustrated in (Figure 33).

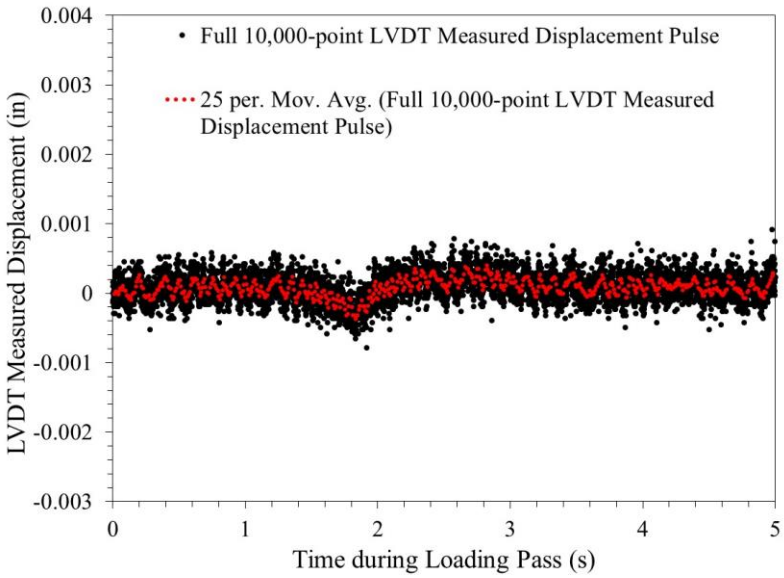

Figure 33. Example of measured and reduced displacement measurements recorded by LVDT during HVS loading pass.

Figure 34a presents a joint displacement pulse that is representative of the typical LVDT measurements recorded during each HVS loading pass. The joint displacement pulse measured during each loading pass consisted of four phases which corresponded

with the movement of the HVS test wheel across the test section (Figure 34b). In the first phase of joint displacement the measured joint displacement remained relatively constant as the wheel approached the joint from the approach slab. In the second phase of joint displacement, the displacement measured by the LVDT decreased to a minimum value (i.e., the joint spacing decreased) as the HVS test wheel moved over the joint. This joint movement was due to the vertical deflection of the approach slab. In the third stage of joint displacement the LVDT measurements increased to a maximum value (i.e., joint spacing increased). This joint displacement occurred due to the residual deflections of the PCC slab as the HVS test wheel moved over the edge of the leaving PCC slab. In the fourth stage of joint displacement, the LVDT measurements decreased towards the initial joint displacement measurement. This was because the influence of the HVS test wheel on PCC slab deflection decreased as the wheel moved further away from the joint.

The second step of the LVDT data analysis procedure involved the computing the maximum joint displacement (ΔJD_{max}) that occurred in the test sections during each HVS wheel pass. The joint displacement within the PCC layer of the composite pavement test sections was of particular concern because it simulated the behavior of cracks or joints in existing (deteriorated) rigid pavements due to repeated traffic loading. It was important to investigate the joint movements within the full-scale test sections because these joint movements typically lead to reflection crack initiation in the HMA overlays.

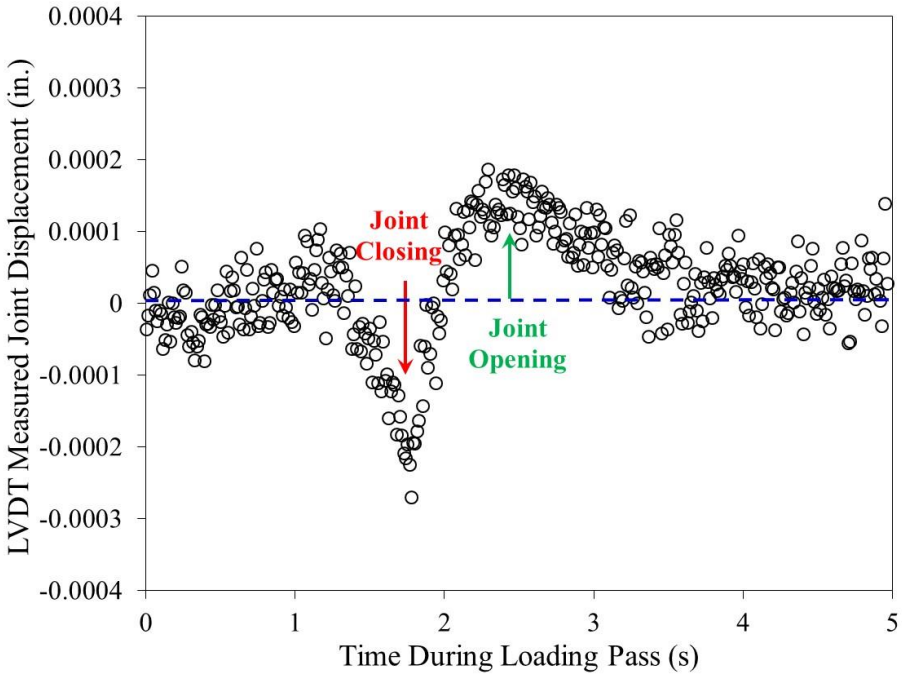

(a)

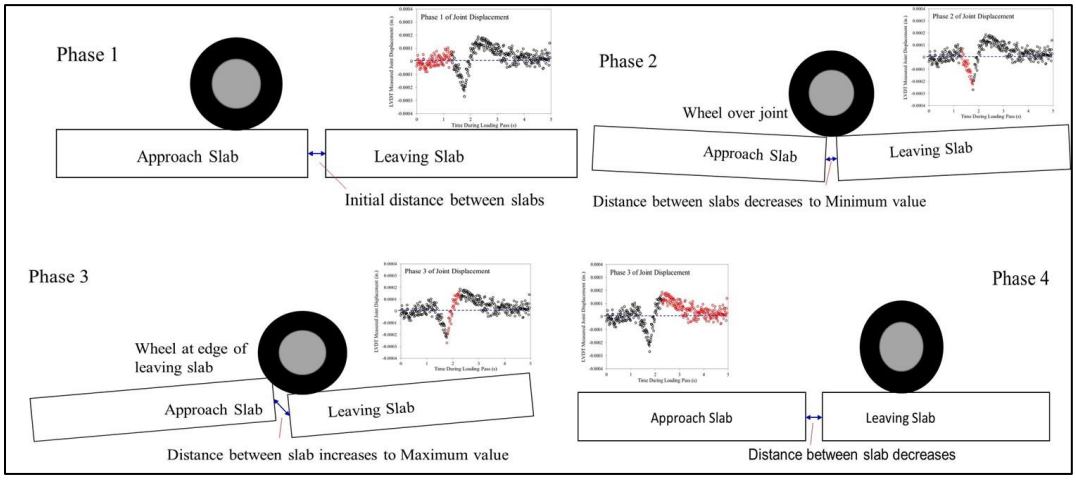

(b)

Figure 34. Joint displacement measured during wheel pass (a) typical joint displacement pulse recorded by embedded LVDTs and (b) Phases of joint displacement during loading pass.

The total joint displacement (ΔJD_{max}) in the composite test sections was computed using (Equation 20). The (ΔJD_{max}) accounted for the overall change in joint displacement

in the test sections during each loading pass. That is, the total joint displacement incorporated the cumulative increase in joint displacement between the initial wheel pass and a particular wheel pass as well as the increase in joint displacement during the particular wheel pass being considered. An example of the computational procedure to determine total joint displacement is illustrated in (Figure 35). From this figure, it can be observed that the total joint displacement accounted for the most critical joint movement the HMA overlays experienced during each HVS loading pass.

$$\Delta JD_{max\,Pn} = JD_{Pn-Pref} + \Delta O_{Pn} \quad \text{.....(20)}$$

Where

$\Delta JD_{max\,Pn}$ Total joint displacement in composite test section during pass: n.

$JD_{Pn-Pref}$ Cumulative joint displacement in composite test section before pass: n

ΔO_{Pn} Maximum joint displacement in composite test section during pass: n.

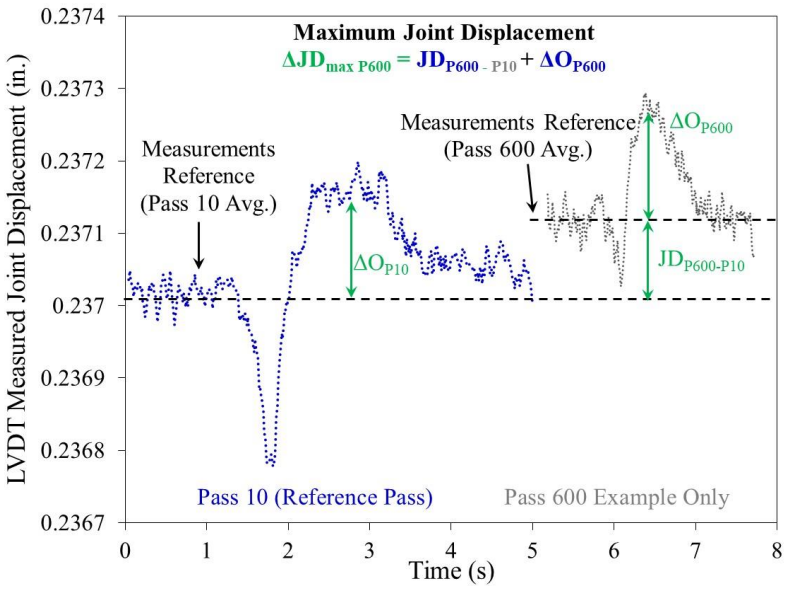

Figure 35. Computational method used to obtain total joint displacement.

It has been well documented that the magnitude of the stress concentrations and tensile strain at the HMA overlay-PCC interface and at the bottom of asphalt overlays, respectively increase as the movement of cracks and joints in the underlying PCC layer increases [33]. Therefore the total joint displacement values computed for each test section provided a means to directly compare the relative reflective cracking potential of the HMA overlays. Figure 36 presents the total joint displacement values computed from LVDT measurements that were recorded during APT on each test section. The total joint displacement calculated from LVDT-1 in each test section (i.e., the LVDT on the right side of the test section in relation to the direction of loading) is shown in (Figure 36a). The ΔJD_{max} obtained from LVDT-2 in each test section (i.e., the LVDT on the left side of the test section in relation to the direction of loading) is illustrated in (Figure 36b). In order to facilitate the comparison of joint displacements test section at a similar damage level; the number of HVS wheel passes applied (i.e., load repetitions) were converted to equivalent single axle loads (ESALS). This is because ESALs relate the damage caused by axles with different loads to the damage caused by a standard 80 kN (18-kip) single axle load. The HVS load repetitions was converted to ESALs using (Equation 21).

$$\text{ESALS} = \left(\frac{\text{HVS Load Magnitude}}{40}\right)^4 \text{x No. of HVS Loading Repetitions} \qquad (21)$$

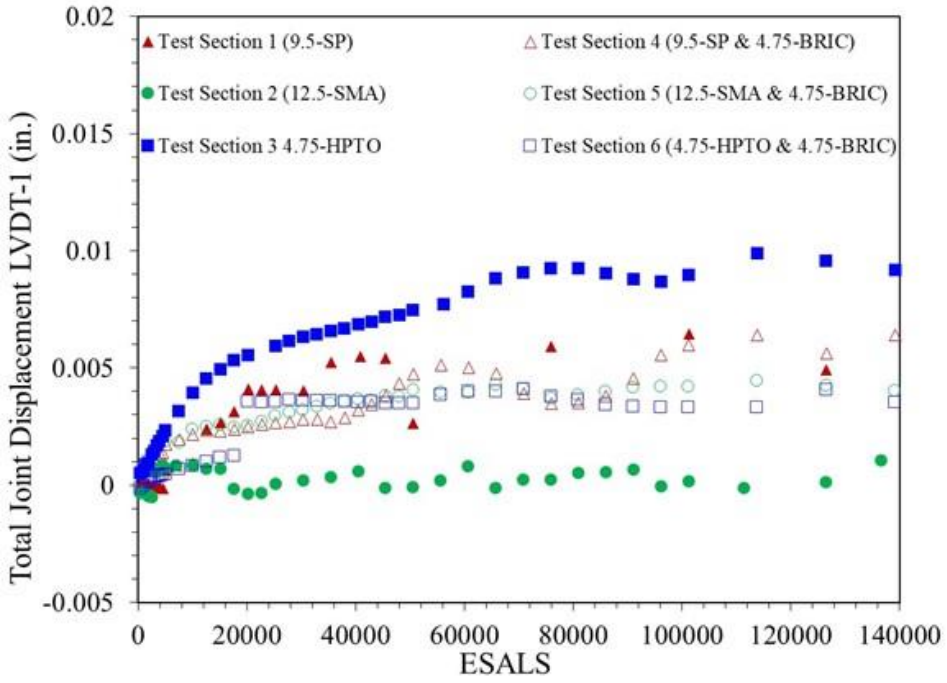

(a)

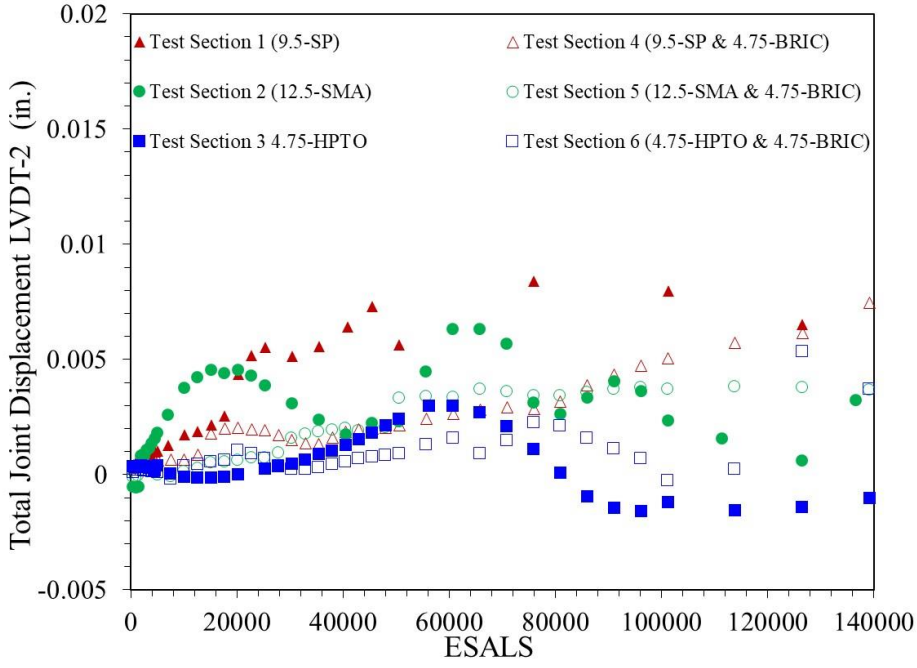

(b)

Figure 36. Total joint displacement computed for test sections: (a) total joint displacement obtained from LVDT-1and (b) total joint displacement obtained from LVDT-2.

Based on the results presented in (Figure 36a) and (Figure 36b) it can be observed that the total joint displacement computed from LVDTs 1 and 2 on each test section generally ranged between 0 mm (0 in.) and 0.254 mm (0.01-in.). It can also be seen that the measurements recorded by LVDT 2 yielded higher total joint displacements values than those obtained from LVDT 1 for all test sections except Test Sections 3 (4.75-HPTO). The total joint displacements; computed from the LVDT measurements, was used to determine the total joint displacement values directly under the embedded asphalt strain gauge in each test section. Since the joint spacing between the PCC slabs in each test section was constant (i.e. 25.4 mm (1 in.)), the joint displacement directly under the embedded asphalt strain gauge was computed using the geometrical relationship expressed in (Equation 22). The factors in (Equation 22) were determined based on the location of embedded strain gauges in reference to the location (i.e., distance) of the LVDTs.

$$\Delta \mathrm{JD}_{\max \mathrm{ASG}} = \left(\frac{65.5\ in}{144\ in}\right)(x_{\mathrm{LVDT\ 2}}) + \left(\frac{78.5\ in}{144\ in}\right)(x_{\mathrm{LVDT\ 1}}) \qquad (22)$$

Where

$\Delta \mathrm{JD}_{\max \mathrm{ASG}}$ Total joint displacement computed directly under asphalt strain gauge.

$x_{\mathrm{LVDT\ 2}}$ Displacement measured by LVDT 2

$x_{\mathrm{LVDT\ 1}}$ Displacement measured by LVDT-1.

The results obtained for the total joint displacement measured directly under the ASGs in the test sections is presented in Figure 37. From this figure it can be observed that Test Section 1 (9.5-SP) had the largest total joint displacement below the ASG during APT. Test Section 3 (4.75 HPTO) and Test Section 4 (9.5-SP & 4.75-BRIC)

experienced the next highest total joint displacement below the ASG with $\Delta JD_{max\ ASG}$ values of (0.006 in.). Test Section 6 (4.75 HPTO & 4.75-BRIC) and Test Section 5 (12.5-SMA & 4.75-BRIC) has similar $\Delta JD_{max\ ASG}$ values (i.e., 0.004 in.) while Test Section 2 experienced the lowest $\Delta JD_{max\ ASG}$ (i.e., 0.003 in.). The results obtained for total joint displacement directly below the ASG suggested that Test Section 2 (12.5-SMA) had the best load transfer efficiency across the joint while Test Section 1 (9.5-SP) had the worst load transfer efficiency across the joint. This implied that the overlay in Test Section 1 was the most at risk to undergo reflection cracking while the overlay in Test Section 2 was least at risk to experience reflection cracking. It should be noted however that the $\Delta JD_{max\ ASG}$ in all test sections was well below 0.01 in: the maximum crack or joint displacement that dense-graded overlays are capable of withstanding [52]. Hence it was unlikely that reflection cracking initiated in any of the HMA overlays.

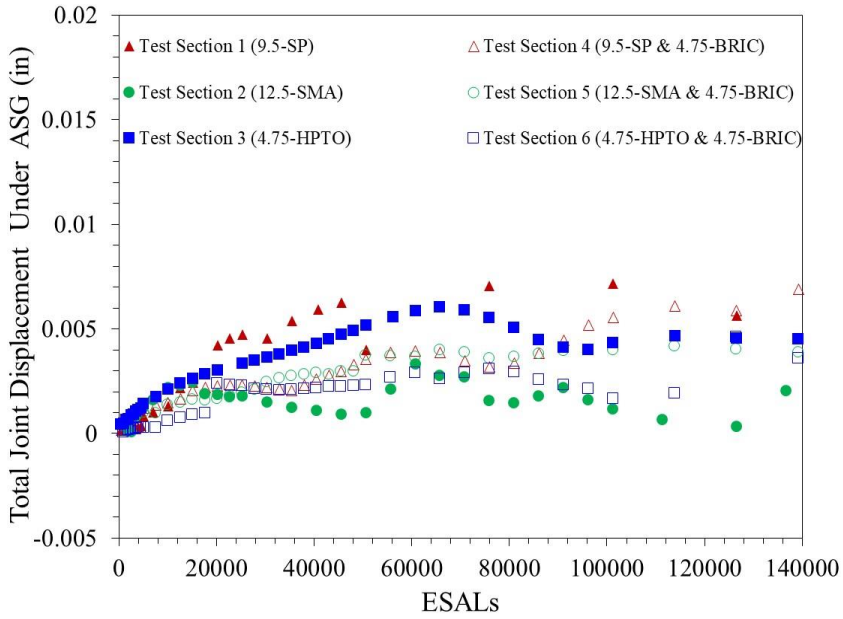

Figure 37. Total joint displacement computed directly under ASGs embedded in test sections.

Asphalt Strain Gauge Results

The measurement of reliable and repeatable pavement strain responses during APT provides the foundation for understanding the overall fatigue or reflection cracking performance of pavements. This is because measured strains provide an indication of pavement fatigue life [73]. The strain at the bottom of an asphalt layer in full scale test sections is typically monitored to capture the loads-associated cracking failure mechanism in the asphalt layers. Hence strain gauges were embedded in the HMA overlays to assess the relative field cracking performance of the overlays. The results of the strain measurements recorded in each test section during loading are presented in this section.

Overview of ASG data analysis procedure. A generalized procedure was developed as part of this study to process and analyze data collected from embedded strain gauges in full-scale test sections. This generalized procedure was developed because there is currently no standardized analysis method to evaluate the fatigue cracking performance of full-scale sections; subjected to APT. The procedure was conceived as a first step towards establishing a standardized procedure to analyze strain data. The establishment of such a procedure is crucial because it will ensure an efficient, and effective characterization of pavement responses and performance by correlating strain data and fatigue life. A standardized strain data analysis procedure is especially important because it lays the foundation to establish a performance parameter(s) through which the fatigue life of various full-scale pavement sections can be adequately predicted, compared, and contrasted. The strain data analysis procedure developed in this

study is presented in the following sections. The procedure consisted of four steps: which are discussed in detail in the proceeding sections.

Step 1: processing strain data. In the first step of the strain analysis procedure, strain measurements were obtained by converting the voltage signal recorded by H-gauges embedded in a pavement section. Calibration factors, which are typically provided by manufacturers, were used for this purpose. The strain-time history response was then filtered using signal processing techniques to remove any noise that may be present in the data [74]. This is because typical strain-time history signals are generally obtained from a large dataset of recorded measurements (i.e., datasets ranging from 1000–2000 data points per second per strain gauge installed) [75]. As such, a 25-data-point moving average of 10,000 data-points was used to reduce the number of data-points required to capture the strain response at a particular loading pass. This process used to reduce the amount of data point per loading pass was found to accurately capture the trend in strain response as will be highlighted in subsequent sections.

Step 2: defining phases of strain response pulse. Step 2 of the analysis procedure also involved defining the various phases that represent the change in strain response recorded for a particular pass. To establish these phases, it was necessary to first identify critical (or turning) points on the strain time history for each loading pass (Figure 38). The critical points were defined as a local maximum or minimum point on the strain time history pulse where the slope changed from positive to negative or vice versa. Using these turning points, four phases in the strain signal time history pulse were defined (Figure 38). As illustrated in (Figure 38), Phase I represents the start of the strain time history pulse up until Turning Point 2 (TP2). This phase captured the initial compressive

strain that the overlay experienced at the joint when the load approached the joint. Phase II (TP2 to TP3) captured the tensile strain the overlay experienced when the load was directly on top of the joint. Phase III (TP3 to TP4) captured the compressive strain the overlay experienced as the load departed from the joint. Phase IV (TP4 to End Point) captured the gradual increase in strain after the load no longer directly impacted joint or PCC slab deflection (i.e., as the load moved further away from the joint). The establishment of these critical phases was necessary in order to perform calculations required in subsequent steps of the proposed strain data analysis procedure.

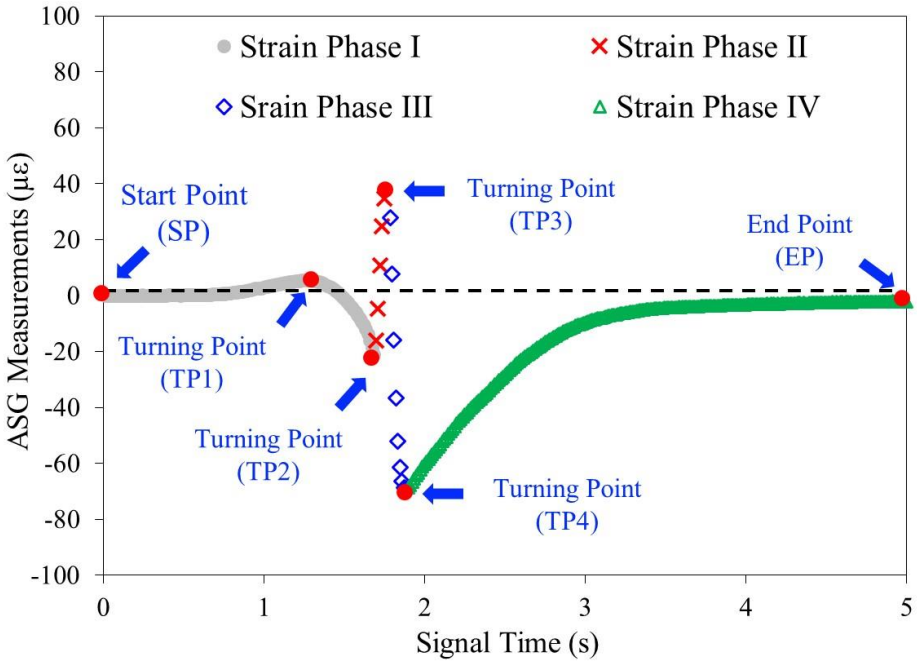

Figure 38. Typical joint displacement pulse recorded by embedded LVDTs.

The strain-time history pulse shown in (Figure 38) was obtained from an H-type, strain gauge, installed to measure the longitudinal strain of an asphalt layer loaded using

a dual-tire single axle configuration as previously discussed. Researchers have previously shown that different strain-time history responses can be obtained by varying the loading configurations in APT [74] and [75]. Despite this fact, the definition of the critical strain phases still holds regardless of the strain-time history pulse obtained.

Step 3: calculating maximum strain and strain ratio. For each loading pass, the phases of the strain-time history pulse defined in Step 1 were utilized to compute two parameters which characterize the strain response of the pavement structure. The first parameter, referred to as the Maximum strain ($\varepsilon_{t\text{-}max}$) was computed as absolute difference between the maximum tensile strain (TP3: Figure 38) and the maximum compressive strain (TP4: Figure 38) for each loading pass. The $\varepsilon_{t\text{-}max}$ characterized the most critical tensile strain that the HMA overlays experienced during each loading pass. This critical tensile strain was the instantaneous strain the overlays experienced when the load was directly above the joint. Higher $\varepsilon_{t\text{-}max}$ values indicated that more damage was being applied to HMA overlays during a particular loading pass. Thus, the $\varepsilon_{t\text{-}max}$ parameter was used to gain insights about the amount of damage that was applied to the asphalt overlays: strictly due to movement of the wheel load directly over the joint during each loading pass. It is noted that the $\varepsilon_{t\text{-}max}$ has been successfully used in other studies [75] and [76] to compare the response of different asphalt overlays to various APT conditions such as: distance from the wheel path, load magnitudes, and loading rates.

The second parameter referred to as the strain ratio (SP_R), was also computed from the strain-time history pulse. The strain ratio was computed using by (Equation 23). The strain ratio was defined as the ratio of the compressive strain that represented the smaller of Phases I or III (Figure 38) to the other compressive strain that represented the larger of

Phases I or III (Figure 38). This mathematical definition was adopted to ensure that the SP_R values obtained for a particular HMA overlay followed a logarithmic growth trend as the loading passes increased: regardless of the strain response obtained from H-gauges. This was important because strain-time history pulses in APT depends on the wheel loading configurations and asphalt mixtures types [75] and [75]. The SP_R captured the net compressive strains the HMA overlays experienced due to the residual PCC slab deflections. These residual slab or joint deflections occurred when the wheel load was on the edge of the approach slab or leaving slab as the wheel load approached and exited the joint vicinity. Similar to $\varepsilon_{t\text{-}max}$, higher SP_R indicated that the asphalt layer experienced a higher compressive strains due to residual joint or PCC slab deflections during a particular loading pass. Therefore, the SP_R was used to determine the rate at which the compressive stains (or damage) in the overlays increased due to residual slab deflection during APT..

$$SP_R = \begin{cases} \frac{\text{Phase I}}{\text{Phase III}} & \text{if } |TP2 - TP1| < |TP4 - TP3| \\ \frac{\text{Phase III}}{\text{Phase I}} & \text{if } |TP2 - TP1| \geq |TP4 - TP3| \end{cases} \quad (23)$$

Where

SP_R Strain ratio.

TP1 Turning Point 1 (Figure 38).

TP2 Turning Point 2 (Figure 38).

TP3 Turning Point 3 (Figure 38).

TP4 Turning Point 4 (Figure 38).

Step 4: determining stiffness index and damage index parameters. Step 4 involved the computing the stiffness index (SI) and damage index (DI) parameters. The

stiffness index was conceptualized as parameter that would give some insight about the relative reduction in asphalt overlay stiffness directly over the joint, as loading progressed. This is because the stiffness index incorporated the change in maximum strain ($\varepsilon_{t\text{-}max}$) the overlays experienced with increasing loading passes. The stiffness index was defined by (Equation 24). The damage index was conceptualized as a parameter the represented the cumulative damage the overlays experienced at the end of each loading cycle. This is because the DI incorporated the total damage the overlays experienced due to loading and residual slab deflection during each loading cycle. Prior to computing the damage index, the total damage the overlays experienced due to loading and residual slab deflection during each loading cycle was computed using (Equation 25). The damage index was then determined using (Equation 26) as the summation of damage applied for all loading passes. Based on the definition of the damage index, the DI was utilized as a potential comparative tool to assess the relative damage accumulation experienced in each asphalt overlay due to APT. It was also used as a means to give an overall assessment of the relative fatigue cracking or reflection cracking resistance of the asphalt overlays.

$$\text{Stiffness Index} = \frac{1}{\varepsilon_{t-max}} \qquad (24)$$

$$PD_i = (SI \times \Delta SP_R)_{pass\ i} \text{.....(25)}$$

$$DI = \sum PD_i \text{.....(26)}$$

Where

$\varepsilon_{t\text{-}max}$, Maximum Strain.

PDi Total damage during each HVS loading pass

SI Stiffness index.

ΔSP_R Change in strain phase ratio.

DI Damage index.

Application of proposed strain data analysis procedure.

Filtering and processing of strain data. Figure 39 presents an example strain-time history pulse obtained from an H-Type strain gauge embedded in one of the sections evaluated in this study. The strain-time history response pulse illustrated in Figure 39 is similar to the strain response reported in a previous study for the longitudinal gauges subjected to dual wheel-single axle loads [76]. That is, a strain-time history pulse which consisted of two consecutive cycles of compression (negative strain) and tension (positive strain); with little permanent deformation at the end of the strain pulse.

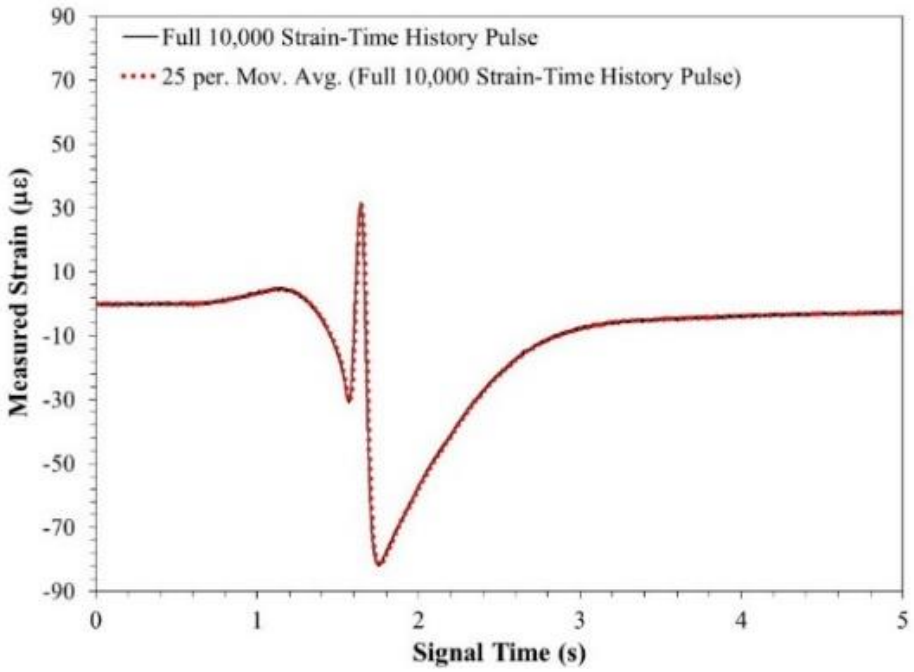

Figure 39. Example of measured and reduced strain time history response obtained from a strain gauge embedded in full-scale test sections.

As can be seen from Figure 39, the strain-time history response for this particular HVS loading pass was smooth with low noise in the recorded data. This was the case for all strain-time history responses collected from all the full-scale test sections considered in this study. Figure 39 also illustrates the reduced strain-time history pulse obtained from the 25-datapoint moving average. Based on the strain-time history response pulses presented in Figure 39 it was determined that the reduced strain-time history response accurately captured the trend of the full strain-time history response. To automate the process of reducing all recorded strain-time history responses, an Excel Macro was developed. The Excel Macro was also utilized to establish the various turning points and phases of the strain-time history response pulse outlined in Step 2 of the proposed analysis procedure.

Maximum tensile strain and strain phase ratio. The $\varepsilon_{t\text{-}max}$ and SP_R parameters were computed for all strain-time history pulses recorded during APT on five of the six full-scale test sections. No strain data was available for Section 1 (9.5-SP) because the ASG was damaged during the construction of the field section. Therefore Test Section 1 was omitted from the strain data analysis. Figure 40 presents the results obtained for the maximum strain ($\varepsilon_{t\text{-}max}$) on all test sections considered. The $\varepsilon_{t\text{-}max}$ was plotted against ESALS to facilitate the comparison of $\varepsilon_{t\text{-}max}$ of the HMA overlays at a similar damage level. It can be observed from Figure 40 that the maximum strain for all test sections followed a logarithmic growth trend as the amount of applied ESALs increased on the full-scale test sections. This trend was expected because the increase in applied loading passes typically amounts to an increase in permanent strain (or damage) within the asphalt layer of pavement sections. In addition, given the constant loading (60kN) applied

to the test section, it can be observed from Figure 40 that the $\varepsilon_{t\text{-}max}$ was able to differentiate between asphalt overlays in the test sections. This is because maximum strain values for Section 2 (12.5-SMA) were highest followed by those obtained for Section 4 (9.5-SP & BRIC), Section 6 (4.75-HPTO & 4.75-BRIC), Section 3 (4.75-HPTO) and Section 5 (12.5-SMA & BRIC) respectively.

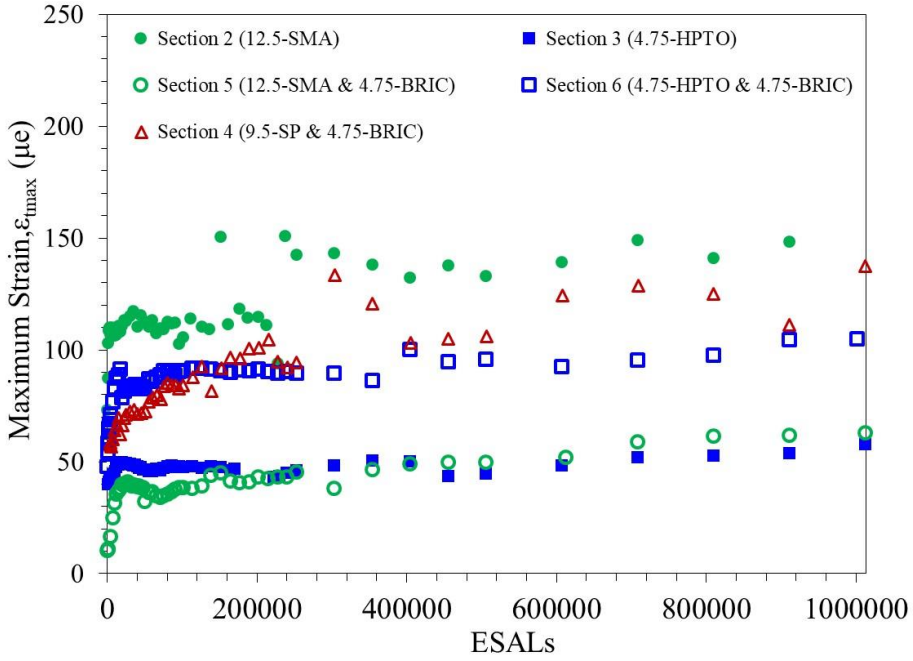

Figure 40. Maximum strain versus number of applied ESALs.

The rate of change in $\varepsilon_{t\text{-}max}$ of the HMA overlays were assessed to gain some insights about the relative damage that occurred in the overlays due to the application of the wheel load directly above the joint. In order to perform this comparison, an empirical relationship between the maximum strain and applied ESALs was established through regression analysis. A logarithmic function was used to model the relationship between

maximum strain and applied ESALs for all the overlays (Equation 27). The coefficients of the empirical relationships established is shown in Table11. All the logarithmic relationships developed for maximum strain and applied ESALs had a relatively low adjusted R^2 value. However since the slope of the logarithmic relationships were significantly different from 0; at a 95% confidence interval, it was determined that the correlation between $\varepsilon_{t\text{-}max}$ and ESALs was relatively good for all overlays. The empirical relationships developed between $\varepsilon_{t\text{-}max}$ and ESALs were used to determine the rate of change of $\varepsilon_{t\text{-}max}$ with respect to applied ESALs (Table 12). Based on the relationships presented in this table it can be observed that the 9.5-SP & 4.75-BRIC overlay experienced the highest rate of increase in $\varepsilon_{t\text{-}max}$ as applied ESALs increased followed by, the 12.5- SMA overlay 4.75-HPTO & 4.75-BRIC overlay, 4.75-HPTO overlay, 12.5-SMA overlay, and 12.5-SMA & 4.75-BRIC overlay respectively. These results suggested that most damage was applied to the 9.5-SP & 4.75-BRIC as the wheel load moved directly over the joint. The results also implied that least damage was applied to the 4.75-HPTO overlays as the wheel moved over the joint.

$$\ln\left(\varepsilon_{t\text{-}max}\right) = a \ln (ESALs) + b \text{……..(27)}$$

Where

$\varepsilon_{t\text{-}max}$	Maximum strain
ESALs	Equivalent single axle loads
a and b	Coefficients of logarithmic relationship between maximum strain and ESALS.

Table 11

Empirical Relationships Established between Maximum Strain and Applied ESALs

Test Section Designation	**Coefficients**		**Adjusted R^2**	**Slope**	**Significance at $\alpha = 0.005$**
	a	**b**			
Test Section 2 (12.5-SMA)	6.4221	47.071	0.51	3.2 E-05	7.8 E-10
Test Section 3 (4.75-HPTO)	1.4886	30.659	0.45	8.4 E-06	4.3 E-09
Test Section 4 (9.5-SP & 4.75-BRIC)	13.401	-64.554	0.72	7.1 E-5	2.3 E-14
Test Section 5 (12.5-SMA & 4.75-BRIC)	5.827 -	-25.746	0.62	3.3 E-6	1.7 E-12
Test Section 6 (4.75-HPTO & 4.75-BRIC)	5.917	20.212	0.39	2.9 E-5	7.7 E-8

Table 12

Rate of Change in $\varepsilon_{t\text{-}max}$ Obtained from E*mpirical Relationships Established between Maximum Strain and Applied ESALs*

Test Section Designation	Rate of Change in $\varepsilon_{t\text{-}max}$ during each loading cycle. ($\Delta\ \varepsilon_{t\text{-}max\ R}$)
Test Section 2 (12.5-SMA)	$\frac{6.4221}{ESALs}$
Test Section 3 (4.75-HPTO)	$\frac{1.4886}{ESALs}$
Test Section 4 (9.5-SP & 4.75-BRIC)	$\frac{13.401}{ESALs}$
Test Section 5 (12.5-SMA & 4.75-BRIC)	$\frac{5.827}{ESALs}$
Test Section 6 (4.75-HPTO & 4.75-BRIC)	$\frac{5.917}{ESALs}$

Figure 41 presents the results obtained for the strain ratio (SP_R) on all test sections considered. The strain ratio obtained for the asphalt overlays on for all test sections followed a logarithmic growth trend as the amount of applied ESALs increased. It should

be noted that the SP_R for each mixture generally converged towards a particular value as the amount of ESALs applied to the test sections increased. Physically, this meant that the overlays experienced less damage due to residual PCC slab deflections (compressive strain) during the initial stages of APT. However as more ESALs were applied to the test sections, the overlays experienced higher compressive strains as the wheel approached and left the vicinity of the joint. Based on the definition of the strain ratio and the overall trend observed in (Figure 41), it was determined that the compressive strains in the smaller strain phase (Phase I or Phase II in Figure 38) increased at a more rapid rate than the larger strain phase in all overlays. This implied that the overlays experienced more flexure (i.e. stretching) due to residual slab deflections as applied ESALs increased.

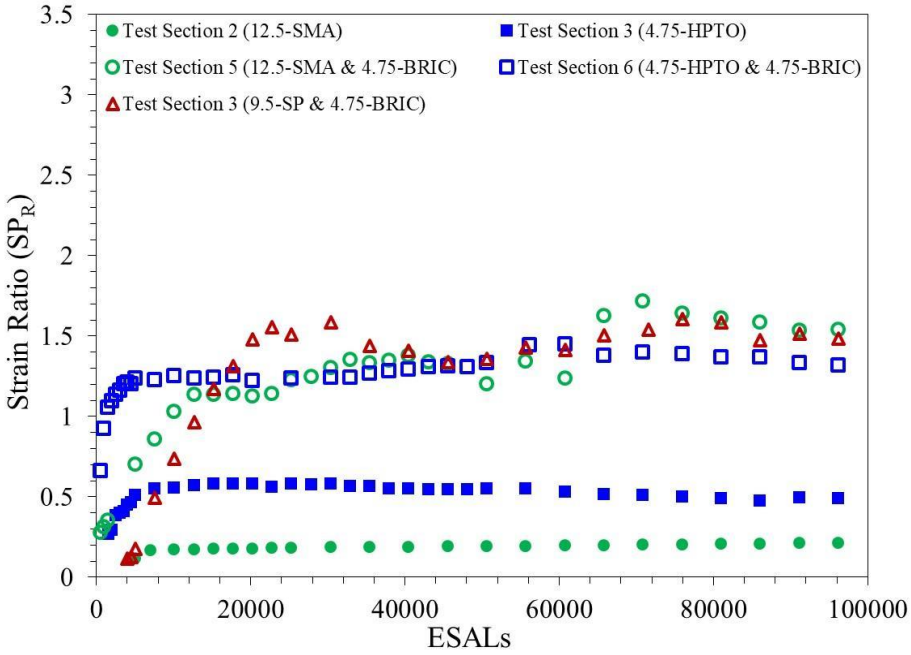

Figure 41. Strain ratio versus number of applied ESALs.

The rate of change in SP_R was utilized to commute the damage index parameter as discussed previously, Therefore a correlation was made between SP_R and applied ESALs. A logarithmic function; similar to the model outlined in (Equation 27), was used to model the relationship between SP_R with applied ESALs. Table 13 shows the model coefficients obtained for the empirical relationship between SP_R and ESALs. From this table it can be seen that the adjusted R^2 was relatively low However all relationships had a slope that was greater than 0 at a 95% confidence interval. Therefore the relationships established for SP_R and ESALs were deemed to be valid. The rate of change of SP_R with respect to applied ESALs was determined from the logarithmic relationships developed from SP_R. The relationships obtained for the rate of change of SP_R is shown in Table 14. From this table it can be observed that the SP_R increased at a faster rate in the 9.5-SP & 4.75-BRIC overlay followed by the 12.5-SMA & 4.75-BRIC overlay, 12.5-SMA overlay, 4.75-HPTO & 4.75-BRIC overlay and the 4.75-HPTO overlay respectively. These results suggested that the 9.5-SP & BRIC overlay experienced more damage due to residual slab deflections while the 4.75-HPTO experienced the least damage due to residual slab deflections.

As was the case for the maximum strain, the trend strain ratio was expected because the increase in applied loading passes typically amounts to an increase in permanent strain (or damage) within the asphalt layer of pavement sections. In addition, given the constant loading (60kN) applied to the test section, it can be observed from Figure 40 that the $\varepsilon_{t\text{-}max}$ was able to differentiate between asphalt overlays in the test sections. This is because values maximum strain for Section 2 (12.5-SMA) were highest

followed by those obtained for Section 4 (9.5-SP & BRIC), Section 6 (4.75-HPTO & 4.75-BRIC), Section 3 (4.75-HPTO) and Section 5 (12.5-SMA & BRIC) respectively.

Table 13

Empirical Relationships Established between Strain Ratio and Applied ESALs

Test Section Designation	**Coefficients**		**Adjusted R^2**	**Slope**	**Significance at $\alpha = 0.005$**
	a	**b**			
Test Section 2 (12.5-SMA)	0.08436	-0.6804	0.87	3.5 E-05	2.2 E-23
Test Section 3 (4.75-HPTO)	0.0362	0.1397	0.53	2.0 E-07	7.0 E-10
Test Section 4 (9.5-SP & 4.75-BRIC)	0.2663	-1.6041	0.63	1.19 E-6	5.4 E-06
Test Section 5 (12.5-SMA & 4.75-BRIC)	0.1509	-0.36	0.59	2.8 E-7	6.5 E-07.
Test Section 6 (4.75-HPTO & 4.75-BRIC)	0.0531	0.7042	0.61	2.1 E-7	7.9 E-8

Table 14

Rate of Change of SP_R Obtained from Empirical Relationships Established between SP_R and Applied ESALs

Test Section Designation	Rate of Change in SP_R during each loading cycle. (ΔSP_R)
Test Section 2 (12.5-SMA)	$\frac{0.0836}{ESALs}$
Test Section 3 (4.75-HPTO)	$\frac{0.0362}{ESALs}$
Test Section 4 (9.5-SP & 4.75-BRIC)	$\frac{0.2663}{ESALs}$
Test Section 5 (12.5-SMA & 4.75-BRIC)	$\frac{0.01509}{ESALs}$
Test Section 6 (4.75-HPTO & 4.75-BRIC)	$\frac{0.0531}{ESALs}$

Determining damage index. In order to determine the damage index, the stiffness index was first computed from the $\varepsilon_{t\text{-}max}$ (Equation 24). The maximum strain and rate of change in SP_R per loading cycle was then combined to obtain the total damage experienced by the overlays during each loading cycle (Equation 25). The damage index was computed as the cumulative damage applied to the overlays after each loading pass (Equation 26). Figure 42 presents the cumulative DI values that were computed using Equation 26 for each overlay mixtures after each HVS pass. The DI values shown in Figure 42 increased at different rates for the different asphalt overlays (or sections). This suggested that the damage index was capable of differentiating between the mixtures.

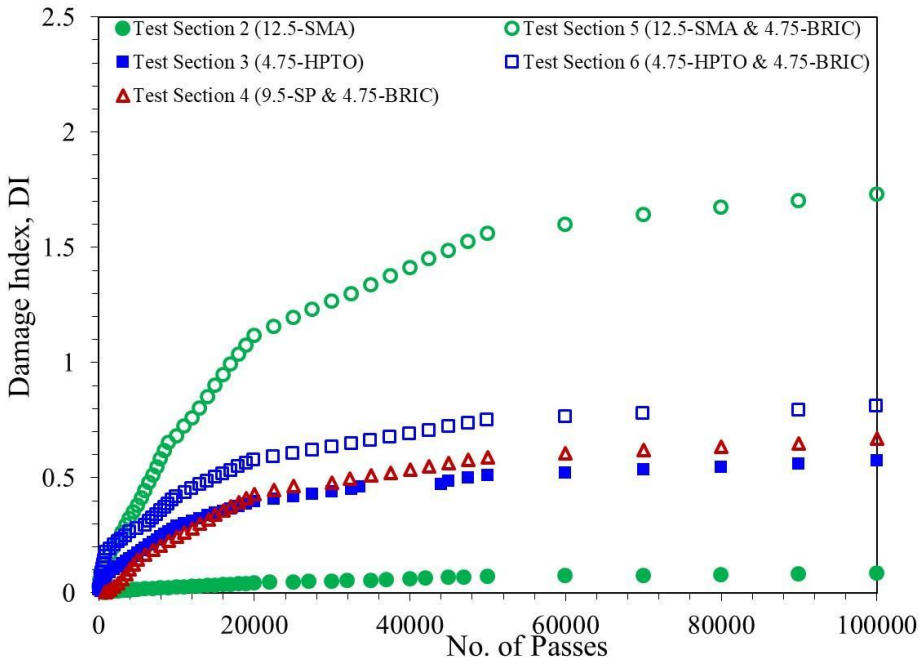

Figure 42. Damage index versus number of applied ESALs.

Logarithmic functions were used to model the evolution of damage in the overlays due to residual PCC slab deflection and the application of the wheel load directly over the joint. The empirical relationships that were developed between DI and applied ESALs is shown in Table 15. From this table it can be observed that the relationships had a very high adjusted R^2 and the slope of these relationships significantly higher than 0. This implied that the damage index had a strong correlation with applied ESALs. The rate of change in damage with respect to ESALs was obtained from the empirical relationships established in Table 16. This rate of change in DI with applied loading was used to assess the relative rate of damage accumulation in the overlays. From the relationships presented in Table 16 it can be observed that the rate of damage accumulation per unit cycle was highest in the 12.5-SMA & BRIC overlay followed by the 9.5-SP & BRIC overlay, 4.75-HPTO & 4.75-BRIC overlay, 4.75-HPTO overlay and 12.5-SMA overlay respectively. These results implied that the overlays which contained the 25.4 mm (1.in.) layer of BRIC (i.e., composite overlays) were potentially more crack susceptible than the surface course overlays more likely to undergo cracking. This observation generally coincided with the trends found with respect to the laboratory fatigue cracking performance of the overlay mixtures. Since no reflection cracking was observed in the full-scale test sections after accelerated loading, the observed trend with respect to DI was logical. This is because fatigue cracking typically occurs in HMA overlays before the on-set and propagation of reflection cracking.

Table 15

Empirical Relationships Established between Damage Index and Applied ESALs

Test Section Designation	**Coefficients**		**Adjusted R^2**	**Slope**	**Significance at $\alpha = 0.005$**
	a	**b**			
Test Section 2 (12.5-SMA)	5.481	-20.583	0.81	8.15-08	2.49 E-19
Test Section 3 (4.75-HPTO)	12.102	-3.7511	0.61	5.12 E-07	1.39 E-13
Test Section 4 (9.5-SP & 4.75-BRIC)	28.535	-66.798	0.66	7.68 E-7	3.4 E-12
Test Section 5 (12.5-SMA & 4.75-BRIC)	34.212 -	-148.97	0.63	1.88 E-6	8.9 E-13
Test Section 6 (4.75-HPTO & 4.75-BRIC)	14.944	92.049	0.58	8.38 E-5	2.13 E-8

Table 16

Rate of Change in Damage Index Obtained from Empirical Relationships Established between DI and Applied ESALs

Test Section Designation	Rate of Change in SP_R during each loading cycle. (ΔSP_R)
Test Section 2 (12.5-SMA)	$\frac{5.481}{ESALs}$
Test Section 3 (4.75-HPTO)	$\frac{12.102}{ESALs}$
Test Section 4 (9.5-SP & 4.75-BRIC)	$\frac{28.535}{ESALs}$
Test Section 5 (12.5-SMA & 4.75-BRIC)	$\frac{34.212}{ESALs}$
Test Section 6 (4.75-HPTO & 4.75-BRIC)	$\frac{14.944}{ESALs}$

It is noted that the DI parameter differentiates between the damage accumulations in different asphalt mixtures, strongly correlates with applied ESALs, and indicates similar trends to those observed in laboratory testing. Therefore the DI has the potential

to be used as a parameter to compare the relative field cracking performance of HMA mixtures. However further studies must be performed to determine whether the DI correlates to changes in material properties of HMA mixtures.

Transverse Pavement Profile Evaluation Results

Transverse pavement profile evaluation was conducted in this study in order to assess the extent of permanent deformation on the surface of pavement sections due to applied HVS loading. Pavement profiles were taken at seven locations along each test section however, particular focus was placed on the pavement profiles obtained at the joint in each test section. The transverse pavement profiles obtained on each test section at the joint; after 200,000 HVS passes, were used for the comparisons presented in this section. (Figure 43) illustrates the methodology utilized to compute the surface permanent deformation on each of the six test sections. From this figure, it can be seen that the permanent surface deformation on each test section was computed by finding the difference in depth between a transverse reference line and the surface depression recorded in each test section.

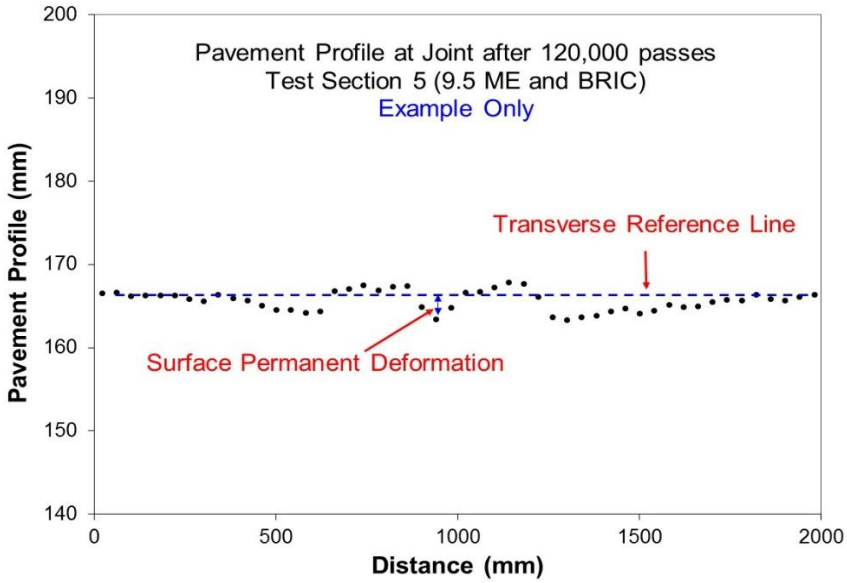

Figure 43. Methodology used to quantify field rutting.

Figure 44 presents the rutting (permanent surface deformation) obtained on each test section at the joint; after 200,000 HVS passes. It can be observed that Section 2 (12.5-SMA) had the lowest surface permanent deformation followed by Section 1 (9.5-SP), Section 4 (9.5 ME & 4.75-BRIC), Section 3 (4.75-HPTO), Section 5 (12.5-SMA & 4.75-BRIC), and Section 6 (4.75-HPTO & 4.75-BRIC) respectively. This trend in the permanent surface deformation results was expected because SMA mixes are typically designed to resist rutting while binder rich asphalt mixtures such as 4.75-HPTO and 4.75-BRIC are highly susceptible to rutting. It can also be observed that the rutting on the sections that contained a composite overlay was generally higher than those that contained one overlay mixture. This result was logical because the stress relieving interlayer contained a softer binder which caused the mixture to provide less support for the surface course overlays.

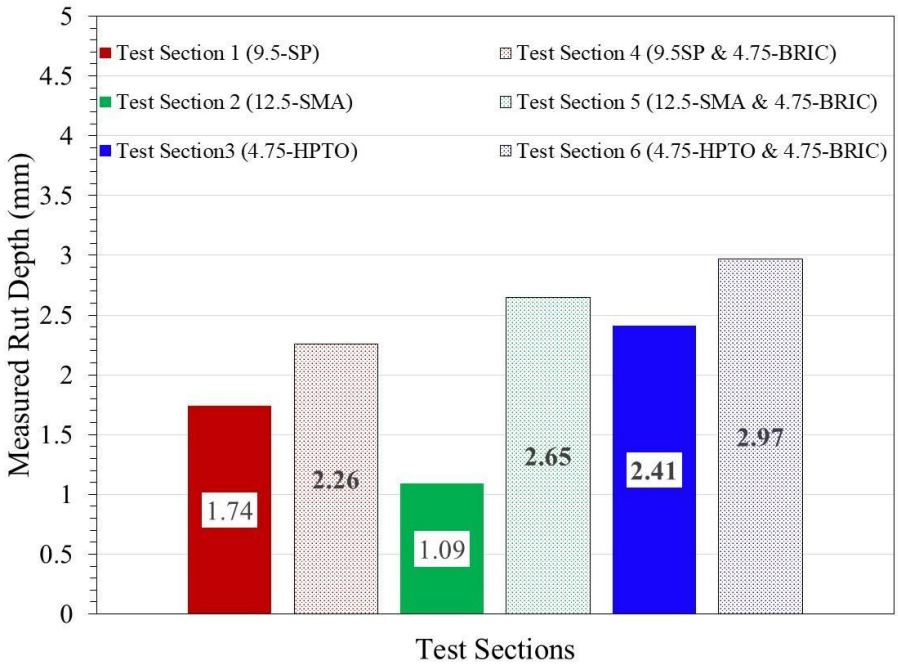

Figure 44. Rutting performance of full-scale, field test sections.

Chapter 7

Performance Comparison & Cost Analysis of HMA Overlays

This chapter presents the results of a performance comparison and cost analysis that was conducted to determine the best performing and most cost effective HMA overlay mixture. The laboratory testing results of phase 2 of laboratory testing (i.e., laboratory performance comparison of the field-extracted HMA overlays) was used for the performance comparison. These results were also used to perform the cost analysis.

Performance Ranking of HMA Overlays

The results obtained during phase 2 of laboratory testing was used to rank the overall laboratory performance of the overlay mixtures. That is, the laboratory fatigue cracking performance ranking, reflection cracking performance ranking, rutting performance ranking of the field-extracted HMA overlays were determined from the results of the bending beam fatigue test, overlay test and APA rut test, respectively.

Table 17 presents the ranking system that was developed to compare the relative laboratory performance of the mixtures. The ranking system was based on 5 criteria which included: average number of BBF cycles to failure, average number of OT cycles to failure, critical fracture energy (G_C) crack progression rate, and APA rut depth. The overlay mixtures were rated on a (1-5) scale for each performance ranking criterion with 5 being the best score and 1 being the worst score. The overall ranking score for each mixture was computed as a weighted average. Greater importance was placed on the average number of OT cycles and crack progression rate criteria because these criteria are closely related to reflection cracking resistance: the primary purpose of HMA overlays.

The least importance was placed on the APA rut depth because rutting is not a primary concern for HMA overlays.

Table 17

Performance Ranking Criteria of HMA Overlay Mixtures

Performance Measure	**Performance Ranking Criterion**	**Ranking Criterion Weight (%)**
Fatigue Cracking	No. of BBF Cycles to Failure	20
Reflection Cracking	No. of OT Cycles to Failure	50
	Crack Progression Rate	20
Rutting	Rutting	10

The average number of BBF cycles to failure and average crack progression rates of the mixtures were ranked based on their actual values. The rating scale for the number of OT cycles to failure was based on the ratio between the average number of cycles to failure for each mix and the OT design criteria proposed by Scullion et al. [14] for crack resistant HMA mixtures (i.e., 700 cycles). Ratio increments of 0.5 were used to distinguish the ranking scores on the number of OT cycles to failure rating scale. For instance ratios between 0 and 5 were given a score of 1; ratios between 5.1 and 10 were given a score of 2; ratios between 11 and 15 were given a score of 3; ratios between 15.1 and 20 were given a score of 4; and ratios greater than 20 were given a score of 5.

The rutting scale depended on the ratio between the average rut depth of each mixture and their respective NJDOT rutting threshold. Similar rut depth threshold that were used for surface course mixtures (i.e., 9.5-SP, 12.5-SMA, and 4.75-BRIC): were used for the composite HMA overlays (i.e. 9.5-SP& 4.75-BRIC, 12.5-SMA & 4.75-BRIC

and 4.75-HPTO & 4.75-BRIC). Increments of 20% were used to distinguish the ranking scores on the rutting scale. For instance ratios between 0 and 20% were given a rutting score of 5 and ratios between 21 and 40% were given a rutting score of 4.

Table 18 presents the performance ranking used to compare the relative performance of the specialty and composite HMA overlay mixtures. From the rankings presented in this table it can be observed that the 4.75-HPTO mixture had the best overall performance followed by the 9.5-SP & BRIC mixture, 9.5-SP, 9.5-SP & BRIC, and 12.5-SMA & BRIC mixtures. In addition, the overall performance rankings also indicated that the 12.5-SMA mixture had the worst overall performance. Based on the overall performance ranking scores it can be observed that the addition of the layer of 4.75-BRIC below the surface course mixtures (i.e., 9.5-SP, 12.5-SMA, and 4.75-HPTO) had little or no effect on the overall performance of the HMA mixtures. However when the rankings of the reflection cracking performance was considered it can be seen that the 4.75-BRIC layer improved the number of OT cycles to failure of the 9.5-SP and 12.5-SMA mixtures. It can also be observed that the 4.75-BRIC layer substantially improved the crack progression rate rankings of the 9.5-SP, 12.5-SMA, and 4.75-HPTO, respectively.

Table 18

Performance Rankings of Specialty and Composite New Jersey Mixtures

Performance Ranking Criterion	**Performance Ranking Score (5:best, 0: worst)**					
	9.5-SP	**12.5-SMA**	**4.75-HPTO**	**9.5-SP & 4.75-BRIC**	**12.5-SMA & 4.75-BRIC**	**4.75-HPTO & 4.754-BRIC**
No. of BBF Cycles to Failure	5	3	4	3	2	2
No. of OT Cycles to Failure	1	1	4	2	2	4
Crack Progression Rate	3	2	2	4	5	3
Rutting	4	3	1	1	1	1
Overall Ranking Score	2.5	1.8	3.3	2.5	2.5	3.1

Cost Analysis

Construction costs of HMA overlays. The results obtained from the beam fatigue tests and overlay tests were used to determine the relative cost effectiveness of the HMA overlay mixtures evaluated in this study. In order to determine the cost effectiveness of utilizing the mixtures as potential treatments for deteriorated rigid pavements, a hypothetical pavement section was considered. This pavement section had the following dimensions: 5280 ft. (1.6 km) length, and 12 ft. (4.57 m) width. The pavement section contained a similar structure as the full-scale composite field sections evaluated in this study. The sections contained a 3 in., HMA overlay, 8 in., PCC base layer, 16 in., New Jersey I-3 granular base layer, and a 12 in. compacted natural soil layer. The overlays in the sections consisted of 76.2 mm (3 in.) thick, 9.5-SP overlay, 12.5-SMA overlay, 4.75-HPTO overlay and 3 composite overlays. The composite overlays consisted of a combination of a 50.8 mm (2 in.) thick 9.5-SP mixture; placed

over a 25.4 mm (1 in.) thick layer of 4.75-BRIC mixture, 50.8 mm (2 in.) thick 12.5-SMA mixture; placed over a 25.4 mm (1 in.) thick layer of 4.75-BRIC mixture., and 50.8 mm (2 in.) thick, 4.75-HPTO mixture; placed over a 25.4 mm (1 in.) thick layer of 4.75-BRIC mixture, respectively. Therefore, the only difference in the pavement section was the type of HMA overlay used in the mixture. Based on this fact, only the construction costs of the HMA overlay in the hypothetical pavement sections were considered for the cost analysis. An assumed HMA density of 2349 kg/m^3 (147 lb/ft^3) was used to determine the quantity of asphalt required for the hypothetical pavement section [77]. The mass of HMA material required for the hypothetical pavement section was determined using (Equation 28). The mass of asphalt required for the overlays was determined as 322 tons. The breakdown of the production costs of the HMA overlay mixtures is illustrated in (Table 19) and the final cost of construction for each HMA overlay in the hypothetical pavement sections is shown in Table 20.

$$\text{Mass} = \text{Density} \times \text{Volume (of HMA overlay layer)} \quad \text{.....(28)}$$

Table 19

Production Cost of HMA Overlays

Production Criteria	**Cost Computational Formula**
Mass of Binder	Optimum binder content x total mass of mixture
Total cost of Binder	Mass of binder x cost of binder (506 per ton) [72]
Mass of aggregates	Volume x Density (1681 kg/m^3) of Aggregate
Total cost of Aggregate	Mass of Aggregate x cost of aggregate ($14 per ton) [71]
Cost of plant production	$2500 per 100 ton of HMA [71]

Table 20

Breakdown of Production and Construction Cost of HMA Overlays

HMA Overlay	9.5-SP	12.5-SMA	4.75-HPTO	9.5-SP & 4.75-BRIC	12.5-SMA & 4.75-BRIC	4.75-HPTO & 4.75-BRIC
Binder Mass (tons)	662	813	883	728	828	875
Binder Cost ($)	334,946	411,337	446,594	368,275	419,207	442,714
Aggregate Mass (tons)	7,237	7,124	7,196	21,245	21,139	21,265
Aggregate Cost ($)	115,789	113,978	115,138	339,915	338,228	340,237
Total Material Cost ($)	450,735	525,315	561,732	708,190	757,435	782,950
Construction Cost ($)	197,469	198,414	201,968	549,312	549,193	553,493
Total Cost ($)	648,204	723,729	763,700	1,257,502	1,306,628	1,336,444

Based on the results presented in Table 20 it can be observed that the 9.5-SP mixture had the lowest total construction cost while the construction cost of the 12.5-SMA and 4.75-HPTO mixtures were slightly higher than that of the 9.5-SP mixture. This was expected because the 12.5-SMA and 4.75-HPTO had a higher binder content (7.0% and 7.6% respectively) than the 9.5-SP mixture which had a binder content of 5.7%. It can also be seen in (Table 20) that the cost of the HMA overlays which contained the 4.75-BRIC was approximately 3 times higher than those which contained only one mixture. This was expected because the 4.75-BRIC mixture contained a smaller NMAS and had a higher binder content. Thus the surface area of the aggregates in the mixture was higher and more binder was required in order to effectively coat the aggregates in the 4.75-BRIC mixture.

Cost effectiveness of HMA overlays. A cost effectiveness economic analysis is typically performed in order to compare the cost to benefit ratio of various alternatives or treatments to assess their viability [71]. For the purposes of this study, the cost effectiveness of the HMA overlay mixtures considered was assessed using a simple approach. This approach involved computing a cost effectiveness ratio for each mixture (Equation 29) based on their respective total construction cost and laboratory reflection cracking performance.

$$\text{Cost Effectiveness Ratio} = \frac{Total\ Construction\ Cost\ of\ Overlays}{Expercted\ Performance} = \frac{Const_{Total}}{N_{f-OT}} \quad (29)$$

Where

$N_{f\text{-}OT}$ Average number of OT cycles to failure

$Const_{Total}$ Total construction cost of HMA overlays

The expected performance (Equation 29) considered only the average number of OT cycles to failure because the main concern for HMA overlays is their reflection cracking performance [17]. Typically, a mixture with a low cost effectiveness ratio is desirable because it suggests that the HMA mixture yields a lower cost per OT loading cycle. The cost effectiveness ratio obtained for of the specialty and composite New Jersey overlay mixtures is presented in (Table 21). Based on the results presented in (Table 21) it can be observed that the 4.75-HPTO lowest cost effectiveness ratio. The 4.75-HPTO & 4.75-BRIC, 9.5-SP & 4.75-BRIC, 12.5-SMA & 4.75-BRIC mixtures had the next lowest cost effectiveness ratios respectively. The 9.5-SP had the highest cost effectiveness ratio followed by the 12.5-SMA. These results implied that the 4.75-BRIC yielded the lowest cost per OT loading cycle and was therefore the most cost effective HMA mixture. The

results also suggested that the addition of a stress relieving interlayer (i.e., a 25.4 mm (1 in.) layer of 4.75-BRIC) generally provided a better "bang for the buck." This is because the cost effectiveness ratios of the composite overlay mixtures were approximately 30% lower than that of their corresponding specialty overlay mixture (with the exception of 4.75-HPTO and 4.75-HPTO & 4.75-BRIC).

Table 21

Cost effectiveness Ratios Obtained for HMA Overlays on Hypothetical Pavement Sections

HMA Overlay	**Average Number of OT Cycles to failure (Cycles)**	**Total Cost ($)**	**Cost Effectiveness ($ per Cycle)**
9.5-SP	2,017	648,204	3.21
12.5-SMA	2,300	723,729	3.15
4.75-HPTO	11,107	763,700	**0.69**
9.5-SP & 4.75-BRIC	5,498	1,257,502	2.29
12.5-SMA & 4.75-BRIC	4,518	1,306,628	2.90
4.75-HPTO & 4.75-BRIC	13,603	1,336,444	0.98

Chapter 8

Summary of Findings, Conclusions, Limitations & Recommendations

Summary of Findings

The main objective of this study was to evaluate the cracking and rutting performance of specialty and composite HMA overlay mixtures utilized in New Jersey to rehabilitate deteriorated rigid pavements. The study was conducted in three components. In the first component of the study, the laboratory performance of four plant -produced specialty New Jersey mixtures were assessed to determine the most appropriate (i.e. best performing) HMA mixture that can be utilized as an asphalt overlays.. These mixtures assessed in this component of the study included: a dense-graded, 9.5-SP mixture, a gap-graded, 12.5-SMA mixture, a dense graded, 4.75-HPTO mixture, and a uniformly graded, 4.75-BRIC mixture. The NMAS of the 9.5-SP, 12.5-SMA, 4.75-HPTO, and 4.75-BRIC mixtures was 9.5 mm, 12.5 mm, 4.75 mm, and 4.75 mm, respectively. The 9.5-SP, 12.5-SMA, and 4.75-HPTO was produced using a PG 76-22 binder while the 4.75-BRIC mixture was made using a PG 70-28 polymer modified binder. The approach utilized during this phase of the study involved conducting the DCM test, S-VECD test, overlay test and APA tests to evaluate the fatigue cracking, reflection cracking, and rutting performance of the mixtures.

The second component of this study involved the laboratory assessment of field-cores, extracted from HMA overlays that were constructed on a full-scale pavement test section. A total of six HMA overlay mixtures were evaluated during the second phase of this study. These mixtures include a 9.5-SP mixture, 12.5-SMA mixture, 4.75-HPTO

mixture and three composite overlay mixtures. The composite mixtures consisted of a 9.5-SP mixture, 12.5-SMA mixture, and 4.75-HPTO mixture, respectively overlaid on a 25.4 mm (1 in.) layer of 4.75-BRIC.The main objective of the second phase of laboratory testing was to determine whether the overall performance of the HMA overlays improved due to the addition of a stress relieving interlayer (i.e., 4.75-BRIC) below the specialty surface course mixtures. The laboratory fatigue cracking, reflection cracking, and rutting performance of the mixtures were assessed using the bending beam fatigue test, overlay test and APA tests, respectively.

The third component of the study involved the field evaluation of six full-scale composite pavement sections which contained a 9.5-SP overlay, 12.5-SMA overlay, 4.75-HPTO overlay, 9.5-SP & 4.75-BRIC composite overlay, 12.5-SMA & 4.75-BRIC composite overlay, and 4.75-HPTO & 4.75-BRIC composite overlay respectively. The main objective of this component of the study was to assess the field reflection cracking and rutting performance of the HMA overlays. The sections were subjected to accelerated pavement testing using a heavy vehicle simulator. The accelerated pavement testing involved the application of a 60 kN dual-tire, single axle load for 200,000 load repetition and pavement responses were measured during APT.

The results of the laboratory and field testing conducted during each component of this study was used to draw conclusions about the relative performance of the mixtures evaluated in the study. The results of the laboratory testing during the first component of the study were as follows:

- The dynamic modulus mastercurves of the mixtures indicated that the 4.75-HPTO mixtures had the highest overall stiffness across the range of testing temperatures and loading frequencies adopted in this study. The 12.5-SMA had the next highest stiffness followed by the 9.5-SP and 4.75-BRIC mixtures respectively. The 4.75-HPTO had the highest potential for rutting of all mixtures because it had the lowest stiffness at higher loading frequencies, The 4.75-HPTO master curve had the most gradual slope in the 10 Hz frequency domain which implied that the 4.75-HPTO mixture had the least susceptibility to fatigue cracking. The 12.5-SMA may be most prone to brittle failure (cracking) because its overall stiffness was high and the overall slope of the master curve was steepest as loading rate increased.
- The 4.75-BRIC mixture experienced the highest rate of reduction in pesuedostiffness followed by the 4.75-HPTO, 12.5-SMA and 9.5-SP mixtures respectively. This suggested that damage accumulation occurred more rapidly in the unconventional, (4.75-BRIC and 4.75-HPTO) mixtures during cyclic loading: when compared to the conventional mixtures (9.5-SP and 12.5-SMA). The higher reduction in the damage characteristic curve of the unconventional mixtures may have been due the fact that the unconventional mixtures were compacted to a lower air void content than the conventional mixtures.
- The 4.75-BRIC.mixture had the highest average number of OT cycles to failure followed by the 9.5-SP, 4.75-HPTO, and 12.5-SMA. The average number of OT cycles obtained for the 9.5-SP and 4.75-HOT mixtures were similar. This implied that the 4.75-BRIC mixture had the highest resistance to reflection cracking while

the 12.5-SMA was most susceptible to reflection cracking. The 4.75-BRIC was expected to have a higher average number of OT cycles to failure because it is specifically designed with a fine gradation, low air void content, and softer, polymer modified binder. The poor reflection cracking performance observed for the 12.5-SMA mixture may have been due to the mixtures' gap-gradation. The lack of intermediate sized aggregates makes the mixture less resistant to shear stresses that develop ahead of the crack tip of macro-cracks during OT loading.

- The 12.5-SMA and 4.75-HPTO mixtures had the highest average critical fracture energy followed by the 4.75-BRIC and 9.5-SP mixtures, respectively. This implied that 12.5-SMA, 4.75-HPTO, 4.75-BRIC mixtures were more resistant to macro-crack initiation than the 9.5-SP control mixture The 4.75-BRIC had the lowest crack progression rate which, was approximately three times lower than the 9.5-SP control mixture. The 12.5-SMA had the highest crack progression rate which was 20% higher than that of the 9.5-SP. This indicated that the 4.75-BRIC had the highest resistance to crack propagation while the 12.5-SMA had the least resistance to crack propagation.
- The APA results indicated that the average rut depth of all the specialty mixtures fell well below their respective NJDOT rut depth thresholds. Therefore, all mixtures performed well in rutting.

The results of the laboratory testing during the second component of the study were as follows

- The 9.5-SP overlay mixture had the highest average number of BBF cycles to failure followed by the 4.75-HPTO, 12.5-SMA. This result coincided with the

results obtained of the S-VED tests. The average number of cycles to failure for the 9.5-SP, 12.5-SMA, and 4.75-HPTO mixtures decreased by 60%, 40% and 67% respectively when a layer of 4.75-BRIC was added to the mixtures. This implied that the use of a 4.75-BRIC mixture in conjunction with the 9.5-SP, 12-SMA, and 4.75-HPTO made the mixtures more susceptible to fatigue cracking

- The average number of OT cycles to failure of the 4.75-HPTO mixture was larger than that of the 12.5-SMA and 9.5-SP mixtures, respectively. These results suggested that the reflection cracking resistance of the HMA overlays increased as the binder content of the mixtures increased. This is because the binder content of the 9.5-SP, 12.5-SMA, and 4.75-HPTO mixtures was: 4.7%, 7.0%, and 7.6%, respectively. The reflection cracking performance of the surface course mixtures generally improved when a layer of 4.75-BRIC was added at the bottom of the mixtures. This is because the average number of OT cycles to failure increased by 60%, 50%, and 18% of the 9.5-SP, 12.5-SMA, and 4.75-HPTO
- The crack progression rates mirrored the trends observed with respect to the average number of OT cycles to failure. The crack progression rates of the HMA overlays decreased when a layer of 4.75-BRIC was placed at the bottom of the surface course mixtures. This implied that the 4.75-BRIC layer retarded the rate of reflection crack propagation in the overlays.
- Average rut depth of the mixtures increased as binder content increased. This trend was logical because the stability and load transfer efficiency of mixtures with higher binder contents decreases at high temperatures. The addition of the 4.75-BRIC layer at the bottom of the HMA surface course mixtures appeared to

have little to no effect on mixture rutting performance since the average rut depth for the composite overlays were similar to the average rut depth of surface course overlays.

The results of the field testing conducted on the six full scale composite pavement sections were as follows:

- The general APT strain data processing and analysis approach presented in study was successfully used to rank all five of the six test sections that were considered during the field testing based on their relative fatigue performance. This is the case because the computed analysis parameter (i.e., cumulative DI) was able to distinguish between the damage that accumulated in the overlays during APT.
- Two measures, maximum strain ($\varepsilon_{t\text{-}max}$) and strain ratio ($SP_R$) were directly computed from the strain-time history pulses measured during APT. These parameters quantify the response of pavement layers to applied loading. The $\varepsilon_{t\text{-}ma}$ represented the most critical tensile strain that the overlays experienced due to PCC slab deflections associated with the wheel load being directly over the joint. The SP_R captured the compressive strains that were applied to the HMA overlays due to residual slab deflections. That is, when the wheel load is on the edge of the slabs.
- A proposed damage index (DI) parameter was used to compare the relative cracking susceptibility of the HMA overlays. This parameter accounted for the total damage that was applied to the overlay strictly due to the wheel load and as a result of residual PCC slab deflection. The DI parameter differentiated between the damage accumulations in different asphalt mixtures, strongly correlated with applied ESALs, and indicated similar trends to those observed in laboratory testing.

Therefore the DI has the potential to be used as a parameter to compare the relative field cracking performance of HMA mixtures.

Conclusions

Based on the results of the laboratory testing and field testing performed on the specialty and composite New Jersey overlay mixtures considered in this study, the following conclusion can be drawn:

- The use of a stress relieving interlayer (i.e., 4.75-BRIC) in conjunction with specialty conventional surface course mixture (i.e., composite overlay) is the best alternative to extend the service life of deteriorated rigid pavements. This is because the 4.75-BRIC mixture retards the rate of reflection crack propagation in the overlay. It should be noted however that the 4.75-BRIC interlayer generally increases the fatigue cracking susceptibility of the overlays.
- Composite overlay (i.e., overlays which contained a surface course mixture placed over a 4.75-BRIC mixture) proved to be generally more cost effective than surface course mixtures. However, the 4.75-BRIC mixture was determined as the most cost effective of all mixtures considered in this study.

Limitations

This study had several limitations which included the following:

- The HMA overlays on the full-scale, field sections that were evaluated during the field testing component of the study did not undergo reflection cracking. Therefore it was not possible to compare the relative cracking performance of the

HMA overlay mixtures based on actual pavement responses. The reflection cracking performance comparison of HMA overlays was limited to results from laboratory testing.

- Results of laboratory reflection cracking (OT tests) and fatigue test (BBF) are highly variable. This led to the increased sampling to ensure accurate and valid results were obtained.

Recommendations

It is recommended that further field evaluation is required to estimate the life expectancy of the overlays considered in the study. Though the research present in this study provided tools to successfully measure and rank the field performance of the six asphalt overlays considered in this study, further field evaluation is necessary in order to predict the expected life of these overlays. Estimation of the expected life of the six overlays evaluated in this study would provide verification for the parameters developed in this study to characterize the asphalt overlays' reflective cracking susceptibility and overall resistance to horizontal and vertical joint movement..

References

[1] D. Newcomb, "Introduction" in *Thin Asphalt Overlays for Pavement Preservation,* IS 135. Lanham, MD, 2009, ch.1, pp.7-9.

[2] D. E. Watson, "Thin Asphalt Concrete." Transportation Research Board of the National Academies, Washington, D.C., Rep. NCHRP Synthesis 464, 2014.

[3] E. R. Brown, and M. Heitzman, "Thin HMA Overlays for Pavement Preservation and Low Volume Asphalt Roads," National Center for Asphalt Technology, Greensboro, NC, Rep. NCAT Report 13-05, 2013.

[4] T. You et al., "Evaluation of Thin Asphalt Overlay Practice Preserving Nebraska's Asphalt Pavements ," Department of Roads, Nebraska Department of Transportation, Lincoln, NE Rep. SPR-P1(15) M017, 2015.

[5] D. Merritt et al., "Evaluation of Pavement Safety Performance," United States Department of Transportation, Washington, DC, Rep. FHWA-HRT-14-065, 2015.

[6] G. Huber, "Performance Survey on Open-Graded Friction Course Mixes," Transportation Research Board of the National Academies, Washington, D.C., Rep. NCHRP Synthesis 284, 2000.

[7] E. Y. Chou and D. H. Pulugurta, "Effectiveness of Thin Hot Mix Asphalt Overlay on Pavement Ride and Condition Performance," Ohio Department of Transportation, Columbus, OH, Rep. 147950, 2008.

[8] K. T. Hall et al., "Performance of Rigid Pavement Rehabilitation Treatments in the Long-Term Pavement Performance SPS-6 Experiment," *Transportation Research Record: Journal of the Transportation Research Board,* vol. 1823, pp.64-72, Jan. 2003.

[9] N. Suleiman, "Evaluation of North Dakota's 4.75-mm Superpave Mixes for Thin Overlay Applications," *Transportation Research Record: Journal of the Transportation Research Board,* vol. 2204, pp.58-64, Jan. 2011.

[10] F. Rahman et al., "Optimized Design for 4.75-mm NMAS Superpave Mix Thin Overlay," in *First Congress of Transportation Development Institute,* Chicago, IL, 2011.

[11] L. A. Cooley and E. R. Brown, "Potential of Using Stone Matrix Asphalt for Thin Overlays," *Transportation Research Record: Journal of the Transportation Research Board,* vol. 1794, pp.46-52, Jan. 2002.

[12] S. Son et al., "4.75 mm SMA Performance and Cost Effectiveness for Asphalt Thin Overlays," *International Journal of Pavement engineering*, vol. 17, pp.799-809, Mar. 2015.

[13] P. Sebaaly et al. "Field and Laboratory Performance of Superpave Mixtures in Nevada," *Transportation Research Record: Journal of the Transportation Research Board*, vol. 1891, pp.76-84, Jan. 2004.

[14] T. Scullion et al., "Design and Performance Evaluation of Very Thin Overlays in Texas," Texas Department of Transportation, Austin, TX, Rep. FHWA/TX-09/0-5598-2, 2009.

[15] S. Hu et al., "Analysis of Rutting Performance Impacting Factors in HMA Overlay Mixture Design," *Journal of Testing and Evaluation*, vol. 39, no. 6, pp.1078-1088, Jan. 2011.

[16] G. Sherman et al., "Minimizing Reflection Cracking of Pavement Overlays," Transportation Research Board of the National Academies, Washington, D.C., Rep. NCHRP Synthesis of Highway Practice 92, 2014.

[17] D. Jones et al., "Comparison of Full-Depth Reclamation with Portland Cement and Full Depth Reclamation with No Stabilizer in Accelerated Loading Test," *Transportation Research Record: Journal of the Transportation Research Board*, vol. 25, no. 24, pp.133-142, Jan. 2015.

[18] M. Minhoto et al., "The Temperature Effect on the Reflective Cracking of Asphalt Overlays," *Road Materials and Pavement Design*, vol. 10, no. 10, Sep. 2011.

[19] T. Bennert et al., "Comparison of Thin-lift Hot Mix Asphalt Surface Course Mixes in New Jersey," *Transportation Research Record: Journal of the Transportation Research Board*, vol. 1929, no. 1 pp. 59-68, Jan. 2005.

[20] T. Bennert, "Flexible Overlays for Rigid Pavements," New Jersey Department of Transportation, Trenton, NJ, Rep. FHWA-NJ-2009-014, 2010.

[21] J. Paris, "The Reflective Cracking in Flexible Pavements," *Romanian Journal of Transportation Infrastructure*, vol. 2, no. 1, pp. 63-87, Feb. 2015.

[22] A. Abedini, "A Comprehensive Review on Reflective Cracking, Concept, Mechanism, and Laboratory Performance Tests," *International Journal of Civil, Mechanical and Energy Science*, vol. 5, no. 5, pp.1-8, Sep., 2019.

[23] D. Lipomi. *Ep22 Mechanical Properties of Polymers and Viscoelastic Models NANO 134 UCSD Darren Lipomi*. Accessed: Mar. 4, 2020. [Online Video]. Available: http://youtube.com/watch?v=vneTd1eAkE4

[24] F. Moreno and M. C. Rubio, "Effect of Aggregate Nature on the Fatigue-Cracking Behavior of Asphalt Mixes," *Materials and Design*, vol. 47, pp. 61-67, Dec. 2012.

[25] A. Gautam, "Tolerable Strains for HMA Overlays over Concrete Pavements," M.S. thesis, Dept. of Civil Engineering, Univ. of Kansas, Lawrence, KS, 2009.

[26] S. Deilami and G. White, "Review of Reflective Cracking Mechanism and Mitigations for Airport Pavements," in *28th Australian Road Research Board International Conference*, Queensland, Australia, 2018.

[27] R. C. Williams et al., "Reflective Crack Mitigation Guide for Flexible Pavements," Iowa Highway Research Board, Iowa Department of Transportation, Ames, IA, Rep. IHRB Project TR-641, 2015.

[28] M. A. Elseifi et al., "Mitigation Strategies of Reflection Cracking in Pavements," Louisiana Transportation Research Center, Baton Rouge, LA, Rep. FHWA/LA 14/541, 2015.

[29] F. Zhou and L. Sun, "Reflective Cracking in Asphalt Overlay on Existing PCC," in *9th International Conference on Asphalt Pavements*, Copenhagen, Denmark, 2002.

[30] T. Bennert, "A Rational Approach to the Prediction of Reflective Cracking in Bituminous Overlays for Concrete Pavements," Ph.D. dissertation, Dept. of Civil and Environmental Engineering, Rutgers Univ., New Brunswick, NJ, 2009.

[31] F. Tsai, "Prediction of Reflection Cracking in Hot Mix Asphalt," *Transportation Research Record: Journal of the Transportation Research Board*, vol. 2155, pp.43-54, Jan. 2010.

[32] J. N. Prieto et al., "Application of the Wheel Reflective Cracking Test for Assessing Geosynthetics in Anti-Reflection Pavement Cracking Systems," *Geosynthetics International*, vol. 14, no. 5, pp.1-11, Jul., 2007.

[33] P. E. Joseph and R. Haas, "Evaluating Alternative Solutions to Reflective Cracking Through Asphalt Overlays," *Transportation Research Record: Journal of the Transportation Research Board*, vol. 1215, pp.282-291, Jan. 1989.

[34] Y. H. Huang, "Complex Modulus," in *Pavement Analysis and Design*, 2nd ed. Upper Saddle River, NJ, 2004, ap.A, sec.A.4, pp.666-670.

[35] D. Offenbacker, "Evaluation of the Cracking Performance of Geogrid-Reinforced Hot-Mix Asphalt for Airfield Applications," Ph.D. dissertation, Dept. of Civil and Environmental Engineering, Rowan Univ., Glassboro, NJ, 2019.

[36] B. S. Underwood et al., "Improved Calculation Method of Damage Parameter in Viscoelastic Continuum Damage Model," *International journal of Pavement Engineering*, vol. 11, no. 6, pp. 459-476, Dec. 2010.

[37] B. S. Underwood et al., "Simplified Viscoelastic Continuum Damage Model as Platform for Asphalt Concrete Fatigue Analysis," *Transportation Research Record: Journal of the Transportation Research Board*, vol. 2296, pp.36-45, Jan. 2012.

[38] Y. Wang, "Development of the Framework of Performance-Engineered Mixture Design for Asphalt Concrete," Ph.D. dissertation, Dept. of Civil Engineering, North Carolina State Univ., Raleigh, NC, 2019.

[39] G. M. Rowe et al., "The Fatigue Performance of Asphalt Mixtures in the Four Point Bending Beam Fatigue test in Accordance with AASHTO and ASTM Analysis Methods," in 5th *Eurasphalt and Eurobitume Congress*, Istanbul, Turkey, 2012.

[40] E. Hajj et al., "Reflective Cracking of Flexible Pavements Phase I and II Recommendations," Materials Division, Nevada Department of Transportation, Carson City, NV, Rep. 13JF-1, 2018.

[41] V. M. Garcia and A. Miramontes, "Understanding Sources of Variability of Overlay test Procedure," *Transportation Research Record: Journal of the Transportation Research Board*, vol. 2507, pp.10-14, Jan. 2015.

[42]. "Design of Gap-Graded HMA Mixtures," in *A Manual for Design of Hot-Mix Asphalt with Commentary*, NCHRP Research Synthesis 673. Washington, DC, 2011, ch.10, pp.174-193.

[43]. J. P. Guyer "An Introduction to Thin Asphalt Pavement Overlays," unpublished.

[44] T. Bennert and D. Pezeshki, "Performance Testing for HMA Quality Assurance," New Jersey Department of Transportation, Trenton, NJ, Rep. FHWA-NJ-2015-010, 2015.

[45] H. J. Treybig et al., "Overlay Design and Reflection Cracking Analysis for Rigid Pavements," Office of Research and Development, Federal Highway Administration, United States Department of Transportation, Washington, DC, Rep. FHWA-RD-77-66, 1977.

[46] H. L. Von Quintus et al., "Techniques for Mitigation of Reflective Cracks," Airfield Asphalt Pavement Technology Program, Champaign, IL, Rep. AAPTP 05-04, 2009.

[47] G. B. Way, "Prevention of Reflective Cracking in Bituminous Overlays on Rigid Pavements," *Association of Asphalt Paving Technologists*, vol. 49, pp.314-329, Jan. 1980.

[48] A. Gibney et al., "Laboratory Study of Resistance of Bituminous Overlays to reflective Cracking," *Transportation Research Record: Journal of the Transportation Research Board*, vol. 1809, pp.184-190, Jan. 2002.

[49] B. Yu et al., "Evaluation of Anti-Reflective Cracking Measures by Laboratory Test," *International Journal of Pavement Engineering*, vol. 14, no. 6, pp.553-560, Jan. 2013.

[50] G. Montestruque et al., "Stress Relief Asphalt Layer and Reinforcing Polyester Grid as Antireflective Cracking Composite Interlayer System in Pavement Rehabilitation," in 7th *RILEM International Conference on Cracking in Pavements*, Netherlands, 2012.

[51] P. Dumas and J Vecoven, "Processes Reducing Reflective Cracking: Synthesis of Laboratory Tests," in 2nd *RILEM International Conference on Cracking in Pavements*, Liege, Belgium, 1993.

[52] T. Bennert and A. Maher, "Evaluation of Current State of Flexible Overlay Design for Rigid and Composite Pavements in the United States," *Transportation Research Record: Journal of the Transportation Research Board*, vol. 1991, pp.97-108, Jan. 2007.

[53] P. Blankenship et al., "Interlayer and Design Considerations to Retard Reflective Cracking," *Transportation Research Record: Journal of the Transportation Research Board*, vol. 1896, pp.177-186, Jan. 2004.

[54] T. Bennert and A. Maher, "Field and Laboratory Evaluation of a Reflective Crack Interlayer in New Jersey," *Transportation Research Record: Journal of the Transportation Research Board*, vol. 2084, pp.114-123, Jan. 2008.

[55] M. Kim et al., "Field and Laboratory Evaluation of Fracture Resistance of Illinois Hot-Mix Asphalt Overlay Mixtures," *Transportation Research Record: Journal of the Transportation Research Board*, vol. 2217, pp. 146-154, Jan. 2009.

[56] H. S. Chang et al., "Prediction of Thermal Reflection Cracking in West Texas," Transportation Planning Division, Texas State Department of Highways and Public Transportation, Austin, TX, Rep. TTI-2-8-73-18-3, 1976 .

[57] T. Bennert., "Field and Laboratory Forensic Analysis of Reflective Cracking on Massachusetts Interstate 495," *Transportation Research Record: Journal of the Transportation Research Board*, vol. 2126, pp.27-38, Jan. 2009.

[58] L. Makowski., "Wisconsin Experiences with Reflective Crack Relief Projects," *Transportation Research Record: Journal of the Transportation Research Board*, vol. 1905, pp.44-55, Jan. 2005.

[59] Y. Mehta et al., "HVS Evaluation of Flexible Overlays on Composite Pavement," New Jersey Department of Transportation, Trenton, NJ, Rep. FHWA-NJ-2018-008, 2018.

[60] L. Shan et al., "Internal Crack Growth of Asphalt Binders during Shear Fatigue Process," *Fuel*, vol. 189, pp. 293-300, Feb. 2017.

[61] T. Scullion et al., "Design and Performance Evaluation of Very Thin Overlays in Texas," Texas Department of Transportation, Austin, TX, Rep. FHWA/TX-09/0-5598-2, 2009.

[62] H. Zhu et al., "Developing master Curves and Predicting Dynamic Modulus of Polymer-Modified Asphalt Mixtures," *International Journal of Materials in Civil Engineering*, vol. 23, pp. 131-137, Feb. 2011.

[63] R. A. Etheridge et al., "Evaluation of Fatigue Cracking Resistance of Asphalt Mixtures Using Apparent Damage Capacity," *Journal of Materials in Civil Engineering*, vol. 31, no. 11, pp. 1-12, Aug. 2019.

[64] R. Islam, et al., "How the Mix Factors Affect the Dynamic Modulus of Hot-Mix Asphalt," *Journal of Composite Science*, vol. 3, no. 72, pp.1-9, Jul. 2019.

[65] F. Safaei et al., "Linking Asphalt Binder Fatigue to Asphalt Mixture Fatigue Performance using Viscoelastic Continuum Damage Modeling," *Mechanincs of Time-Dependent Materials*, vol. 20, pp. 299-323, Apr. 2016.

[66] S. Sreedhar, and E. Coleri, "Effects of Binder Content, Density, Gradation, and Polymer Modification on Cracking and Rutting Resistance of Asphalt Mixtures Used in Oregon," *Journal of Materials in. Civil. Engineering*. vol. 30, no. 11, Aug. 2018.

[67] S. Kodippily, et al., "Deformation and Cracking Performance of Recycled Asphalt Paving Mixes Containing Polymer-Modified Binder," *Road Materials and Pavement Design* vol. 18 no. 2 pp. 425-439, May 2016.

[68] V. Garcia et al., "Improved Overlay Tester for fatigue Cracking Resistance of Asphalt Mixtures," Texas Department of Transportation, Austin, TX, Rep. TxDOT 0-6815-1, 2017.

[69] A Ali. and Y. Mehta., "Heavy Vehicle Simulator and Accelerated Pavement Testing Facility at Rowan University," in 5th *International Conference on Accelerated Pavement Testing*, Costa Rica, 2016.

[70] L. G. Rodrigues de Mello et al., "Using Damage Theory to Analyze Fatigue of Asphalt Mixtures on Flexural Tests," *International Journal of Pavement Research and Technology*, vol. 11, no. 4, pp. 617-626, Nov. 2018.

[71] Y. Huang et al., "Evaluating Pavement Response and Performance under Different Scales of APT Facilities," *Innovations in Characterization and Modeling of Road materials and Pavements*, vol. 18, no. 3, pp. 159-169, Jun. 2017.

[72] D. H. Timm and A. L. Priest, "Dynamic Pavement Response Data Collection and Processing at the NCAT Test Track. National Center for Asphalt Technology," National Center for Asphalt Technology, Auburn, AL, Rep. NCAT Report 04-03, 2004.

[73] X. Qi et al., "Strain Responses in ALF Modified-Binder Pavement Study," in *2nd International Conference on Accelerated Pavement Testing*, Minneapolis, MN, 2004.

[74] N. Garg and G. F. Hayhoe, "Asphalt Concrete Strain Responses at High Loads and Low Speeds at the National Airport Pavement Test Facility (NAPTF)," in *Airfield Pavement Specialty Conference*, Chicago, IL, 2001.

[75] M. Elseifi, "Analysis of Seasonal Strain Measurements in Asphalt Materials under Accelerated Pavement Testing and Comparing Field Performance and Laboratory Measured Binder Tension Properties," Louisiana Transportation Research Center, Baton Rouge, LA, Rep. FHWA/LA.09/444, 2009.

[76] M. I. Souliman et al., "Cost-effectiveness of Rubber and Polymer Modified Asphalt Mixtures as Related to Sustainable Fatigue Performance," in *International Conference on Sustainable Design, Engineering and Construction*, Tempe, AZ, 2016.

[77] *Asphalt Cement and Fuel Price Index*, New Jersey Department of Transportation, Mar. 2020. [Online]. Available: https://www.state.nj.us/transportation/business/aashtoware/PriceIndex.shtm

Appendix A

Phase 2 Laboratory Testing Statistical Analysis Results

Table A1

Tukey's Honest Significant Difference (HSD) Pairwise Comparisons of Laboratory Performance of Field-Extracted Specialty New Jersey Overlay Mixtures at α = 0.05.

Laboratory Test	Test Parameter	Specialty Mixture Type		ANOVA		Tukey's HSD		Bonferroni
				F value	P	Mean Difference	P Adjusted	P Adjusted
Bending Beam Fatigue Test	No. of BBF Cycles to Failure	9.5-SP	12.5-SMA	3.31	0.05	49837	**0.04**	0.06
			4.75-HPTO			41322	**0.05**	0.07
Overlay Test	No. of OT Cycles to Failure	9.5-SP	12.5-SMA	5.55	0.02	47724	0.19	0.26
			4.75-HPTO			-79698	**0.02**	0.02
	Crack Progression Rate	9.5-SP	12.5-SMA	1.14	0.35	0.03	0.51	0.84
			4.75-HPTO			-0.01	0.95	1.00
Asphalt Pavement Analyzer Test	Average Rut Depth	9.5-SP	12.5-SMA	25.20	0.00	-2.32	**0.00**	0.01
			4.75-HPTO			-3.82	**0.01**	0.00

Table A2

Tukey's Honest Significant Difference (HSD) Pairwise Comparisons of Laboratory Performance of Field-Extracted Composite New Jersey Overlay Mixtures at α = 0.05.

Laboratory Test	**Test Parameter**	**Composite Mixture Type**		**ANOVA**		**Tukey's HSD**		**Bonferroni**
				F value	**P**	**Mean Difference**	**P Adjusted**	**P Adjusted**
Bending Beam Fatigue Test	No. of OT Cycles to Failure	9.5-SP & 4.75-BRIC	12.5-SMA & 4.75-BRIC	15.81	0.00	22,364	**0.03**	0.10
			4.75-HPTO & 4.75-BRIC			21,586	**0.03**	0.09
Overlay Test	No. of OT Cycles to Failure	9.5-SP & 4.75-BRIC	12.5-SMA & 4.75-BRIC	3.016	0.09	23,064	0.20	0.28
			4.75-HPTO & 4.75-BRIC			-27,760	**0.04**	0.12
	Crack Progression Rate	9.5-SP & 4.75-BRIC	12.5-SMA & 4.75-BRIC	0.36	0.70	-0.10	0.88	1.00
			4.75-HPTO & 4.75-BRIC			-0.017	0.68	1.00
Asphalt Pavement Analyzer Test	Average Rut Depth	9.5-SP & 4.75-BRIC	12.5-SMA & 4.75-BRIC	10.00	0.00	-1.70	**0.02**	**0.03**
			4.75-HPTO & 4.75-BRIC			-2.56	**0.00**	**0.00**